University of Modena and Reggio Emilia

DEPARTMENT OF ENGINEERING “ENZO FERRARI”

PhD SCHOOL IN

INDUSTRIAL AD ENVIROMENTAL ENGINEERING

XXXV CYCLE

Development of a methodology for the design of a high-performance small-sized vehicle with a hybrid powertrain. Application to a Formula Student single-seater.

CANDIDATE:

Francesco Raimondi

TUTOR:

Prof. Matteo Giacopini

PhD SCHOOL COORDINATOR:

Prof. Alberto Muscio

Table of contents

Abstract (Italiano)

In questa tesi si è cercato di sviluppare una metodologia di progettazione di un veicolo a quattro ruote di piccole dimensioni ad alte prestazioni movimentato da una power unit ibrida. Lo scopo di tale metodologia è quello di trovare il miglior compromesso tra l'esiguo spazio disponibile in tali veicoli, ed i numerosi componenti che costituiscono una power unit. Tali esigenze si ritrovano in una monoposto del campionato Formula Student, che quindi è stata usata come caso di definizione e validazione della metodologia. La realizzazione di una power unit ibrida mira ad ottimizzare l'utilizzo dell'energia accumulata nel veicolo per la sua propulsione. Da analisi bibliografiche si sono ricercati vari modelli matematici che descrivono il funzionamento di questi sistemi. In particolar modo ci si è concentrati sul metodo numerico del Dynamic Programming basato sui principi di Bellman. Questo metodo è utilizzato per risolvere problemi dove è necessario prendere decisioni a più livelli. Esso è in grado di fornire la soluzione ottimale a problemi di qualsiasi complessità. Tuttavia, il metodo è non causale ed è implementabile solo in un ambiente di simulazione, perché richiede informazioni a priori sull'intero campo di ottimizzazione. Però facendo l'ipotesi di utilizzare il veicolo ibrido in un ciclo omologativo, o in un giro di pista nel quale si vuole ottimizzate la velocità media limitando il consumo di energia, il metodo restituisce numerose informazioni sia sulla definizione del layout della power unit, sia su come utilizzare al meglio l'unità propulsiva, che può essere limitata da vincoli normativi o costruttivi. Inoltre, tale metodo può essere sfruttato per anticipare e validare le logiche di un eventuale software di controllo delle due macchine, quella elettrica e quella a combustione interna, che devono cooperare per generare potenza. Tali strumenti sono stati sfruttati, ed a sua volta affinati ed evoluti, nelle fasi di progettazione e realizzazione di una monoposto di Formula Student con power unit ibrida. I vincoli di progetto per una monoposto di questo campionato sono dettati da un regolamento che dà la possibilità di sviluppare motori motociclistici, che devono essere installati all'interno di un telaio che a sua volta deve rispettare determinati vincoli regolamentari riguardanti prevalentemente la sicurezza dei piloti. Quindi tramite le conoscenze già acquisite in dipartimento per la costruzione di vetture con motore a combustione interna, l'idea di base è stata quella di sostituire il motore a combustione interna 4 cilindri in linea di 708cc e circa 73,6kW con una pover unit ibrida che rispettasse tutti i limiti regolamentari, desse le stesse prestazioni, e soprattutto che avesse gli stessi ingombri cercando di limitare il peso totale del veicolo. Con lo sviluppo di codici numerici che seguono le teorie descritte in precedenza, si sono raccolti una serie di dati, che analizzati in modo critico hanno portato alla definizione del layout della power unit. Questa è costituita da un motore monocilindrico di 480 cc di cilindrata sviluppato sulla base del bicilindrico a V di 90 gradi della Ducati "959

Superquadro". Il motore termico è assistito da un motore elettrico realizzato per questa specifica applicazione (30 kW), alimentato da un pacco batterie agli ioni di litio. Il motore Ducati è stato scelto per le sue prestazioni e per sfruttare il layout dell'architettura a V. Infatti, la testata verticale è stata sostituita dal motore elettrico, direttamente collegato all'albero motore tramite la catena di distribuzione originale, ottenendo così un sistema molto compatto. La power unit installata sulla monoposto è stata realizzata e verificata sperimentalmente, ed ha partecipato alle prove dell'evento inglese di Formula Student.

Abstract

In this thesis, an attempt has been made to develop a design methodology for a high-performance small-sized four-wheeled vehicle, powered by a hybrid power unit. The purpose of this methodology is to find the best compromise between the limited space available in such vehicles and the numerous components that constitute a power unit. These requirements are encountered in a Formula Student single-seater, which has been used as a case for defining and validating the methodology. The development of a hybrid power unit aims to optimize the use of the energy stored in the vehicle for its propulsion. Through bibliographic analyses, various mathematical models describing the operation of these systems were researched, with a particular focus on the numerical method of Dynamic Programming based on Bellman's principles. This method is employed to solve problems where decisions need to be made at multiple levels. It can provide an optimal solution to problems of any complexity. However, it is non-causal and can only be implemented in a simulation environment because it requires a priori information about the entire optimization field. Assuming the use of the hybrid vehicle in a homologation cycle or in a track lap where average speed is to be optimized while limiting energy consumption, the method provides numerous pieces of information both on defining the layout of the power unit and on how to best utilize the propulsion unit, which may be constrained by regulatory or construction-related limitations. Additionally, this method can be utilized to anticipate and validate the operating logics of potential control software for both machines, the electric and internal combustion engines, which must cooperate to generate power.

These tools have been utilized, refined, and evolved in the design and implementation phases of a Formula Student single-seater with a hybrid power unit. The design constraints for a single-seater in this competition are dictated by regulations that allow the development of motorcycle-derived engines, to be installed within a chassis that must comply with certain safety regulations primarily concerning driver safety. Leveraging the department's existing knowledge in constructing vehicles with internal combustion engines, the basic idea was to replace the inline 4-cylinder, 708cc, and approximately 73,6kW internal combustion engine with a hybrid power unit that would meet all regulatory limits, deliver the same performance and, most importantly, have the same dimensions while trying to limit the total weight of the vehicle.

By developing numerical codes following the theories described earlier, a series of data were collected. Critical analysis of this data led to the definition of the power unit layout. It consists of a single-cylinder engine with a displacement of 480 cc developed based on Ducati's 90-degree V-twin "959 Superquadro". The

thermal engine is assisted by an electric motor designed for this specific application (30 kW), powered by a lithium-ion battery pack. The Ducati engine was chosen for its performance and to leverage the V-shaped architecture. The vertical cylinder head has been removed and replaced by the electric motor, directly connected to the crankshaft via the original timing chain, resulting in a very compact system. This power unit installed on the single-seater has been designed, tested, and participated in the trials of the Formula Student event in the United Kingdom.

1 Introduction

The automotive industry and its related sectors are crucial to the global economy and employ a significant portion of the workforce. However, the high number of cars in use worldwide has resulted in severe environmental and human health issues [1].

The transport sector is a major contributor to pollution, and its share of CO_2 emissions is increasing in all regions of the world. This share of CO_2 emissions and its continuous increase have garnered the attention of policymakers in the economic, transport and climate change fields [2,3]. Currently, various technologies based on unconventional propulsion systems are being studied to enhance fuel efficiency and decrease environmental impact [4,5]. One of the most discussed innovations is the development and proliferation of zero-emission vehicles (ZEVs). These vehicles do not emit exhaust gases thanks to onboard power sources, usually derived from battery devices. However, it is important to note that battery electric vehicles (BEVs) are only considered zero-emission locally, as they typically produce greenhouse gases at power plants where electricity is generated. Moreover, the range of BEVs is not yet comparable to the internal combustion engine vehicles (ICEVs), as they are still heavier due to the additional weight of batteries [6].

Hybrid electric vehicles (HEVs) combine the high fuel density of gasoline engines with the zero pollution of electric motors. The aim of this work is to define analysis procedures for the optimal integration of the two systems in a small, high performance four-wheeled vehicle. The requirements of the vehicle are similar to those of a two-wheeler with the same performance characteristics. This step is being taken precisely because the motorcycle market will also have to comply with more stringent emission regulations [7-9].

Therefore, the application of hybrid technologies to motorcycle engines is an interesting solution to study in order to reduce fuel consumption and therefore CO_2 emissions [10,11].

For a real application of the hybridization process, an existing vehicle was considered, which allowed for real tests to be conducted and specific control strategies to be developed. The vehicle considered for this case study is the Formula SAE car from the University of Modena and Reggio Emilia. This makes it possible to define the specific boundary conditions and constraints that the hybrid power unit must comply with. Given the regulatory constraints of Formula Student UK [12], this thesis describes the design process to achieve an original and compact solution to this hybridization problem.

The aim is to keep most of the engine components to reduce costs and potential reliability issues, while considering the available space in the single-seater. The designed configuration is especially suitable for V-type engines and provides a *'plug & play'* solution. The process entails replacing one of the engine heads with an electric motor that is connected to the crankshaft through the original valve transmission system. The maximum external dimensions of the original engine must be adhered to, and the weight of the powertrain must be maintained. However, the introduction of additional components, such as the battery pack and inverter, must also be considered to estimate the overall weight of the hybrid powertrain.

The subsequent sections examine the primary stages that lead to the final geometry of the power unit housing in the vehicle. It is essential to consider specific dimensional constraints to enable the replacement of the engine head with the electric motor without requiring further modifications. A volume analysis was conducted to optimize the use of available space and guide the selection of necessary vehicle systems. Various layouts of the electric motor cooling circuit were analysed through 3D CFD simulations to determine the most suitable solution in terms of pressure losses and distribution of heat transfer coefficients (HTC). In the final phase, a detailed finite element thermal-structural analysis is conducted to assess the mechanical behaviour of the component. This is based on the CFD analysis, and the maximum loads derived from the electric motor and transmission chain.

Finally, a preliminary control strategy has been developed that defines how power should be distributed during vehicle operations, referring to the energy management problem. An HEV can avoid low-efficiency operating points of the ICE by storing excess energy in the batteries beforehand and using it later when needed, thus providing part of the torque during short acceleration phases [13].

2 HEV architectures

A vehicle in which the propulsion energy comes from two sources, with at least one being an electric energy accumulator, is defined as a hybrid electric vehicle. A vehicle with two or more internal combustion engines powered by different fuels could also be defined as a hybrid vehicle. The hybrid electric vehicle represents a balanced compromise between the characteristics of the internal combustion engine, which converts the chemical energy of the fuel into mechanical energy with acceptable efficiency at certain operating points, and the electric motor, which converts electrical energy into mechanical energy with higher efficiency. The electric machine is highly versatile and allows for operation in both traction and generation modes, which is one of the strengths of the electric motor, as it enables the conversion of mechanical energy into electrical energy by regenerating the battery during vehicle braking. Unlike a pure electric vehicle, a hybrid electric vehicle does not require an external battery charging system, thus it can be independent of the charging infrastructure [14-17].

A possible classification of vehicles currently on the market can be based on the size of the internal combustion engine and the size of the electric machine, as visible in the *Figure 1* and described below [19]:

1. ***Conventional Vehicles***: where the internal combustion engine is the exclusive source of propulsion.
2. ***Micro-Hybrids***: they are characterized by a low degree of hybridization, thus limiting fuel consumption by utilizing start and stop functionality and mild regenerative braking. Typically equipped with electric motors with a power output not exceeding 10 kW powered by 12-48 V.
3. ***Mild-Hybrids***: allow partial electric propulsion, unable to cover the entire driving cycle, also possessing Micro-Hybrid characteristics. Utilizes batteries with a higher voltage ranging from 100-200 V and electric motor power of about 20 kW.
4. ***Full-Hybrids***: the electric system allows, regardless of battery autonomy, to complete the entire driving cycle. Hence, it enables possible electric propulsion and all characteristics of Mild-Hybrids. Typically employs batteries with voltages between 200-300 V and electric motor power exceeding 50 kW.
5. ***Plug-in Hybrids***: they have the same characteristics as Full-Hybrid vehicles but have the ability to recharge the battery by connecting to the electrical grid.
6. ***Electric Vehicles***: where the electrical motor is the exclusive source of propulsion.

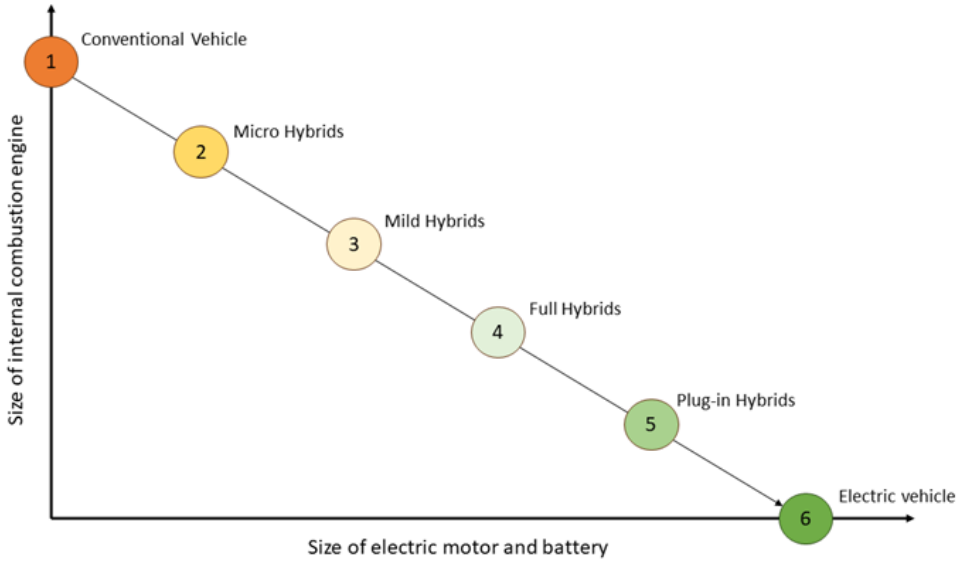

Figure 1 Spectrum of vehicle technologies. [19]

The analysed vehicles can be further classified based on the number and position of the electric machine relative to the internal combustion engine. In fact, they can be defined as [19]:

- ***Series***: the internal combustion engine (ICE) drives a generator, producing electrical power which can be summed to the electrical power coming from the rechargeable energy storage system (RESS) and then transmitted, via an electric bus, to the electric motor(s) driving the wheels.

- ***Parallel***: the power summation is mechanical rather than electrical: the engine and the electric machines (one or more) are connected with a gear set, a chain, or a belt, so that their torque is summed and then transmitted to the wheels.

- ***Power split***: the engine and two electric machines are connected to a power split device (usually a planetary gear set), thus the power from the engine and the electric machines can be merged through both a mechanical and an electrical path, thus combining series and parallel operation.

- ***Series/Parallel***: the engagement/disengagement of one or two clutches allows to change the powertrain configuration from series to parallel and vice versa, thus allowing the use of the configuration best suited to the current operating conditions.

2.1 Series HEV

To better understand how power flows are managed in various architectures of electric hybrid vehicles, diagrams have been created, as shown in Figure 2, representing in this case the vehicle with an internal combustion engine and the purely electric one [17].

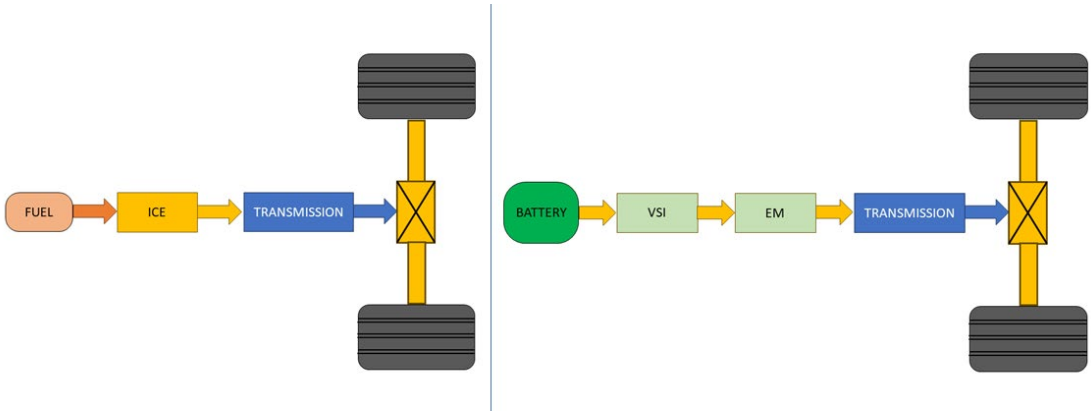

Figure 2 Power flow diagram of an internal combustion engine vehicle and an electric vehicle [17].

The series hybrid electric vehicle, in *Figure 3*, is characterized by an architecture very similar to that of a pure electric vehicle.

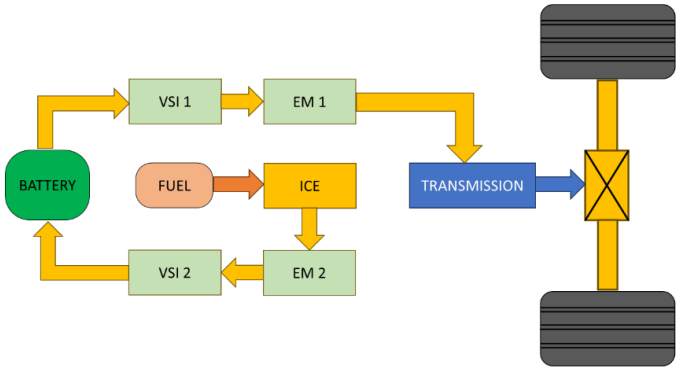

Figure 3 Power flow diagram SERIES HEV [17].

It is mainly composed of an internal combustion engine, an electric motor, a generator, and a battery pack. The internal combustion engine is decoupled from the wheels and provides mechanical power to the generator, which converts it into electrical power. Its task is to generate the current to power the electric motor that provides mechanical power to the wheels for propulsion, while any excess energy is used to recharge the batteries. The vehicle features two electric machines (EMs), one of which is an electric generator, which adds cost and weight to the propulsion system.

The vehicle is propelled solely by an electric traction motor with a motor-generator set that provides the electrical power required for the vehicle's

movement on average. This allows us to say that this architecture has a single energy path; however, the mechanical energy produced by the motor is converted twice (from mechanical to electrical in the generator and from electrical to mechanical in the electric traction motor). The losses in these processes add up, resulting in a reduction in system efficiency. The electric traction motor must be sized for the maximum power of the vehicle; therefore, it needs to be of considerable size, weight, and cost [20].

During moments when a large amount of power is required, electrical energy is drawn from both the generator/internal combustion engine and the battery. The efficiency of internal combustion engines changes with varying engine speeds.

Due to the decoupling with the wheels, in a series hybrid, conditions can be created to optimize the operation of the internal combustion engine, as it only needs to produce electrical energy as efficiently as possible. It will then be the electric motor that varies its operating regime to adapt to the driving needs.

Thanks to the excellent performance of the electric motor in terms of torque and low speeds, it is possible to avoid oversizing the internal combustion engine, as is generally required traditionally to achieve good acceleration and responsiveness. Therefore, downsizing is implemented, and the internal combustion engine is operated at a fixed point or follows the Economic-line, a torque characteristic as a function of the number of revolutions where there is the lowest specific fuel consumption. This setting depends on the type of control unit and numerical method adopted within it. The torque characteristic of the electric motor allows for the elimination of multi-speed gearboxes, simplifying the entire transmission. However, it may be useful to consider the inclusion of a two-speed gearbox for the analysis of regenerative braking and electrical energy recovery purposes [18,21,22].

2.2 Parallel HEV.

The parallel hybrid electric vehicle, in *Figure 4*, is mainly composed of an internal combustion engine, a battery pack, a single electric motor/generator (SEM), and a mechanical transmission node.

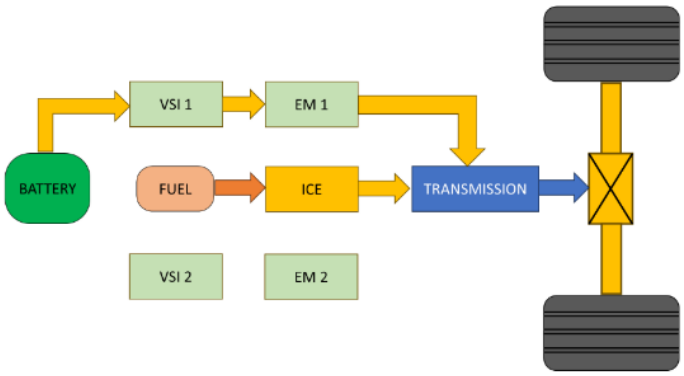

Figure 4 Power flow diagram PARALLEL HEV [17].

The term "parallel" is used because both the internal combustion engine and the electric motor contribute to the vehicle's propulsion. The internal combustion engine is therefore coupled to the wheels, unlike the series architecture, so it is not possible to achieve significant downsizing, and its rotation speed depends closely on the wheel speed.

The internal combustion engine is the dominant component, providing a relatively constant power output, while the electric motor functions to deliver additional power when needed and to compensate for typical shortcomings of the internal combustion engine such as low-speed torque and energy recovery during braking. There is no double conversion, resulting in a single conversion of electrical energy into mechanical energy in the electrical branch, thereby reducing some losses.

Depending on how the thermal and electric systems are connected, the following classification is introduced [23]:

- ***P0*** → belt-driven starter/generator.
- ***P1*** → electric motor mounted on the engine shaft.
- ***P2*** → electric motor mounted on the gearbox input.
- ***P3*** → electric motor mounted on the gearbox output.
- ***P4*** → electric motor mounted on one of the wheels axles.

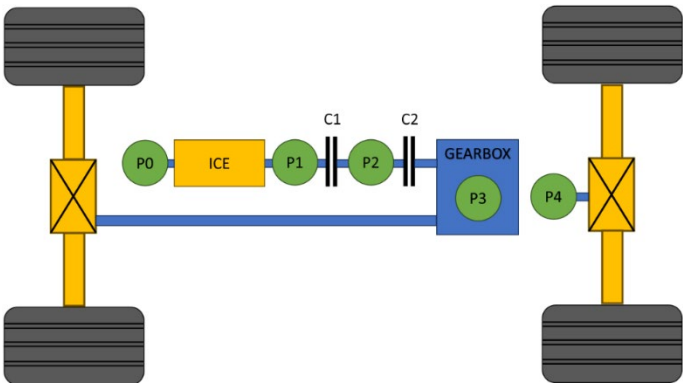

Figure 5 Schematic representation of parallel hybrid electric vehicle configurations [23].

Given the constraint of the connection between the internal combustion engine and the wheels, this architecture requires a multi-speed gearbox, which can be either manual or automatic, making the transmission more complex compared to a series hybrid vehicle. The battery pack is considerably smaller in size compared to series hybrid vehicles, plug-in hybrid vehicles, or pure electric vehicles, allowing for shorter charging times and less volume and weight. This architecture is suitable for diversified missions, suitable for urban rhythms as well as extra-urban cycles [23-25].

2.3 HEV mixed architecture.

Hybrid Electric Vehicles (HEVs) that combine the advantages of both series and parallel architectures can be realized by introducing additional elements to blend the torque from the internal combustion engine with that of the electric motor(s). In the case of a power-split system, a planetary gear set, and clutch actuation are utilized to switch between pure electric, series, or parallel power units, optimizing energy for vehicle propulsion depending on the driving speed [23,24]. Using the same principle, series/parallel vehicles can be implemented where the transition between systems occurs through the actuation of a simple clutch and two electric motors.

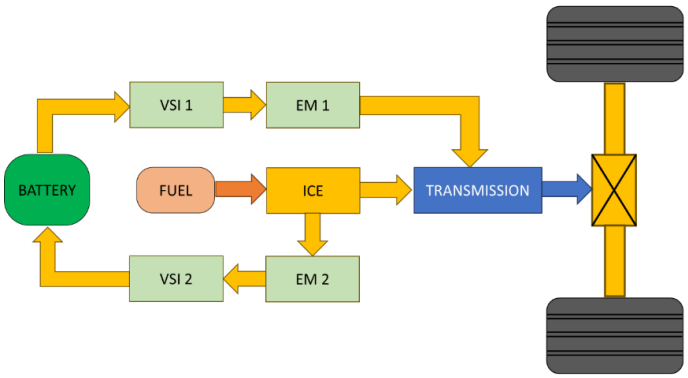

Figure 6 Power flow diagram of HEV mixed architecture.

Another system that has been widely used in motorsport for decades, in the world of Formula 1 and earlier in the World Endurance Championship, is the parallel system in which an electric motor is added, which can function as a motor-generator and is solidly installed on the turbocharger axis [26], as shown in the diagram in *Figure 7.*

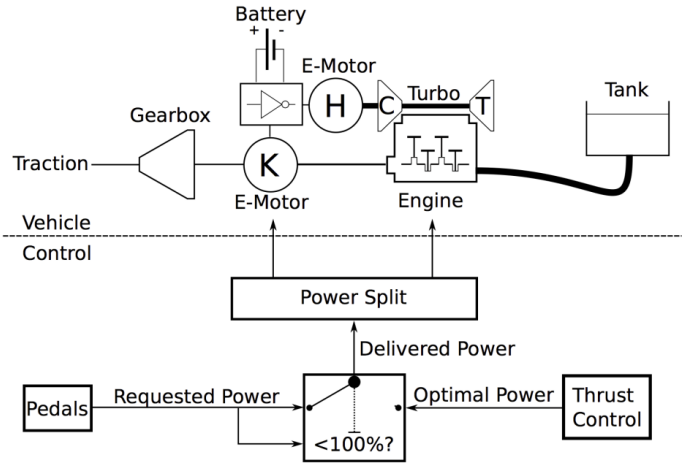

Figure 7 Formula 1 Hybrid power unit layout.

3 The energy management problem in HEVs.

The primary purpose of developing a hybrid electric vehicle is to make the best use of the energy stored in the vehicle while reducing fuel consumption. Hence, the challenge of energy management arises, which can be addressed through the assistance of mathematical models that accurately describe the phenomena involved. Once these phenomena are described, it becomes possible to devise strategies to solve this problem and understand how they can be applied in real-world scenarios.

3.1 Model of a hybrid vehicle.

For the development of an analytical model of a vehicle, the equations of motion of a point mass interacting in the space it moves through are used. Specifically, reference is made to the equation of longitudinal motion expressed as the equilibrium of forces:

$$M_{veh}\frac{dv_{veh}}{dt} = F_{inertia} = F_{trac} - F_{roll} - F_{aero} - F_{grade}$$

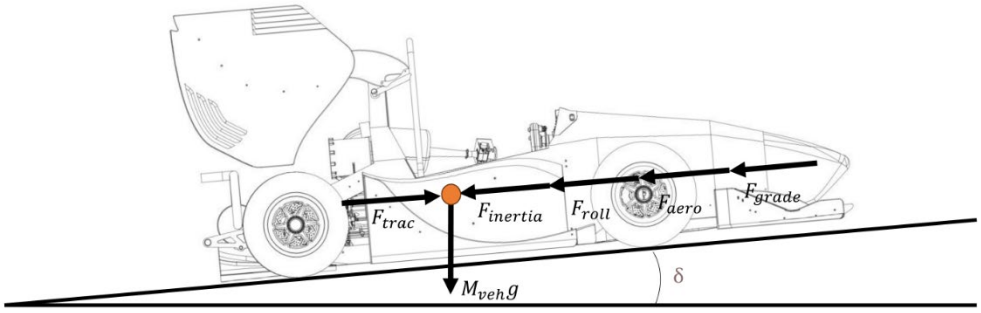

Figure 8 Equilibrium of forces in longitudinal motion.

Where M_{veh} is the actual mass of the vehicle, v_{veh} is the instantaneous velocity, $F_{inertia}$ represents the component of inertia forces, F_{trac} is the traction or braking force from the wheels, F_{roll} is the rolling resistance force, F_{aero} is the sum of forces generated by aerodynamic resistance, and finally, F_{grade} is the resistance force due to road grade. The previous equation can be rearranged to express the traction force, obtaining:

$$F_{trac} = F_{inertia} + F_{roll} + F_{aero} + F_{grade}$$

Multiplying all values by the instantaneous velocity of the vehicle $v_{veh}(t)$, we obtain the power balance:

$$P_{trac} = F_{trac}\, v_{veh}(t) = \left(F_{inertia} + F_{roll} + F_{aero} + F_{grade}\right) v_{veh}(t) \\ = P_{inertia} + P_{roll} + P_{aero} + P_{grade}$$

Integrating this relationship over time yields the energy balance of the system over a certain time interval.

$$E_{trac} = \int_{t_0}^{t_f} P_{trac}\, dt = E_{kin} + E_{pot} + E_{roll} + E_{aero}$$

In detail:

$$E_{kin} = \int_{t_0}^{t_f} P_{inertia}\, dt = M_{veh} \int_{t_0}^{t_f} v_{veh}(t)\dot{v}_{veh}(t)dt$$

$$E_{pot} = \int_{t_0}^{t_f} P_{grade}\, dt = M_{veh} g \int_{t_0}^{t_f} v_{veh}(t) \sin\delta\,(t)dt$$

$$E_{roll} = \int_{t_0}^{t_f} P_{roll}\, dt = M_{veh} g \int_{t_0}^{t_f} c_{roll} v_{veh}(t) \cos\delta\,(t)dt$$

$$E_{aero} = \int_{t_0}^{t_f} P_{aero}\, dt = \frac{1}{2}\rho_{air} A_f C_d \int_{t_0}^{t_f} v_{veh}(t)^3 dt$$

With this formulation, the various energies can be obtained through constants related to the vehicle characteristics, along with knowledge of a defined driving cycle defined by a velocity profile $v_{veh}(t)$ and a function of road grades over time $\delta(t)$.

From this energy balance, one can observe the advantage of a hybrid vehicle. During the phases of a driving cycle where the vehicle needs to increase its velocity and subsequently decrease it, a portion of the acquired potential and kinetic energy, excluding the rolling and aerodynamic resistances which are always present, can be recovered and made available for the following acceleration phase [19].

From an analytical standpoint this concept is expressed as follows, during a transient where the vehicle's velocity increases, and therefore, conventionally defined as positive acceleration, the power unit is required to deliver a positive amount of energy, which will be equal to the sum of all contributions described earlier to bring the vehicle to the new equilibrium point where acceleration becomes zero.

$$\dot{v}_{veh} > 0$$

$$E_{trac}{}^{+} = E_{pwt}{}^{+} = E_{kin}{}^{+} + E_{pot}{}^{+} + E_{roll}{}^{+} + E_{aero}{}^{+}$$

At this new equilibrium point, the vehicle possesses energy equal to the sum of kinetic and potential energy, which in the subsequent deceleration phase must be dissipated, except for the usual rolling and aerodynamic resistances. In a conventional vehicle, this is achieved through the brakes, dissipating it all as heat. However, in a hybrid vehicle, this energy can be recovered and stored in the batteries to be utilized in a subsequent acceleration phase.

$$\dot{v}_{veh} < 0$$

$$E_{regen,pot} = E_{kin}{}^{+} + E_{pot}{}^{+} - E_{roll}{}^{-} - E_{aero}{}^{-} - E_{pot}{}^{-}$$

To better understand this concept, a histogram diagram is provided in *Figure 9*, where moving from right to left subtracts the components related to resistances, obtaining the ideal amount of recoverable energy.

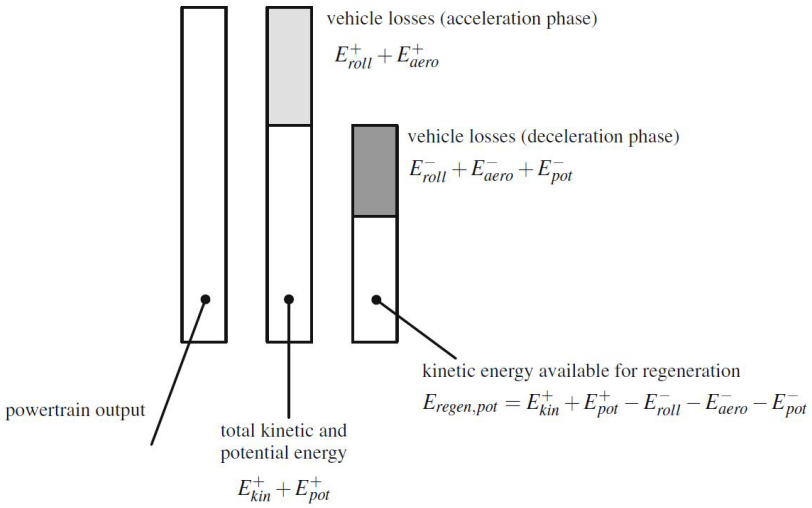

Figure 9 Vehicle energy balance [19].

From what has been described, it can be stated that comparing a conventional vehicle to a hybrid one with the same geometries and therefore the same characteristics of aerodynamic resistance and rolling resistance, and assuming the same masses, under conditions of constant velocity, the latter would have no advantage. However, making the same comparison during one or more transients shows a markedly different behaviour between the two. Therefore, to appreciate the advantages of a hybrid vehicle, it is crucial to define a unique driving cycle. Regarding road vehicles, current regulations define reference driving cycles aimed at evaluating the maximum limits of fuel consumption and pollutant emissions that they must comply with for homologation. An example of a velocity profile is

the one defined in the Worldwide Harmonized Light Vehicles Test Procedure (WLTP), which today realistically simulates average vehicle use on the road.

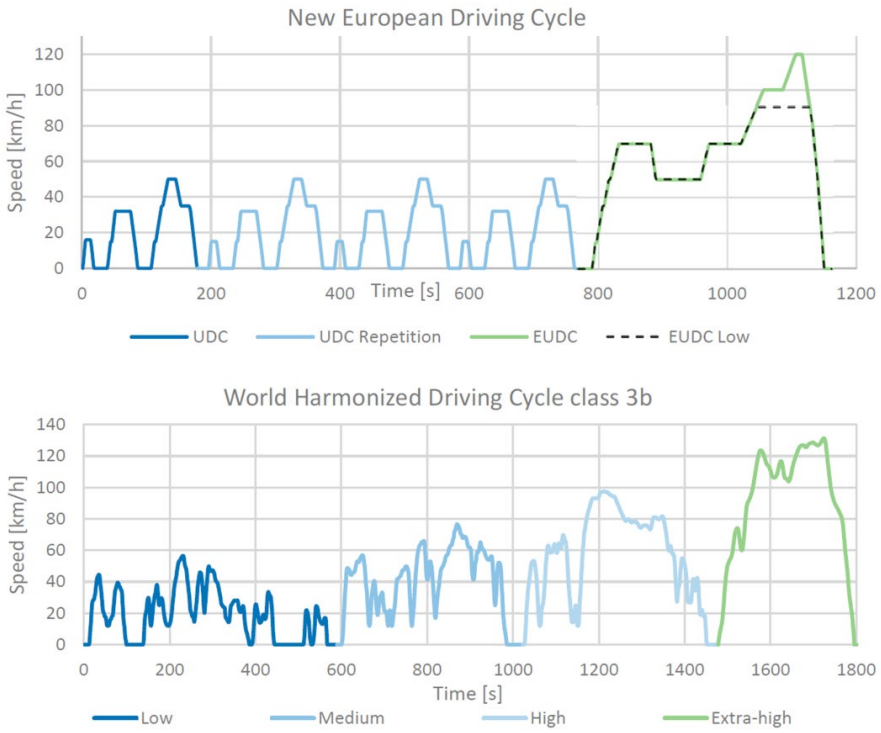

Figure 10 Examples of standard driving cycles [9].

This same approach can also be used in the design and development of a competition vehicle that utilizes a hybrid power unit, where obviously the main target will not only be to optimize fuel consumption but above all to make the best use of the stored energy to achieve the highest average speed around a circuit during a competition [28].

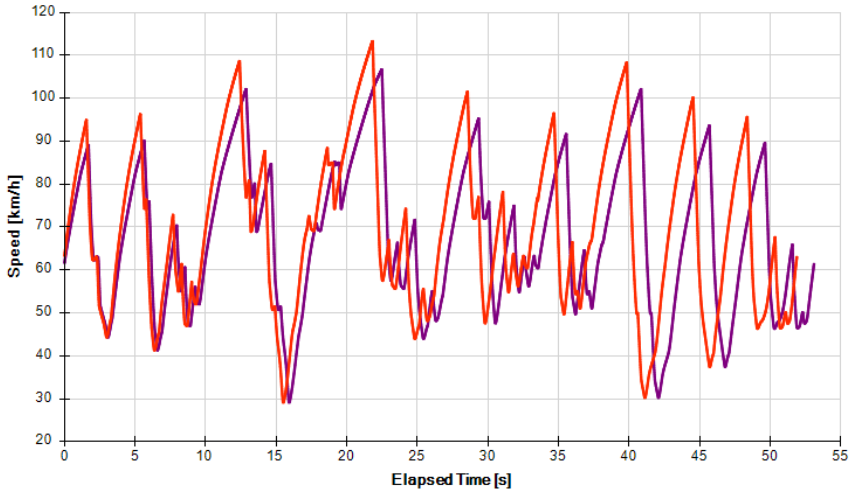

Figure 11 Example of speed profiles of a Foemula SAE vehicle.

In general, it can be stated that these driving cycles must be studied for the acceleration phases of the hybrid vehicle, where efforts are made to operate the combustion engine under conditions of maximum efficiency, also with the assistance of the electric motor, and for the deceleration phases, where the electric motor is tasked with recovering as much potential energy as possible that the vehicle possesses, rather than simply dissipating it due to friction.

To carry out these analyses, there is a need to use numerical models that allow the resolution of the energy balance equations, consisting of sub-models that describe the individual systems comprising a hybrid vehicle.

These models can follow different approaches, but they can generally be grouped into two main categories, where the starting point is the driving cycle [17].

In the first approach, a torque request is imposed on the power unit sub-model, which then interfaces in cascade with others describing the vehicle. From this torque request processing, an operating point of the power unit is obtained to meet the target speed. This approach is called *forward* and is schematized in the following *Figure 12*.

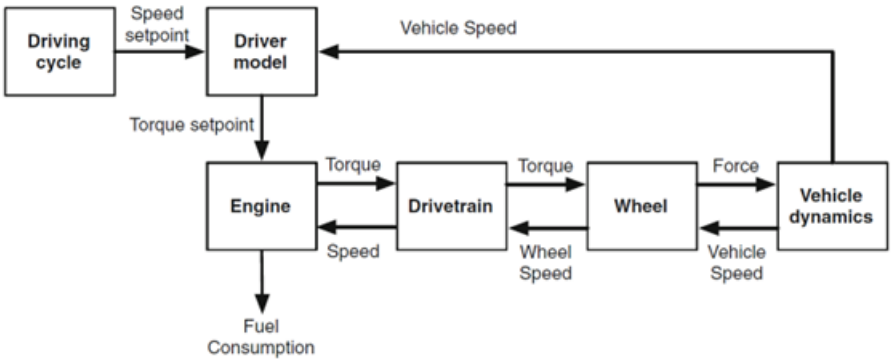

Figure 12 Information flow in a forward simulator [19].

In the second approach, it is assumed that the power unit can always meet any torque request, and a velocity is imposed on the vehicle sub-model, which interacts with the others until reaching the power unit sub-model, which returns an operating point for a given speed and torque. This approach is called *backward*, and the diagram is shown below in *Figure 13*.

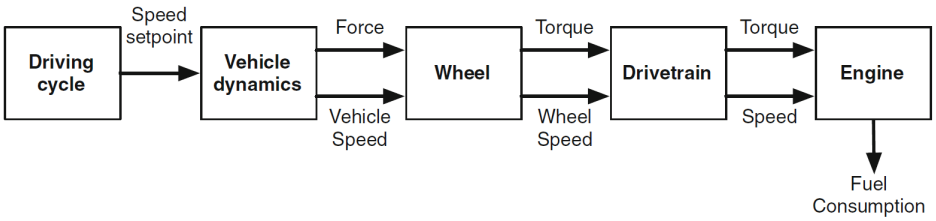

Figure 13 Information flow in a backward simulator [19].

Both approaches provide operating points over time for the power unit and thus the trend of fuel consumption, a fundamental parameter for optimization strategies. In general, depending on how many aspects one wants to control and the degree of precision with which one wants to follow the driving cycle, an approach can be chosen. Certainly, the forward method allows for a more comprehensive analysis, taking into account the dynamic response of the vehicle, but it has the complication of implementing a controller (Drive model) that verifies the convergence of the calculated velocity with the target velocity. In the backward method, there is no need for a controller as the velocity is imposed, and therefore, it is a much more stable method in finding the solution of equations, but it does not fully describe the longitudinal dynamics of the vehicle.

Another important aspect is the definition of sub-models for the various systems comprising the hybrid vehicle. As visible from the diagrams of hybrid vehicle architectures, the necessary components are:

- Internal combustion engine (ICE);
- Any electric motors (EM);
- The battery;
- Transmission elements, brakes, wheels;
- The vehicle for aspects related to aerodynamic resistances.

For each of these sub-models, one can delve into more detail, introducing increasingly complex computational degrees, of course.

For example, the internal combustion engine can be simulated through simple maps where operating points for each regime are collected [22], but one can simulate the engine through one-dimensional models in which real-time operation can be simulated. The same principle can be applied regarding electric machines and even the accumulator. Regarding aspects of transmission, brakes, and wheels, they are often simply treated as flywheels with equivalent inertias, with multipliers that introduce efficiencies and transmission ratios. For the introduction of resistances from aerodynamic or rolling forces, analytical relationships or maps derived from experimental tests can also be used.

In general, it can be stated that such models can be increasingly complicated to delve into the dynamics of individual systems, but this approach is not always necessary for energy utilization optimization analyses, which, as we will see later, introduce significant complications.

3.2 Energy management.

Energy management in hybrid vehicles involves deciding the amount of power to be delivered at each instant from the energy sources present in the vehicle, while simultaneously respecting various constraints.

A control system of a hybrid vehicle, therefore, must perform two tasks. One is the *"low-level control"* or *"component-level control"*, where each component of the powertrain is controlled using classical feedback methods. The second, termed *"high-level control"* or *"supervisory control",* is responsible for optimizing the energy flow onboard the vehicle while maintaining the state of charge of the battery within a certain operating range. This level of control, called the *Energy Management System* (EMS), receives and processes information from the vehicle (ω_{ice}, ω_{gb}, ω_{em}) and the driver (v_{veh}, $\dot{v}_{veh}$,δ) to produce optimal set points that are sent to actuators and executed by low-level controllers.

The EMS also selects the best operating modes of the hybrid power unit, including power split and electric starting. The control scheme of an HEV based on the definitions just given is illustrated in the *Figure 14*.

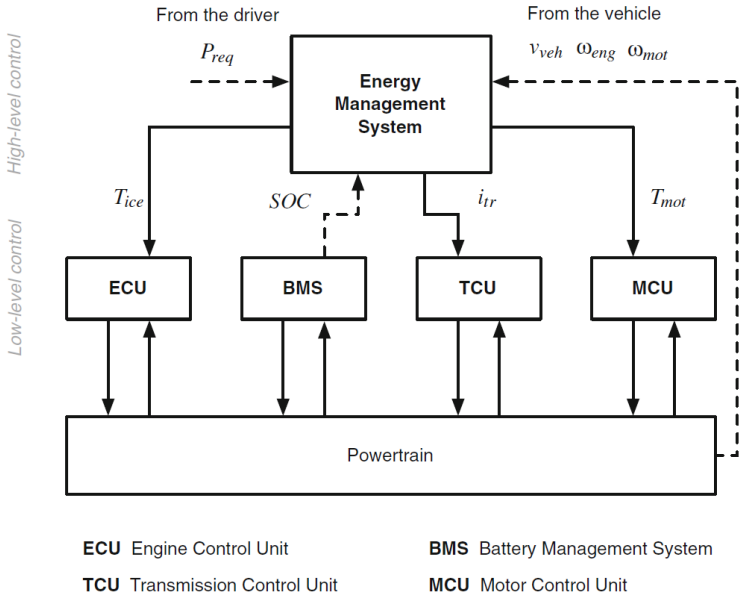

Figure 14 Two-layer control architecture in hybrid vehicle [19].

Therefore, based on these concepts just outlined, it can be easily stated that to obtain advantages from a hybrid power unit, much depends on the definition of control logics established in the high-level controller EMS. In fact, if these control logics are developed following optimization algorithms, it has been observed that fuel consumption reductions ranging from 10% for mild-hybrid systems to up to 30% for full-hybrid systems can be achieved.

In a conventional (non-hybrid) vehicle, there is no need for an energy management strategy: the driver decides the instantaneous power delivery using the brake and accelerator pedals and, in vehicles with manual transmission, selects the gear to engage as needed. The driver's inputs are translated into actions by the low-level control: for instance, the engine control unit (ECU) determines the amount of fuel to inject based on the desired torque request; the automatic transmission control unit (TCU) decides when to shift gears based on engine conditions and vehicle speed, and so forth.

In a hybrid vehicle, however, there is an additional decision to make: the amount of energy provided by each of the energy sources onboard the vehicle. For this reason, all hybrid vehicles include an energy management controller positioned between the driver and the component controllers. As mentioned earlier, the goal of the energy management system is to determine the optimal power distribution among the onboard energy sources. The decision on what to consider optimal depends on the specific application: in most cases, strategies tend to minimize fuel consumption, but optimization objectives may also include minimizing pollutant emissions, maximizing battery lifespan, or, generally, a compromise between all these objectives. The role of the energy management system in a hybrid vehicle can also be depicted as in the *Figure 15.*

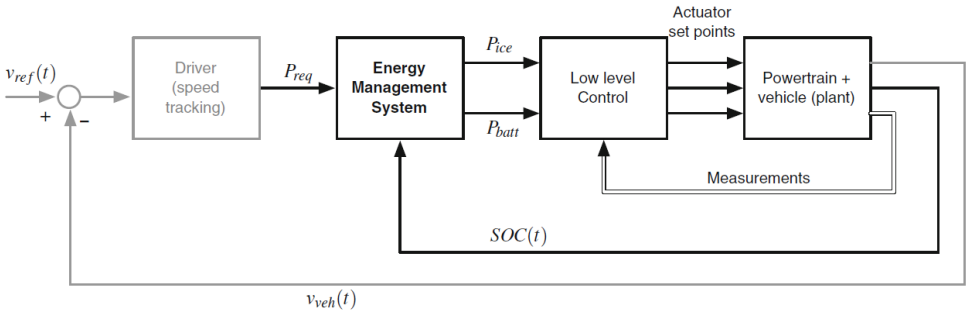

Figure 15 Control flow of the EMS system [19].

The outermost layer of the figure represents the speed control, which embodies the human driver in a real vehicle and a driver model (typically a PI controller) in simulation. The speed controller determines the total power request $Preq$ that the powertrain must deliver to follow the prescribed speed profile. The innermost layer is the energy management system, which decides how to allocate the total power request among the onboard energy sources: the rechargeable energy storage system and the internal combustion engine. In designing the energy management strategy, the separation of the two controllers allows considering only the battery state of charge as the system state and disregarding the vehicle speed, as this is directly controlled by the driver.

3.3 The general problem of the optimal energy strategy.

In the literature, various families of energy management strategies have been proposed [29]. Two general trends can be identified that address the energy management problem: rule-based methods and model-based methods.

The main characteristic of rule-based approaches is their effectiveness in real-time implementation. They do not involve explicit minimization or optimization but rely on a set of rules to decide the control value to apply at each moment. The rules are generally designed based on experience, intuition, or knowledge of an optimal global solution generated with mathematical models through optimization algorithms.

In model-based optimization strategies, the optimal set-points of actuators are calculated through the minimization of a cost function over a fixed and known drive cycle, leading to a global optimal solution. This results in a non-causal solution as it finds the minimum value of the cost function using information about future driving. Although model-based methods cannot be directly used for real-time implementation and do not lend themselves directly to practical implementation due to their preview nature and computational complexity, they constitute a valuable design tool. Indeed, they can be used for designing rules for online implementation or as a reference solution to evaluate the performance of other control strategies. Model-based optimization methods can be further divided into numerical and analytical approaches.

In numerical optimization methods, such as *Dynamic Programming*, *Simulated Annealing*, and *Stochastic Dynamic Programming*, the entire drive cycle is considered, and the global optimum is numerically found.

Analytical optimization methods, on the other hand, use an analytical formulation of the problem to find the solution in closed and analytical form, or at least provide an analytical formulation that makes the numerical solution faster than purely numerical methods. Among these methods, the *Pontryagin's Minimum Principle* is the most important.

Thus, the use of one of these approaches leads to the solution of the problem and to the definition of the so-called Equivalent Consumption Minimisation Strategy (ECMS) or Adaptive ECMS [30-32].

The main idea of ECMS is to minimize a function that takes into account both the energy coming from the fuel and from the battery, formulated as follows:

$$\dot{m}_{eq}(t) = \dot{m}_f(t) + \dot{m}_{bat}(t) = \dot{m}_{eq}(t) + \frac{s}{Q_{LHV}} P_{bat}(t)$$

where $\dot{m}_f$ is the instantaneous fuel consumption of the engine, $\dot{m}_{bat}$ is the fuel consumption equivalent to the used electrical power, P_{bat} is the electrical power demanded at a certain instant, Q_{LHV} is the fuel lower heating value (energy content for mass unit) and s is the equivalent factor, which is used to convert the electrical power from the battery into equivalent fuel consumption [33]. The power requested to the battery can be either positive or negative and, consequently, the equivalent fuel consumption can be higher or lower than the real one. Defining SOC as the State Of Charge of the battery it is possible to write:

$$S\dot{O}C(t) = f(SOC, u, t) = -\frac{I_{bat}(SOC, u, t)}{Q_{bat}}$$

where u is the control action, I_{bat} is the battery current and Q_{bat} is the capacity of the battery. Then, it is possible to define the *Hamiltonian* of the optimal control problem, which has to be minimized:

$$H(SOC, u, \lambda, t) = -\lambda(t) \cdot f(\mathrm{SOC}, u, t) + \dot{m}_f(u, t)$$

The co-state variable $\lambda(t)$ is the solution of:

$$\dot{\lambda}(t) = -\lambda(t)\frac{\partial f(SOC, u, t)}{\partial SOC}$$

In other words, the *Hamiltonian* is the total equivalent fuel consumption including the electric energy. To better understand the meaning of $\lambda(t)$, an auxiliary variable can be introduced, the equivalent factor $s(t)$, formulated as follow:

$$s(t) = -\lambda(t)\frac{Q_{LHV}}{P_{bat}(t)}$$

here $P_{bat}(t)$ is the power request to the battery and Q_{LHV} is the lower heating value of the fuel. Finally, the instantaneous equivalent fuel consumption is:

$$H(SOC, u, \lambda, t) = \dot{m}_{eq}(SOC, u, s, t) =$$

$$= -s(t)\frac{P_{bat}(t)}{Q_{LHV}} \cdot f(\mathrm{SOC}, u, t) + \dot{m}_f(u, t)$$

The optimal control action is the one that satisfies:

$$u^*(t) = argmin_u H(SOC, u, \lambda, t)$$

The optimal control depends on the value of $s(t)$, but this is unknown a priori and this makes the strategy sub-optimal.

Physically, the equivalent factor represents the “cost” of the energy stored in the battery, so if it has a high value, then it is preferable to use the engine and recharge, while if it is low, it’s better to use electrical traction [34].

In this work, an A-ECMS approach has been adopted, with adaptation on feedback values. The formulation of $s(t)$ has two contributions:

- adaptive term, which is related, in this case, to the feedback of the previous SOC (square brackets);
- penalty function that corrects the value of s when it is close to the maximum and minimum accepted values (first curly brackets).

It is defined as follows:

$$s(t) = \left\{1 - k_p \left(\frac{SOC - SOC_f}{\frac{SOC_{max} - SOC_{min}}{2}}\right)^3\right\} \ldots$$
$$* \left[k_a \left(SOC_{ref} - SOC(t)\right) + \left(\frac{s_{k-1} + s_{k-2}}{2}\right)\right]$$

MODE	SPLIT FACTOR	ICE	EM
ICE only	$u^* = 0$	ON	OFF
Boosting	$0 < u^* < 1$	ON	ON
Battery Recharge	$u^* > 0$	ON	OFF
Regenerative Braking	$u^* = 1$	OFF	ON

where $SOC(t)$ is the actual state of charge, SOC_{max} and SOC_{min} are the SOC upper and lower limits defined by the developer, SOC_{ref} is the target value, s_{k-1} and s_{k-2} are the values of s used in two previous time intervals, between two adaptation steps. While k_p and k_a are two gain parameters used to tune the strategy.

The objective of this study was to analyse the numerical method that exploits DP and extrapolate from this analysis a real power unit control strategy for the case in question.

4 Dynamic Programming

4.1 General Formulation.

Dynamic Programming is a numerical method for solving problems where decisions need to be made at multiple levels. It can provide the optimal solution to problems of any level of complexity (within computational limits); however, it is non-causal and can only be implemented in a simulation environment because it requires prior information about the entire optimization horizon. The study of dynamic programming dates to Richard Bellman, who wrote the first book on the subject in 1957, in which he formulated what is now called Bellman's principle of optimality:

"An optimal policy has the property that whatever the initial state and decision are, the remaining decisions must constitute an optimal policy with respect to the resulting state from the first decision." [9]

In other words, from any point on an optimal trajectory, the remaining trajectory is optimal for the corresponding problem initiated at that point.

Consider the discrete-time system:

$$x_k + 1 = f_k(x_k, u_k)$$

where k takes integer values, as $k = 0,1,2, \dots$. Let u_k be the control variable whose value must be chosen at time k. Both the state x and the control u are constrained and discretized, meaning they can take values in their respective domains $u_k \in U_k$ and $x_k \in \Omega_k$.

Consider the following control policy for the first N time steps:

$$u = \{u_0, u_1, \dots, u_{N-1}\}$$

The cost of the policy u, starting at initial conditions x_0, is:

$$J(x_0, u) = L_N(x_N) + \sum_{k=1}^{N-1} L_k\,(x_k, u_k)$$

where L_k it is the instantaneous cost function also called *arc cost* in the context of dynamic programming. The cost function obtained with the optimal solution is:

$$J^*(x_0) = \min_u J(x_0, u)$$

and the corresponding optimal policy is $u^* = \{u_1^*, u_2^*, \dots, u_{N-1}^*\}$.

Now let's consider the "*tail sub-problem*" of minimizing the *cost-to-go* Y from time i (and state x_i) to time N:

$$Y(x_i, i) = L_N(x_N) + \sum_{k=i}^{N-1} L_k\,(x_k, u_k)$$

which corresponds to the final part of the overall problem. The Bellman optimality principle states that the *"tail policy"* $\{u_1^*, u_2^*, \dots, u_{N-1}^*\}$ is the optimal policy for the tail subproblem.

The dynamic programming algorithm is based on the Bellman's principle of optimality. Starting from the final step N, the algorithm proceeds backward using the control sequence that generates the optimal cost-to-go, as follows:

$$u_k = \mu^*(x_k, k) = arg \min_{u \in U_k} \big(L_k(x_k, u) + Y_{k+1}(f_k(x_k, u_k), u_k)\big)$$

for $k = N-1, N-2, \dots, 1$.

Where $Y(x_1, 1)$ generated at the last iteration is equivalent to the optimal minimum cost $J^*(x_0)$. While $Y(x_k, k)$ represents the optimal cost-to-go of state x_k at time k, at the end of the optimization horizon, and $Y_k(x_k, u_k)$ is a function that depends on the control value u_k, representing the alternative values that the cost-to-go can take from the same state, depending on the control x_k. In other words, $Y(x_k, k)$ is the minimum value that $Y_k(x_k, u_k)$ can assume as u_k changes. The optimal control sequence can be derived by proceeding backward from the final state, choosing at each step the control that minimizes the cost-to-go $Y_k(x_k, u_k)$, and storing in a matrix μ^* the optimal choice for each time step k and state x_k. Since the state values are discretized in the algorithm, but most physical systems are defined by a continuous state, applying a specific control action within the discrete control set might cause the system to reach a state that is not one of the discretized values in Ω_k, but rather lies between two of them. In this case, computing the cost at grid values relies on interpolation.

Summarizing:

- The optimal control sequence μ^*depends only on u_k and k.
- The optimal control law is expressed in closed loop form.
- The Bellman equation is solved backward induction: the later choice is decided first.

4.2 Application of DP to the energy management problem in HEVs.

Dynamic Programming can be used to solve energy management problems. The control sequence u_k (decisions) represents the power split between the combustion engine and battery charging in successive time periods. The cost corresponds to fuel consumption, energy consumption, emissions, or any other

design parameter. The set of choices at each time step (set U_k) is determined by considering the state of each engine component and the total power demand. The number of possible solutions that can be considered and evaluated is a trade-off between computational capabilities and result accuracy: indeed, the minimum cost may not exactly coincide with one of the selected points, but the closer they are to each other, the better the approximation of the optimal solution.

Once the grid of possible power splits is created, the procedure described earlier can be used, associating a cost with each solution. Proceeding backward (i.e., from the end of the driving cycle), the optimal cost-to-go for each point on the grid is calculated, and it is stored in a cost matrix. When the entire cycle has been examined, the path with the lowest total cost represents the optimal solution.

As an example, consider the case of a series HEV where the decision variable is the battery power, P_{batt}, which is chosen from a set of permissible values (between a maximum and a minimum limit). Starting from the end of the driving cycle (assumed to be known), at each time instant, the arc costs of all feasible paths are calculated, defined as those corresponding to a change in SOC compatible with the battery power limits. The cost is calculated by the powertrain model as the fuel consumption corresponding to a specific choice of power requested from the battery, which therefore corresponds to the given SOC variation.

The goal of Dynamic Programming is to select the optimal sequence of power supplied by the battery to minimize the total cost. Choosing a specific sequence of power values to request from the battery leads to the decision of a corresponding sequence of SOC values, as the SOC change between time steps is proportional to the integral of the battery power between these steps. The correspondence between the control variable and the state change is one-to-one.

The selection of battery power values and SOC must satisfy the constraints on the maximum and minimum allowable battery power and state of charge, as only permissible values are considered. Additionally, the initial and final SOC values are set effortlessly (global state constraints).

The diagram in *Figure 16* illustrates the implementation of the Dynamic Programming algorithm in its basic form. The state vector x_{vec} is defined and discretized with a step δx from a minimum value x_{min} to a maximum value x_{max}. The length of the x_{vec} vector is N_x. The same applies to the control vector, u_{vec}, which contains N_u components from the minimum value u_{min} to the maximum value u_{max}. At time step $k = N$, the final cost-to-go corresponds to the final cost L_N. This is computed for each admissible state value within x_{vec}. If the final state is constrained to a specific value or range of values, only a subset of x_{vec} is admissible at the final step, which means the cost associated with reaching any of the inadmissible state values is set to infinity. Therefore, as time progresses

backward, the arc cost $L_k(x_k, u_k)$ for all combinations of state and control values is computed and stored in the matrix $L_k(m, n)$, where the indices m and n correspond respectively to the state and control. The matrix L_k contains the costs of transitioning from each admissible node (each element of x_{vec}) at time k to all reachable nodes at time $k+1$ (i.e., the states obtained by applying each element of u_{vec}). Then, the candidates for the cost-to-go $Y_k(m, n)$, representing the cost of reaching the final horizon from state $x_{vec}(m)$ at time k by choosing $u_{vec}(n)$ as the first control action, are computed. The optimal cost-to-go $Y(m, n)$ is obtained by selecting the control u_k that yields the minimum $Y_k(m, n)$.

For each admissible state index m, the control index that generates the optimal cost-to-go at time k is stored in the matrix $\mu^*(m, k)$. This operation is repeated until the initial time is reached $(k = 1)$, at which point the optimal control sequence is found. With the newly calculated optimal control matrix $\mu^*(m, k)$, the cycle then progresses forward in time, and the optimal control and state sequences are computed.

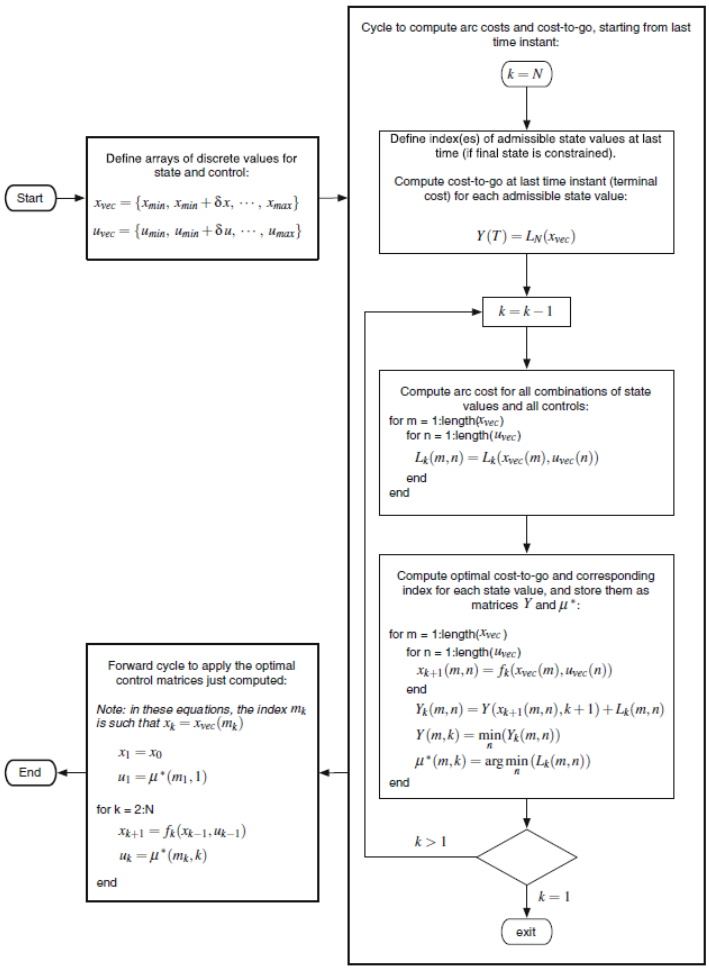

Figure 16 Dynamic Programming implementation flowchart [19].

To better visualize in *Figure 17*, an example illustrating the state calculations over time is provided. The points represent the state values; the arrows out of each

point represent the control choices (u_{vec}), pointing to the state value that would be obtained by applying that control. The numbers on each segment indicate the arc costs $L_k(x,u)$, i.e., the cost incurred (during a single time step) in choosing that control action. While, in *Figure 18*, the optimal path is visualized.

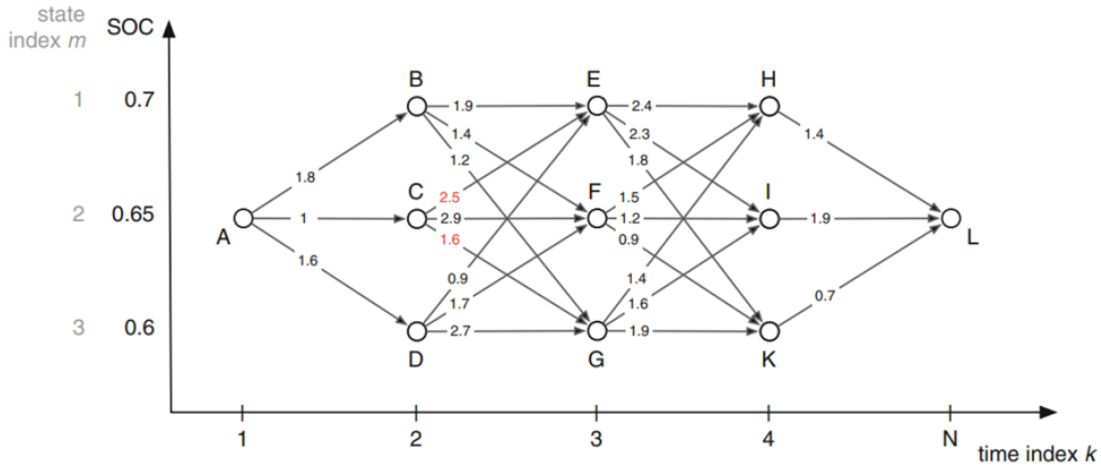

Figure 17 Arc costs simplified example [19].

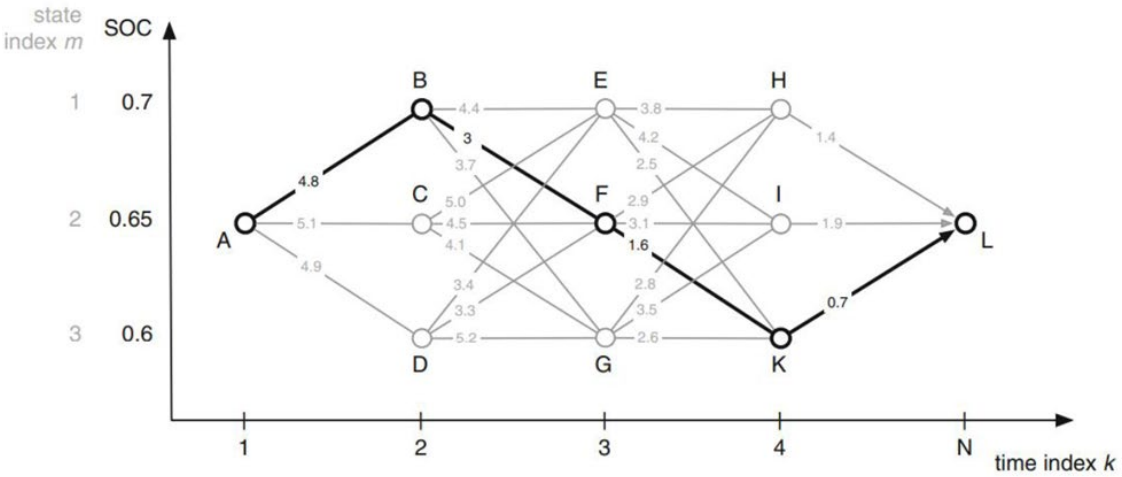

Figure 18 Calculated optimum control example [19].

5 Design of a HEV Formula Student.

The Formula SAE championship is a global university student competition organized by the Society of Automotive Engineers (SAE), in which students design and build a Formula-style single-seater race car. The Formula SAE event consists of a series of static and dynamic tests in which teams compete against each other.

Static tests:

- Engineering Design (150 points)
- Cost and Sustainability analysis (100 points)
- Business Presentation (75 points)

Dynamic tests:

- Skidpad (50 points): evaluates the dynamic characteristics of the vehicle as it navigates an "eight" circuit.
- 0-75 m Acceleration (150 points): the vehicle must accelerate from a standstill and travel the straight line in the shortest possible time.
- 1 km Autocross/sprint (75 points): a single lap of the track testing the driver's abilities, vehicle handling, and roadholding, also used to determine the starting order for the endurance test.
- 22 km Endurance (300 points): the final event of the competition, testing the overall performance and reliability of the vehicle.
- Efficiency (100 points): evaluates the vehicle's performance in terms of energy consumption, fuel consumption for combustion vehicles, and electrical consumption for electric vehicles.

The teams eligible to participate in these tests are those that present a vehicle:

- With internal combustion engine (IC)
- Full electric (EV)
- Driverless (DV)

Each of these categories must comply with specific regulations, primarily concerning:

- Structural characteristics of the chassis.
- Limits on displacement and intake system layout for combustion vehicles.
- Limit on power output from the battery pack for electric vehicles.
- Aerodynamic limits.
- Electronic safety systems.

The compliance with various parts of the regulations is verified by the judges during the preliminary technical inspections, which, if not passed, do not allow the Team to take part in the dynamic tests.

In the official SAE circuit competition, therefore, vehicles with architectures other than those just listed are not allowed. However, the competition held in England, at the Silverstone circuit, called Formula Student UK (FSUK), allows the participation of Teams that present a project not provided for by the official regulations [12]. Therefore, those Teams intending to enter a vehicle with an unconventional architecture must present the project idea to the judges in advance. If the project is approved, the judges will assign additional rules to be followed. In the case of Team MMR-Hybrid and thus the vehicle subject of this thesis, it was required to adhere to both the combustion engine and electric vehicle regulations. To ensure performance uniformity with other vehicles that can regularly participate in the competition, additional rules have been imposed, including:

a. Maximum combustion engine displacement of 500 cm^3.
b. Restriction on the intake system of 20 mm.
c. Maximum power output from the battery pack limited to 30 kW.

5.1 Analysis of volumes of Formula Student vehicle with internal combustion engine.

The development of the single-seater with a hybrid power unit stems from the knowledge of the Vehicle Engineering Department and the related Formula Student MMR Team for the design and construction of the vehicle with an internal combustion engine.

This car is an open-wheel Formula-style prototype with a wheelbase of 1540 mm, a front track width of 1260 mm, and a rear track width of 1210 mm. The wheels have a diameter of 10'' and use 7.5'' wide tires. The suspension system consists of a double wishbone layout made with carbon fibre tubes. A pull-rod arrangement was chosen for the front suspension, while a push-rod solution was adopted for the rear. The braking system features floating steel discs with a diameter of 190 mm, designed to fit into the 10'' wheels. Aluminum brake calipers with 4 pistons at the front and 2 pistons at the rear have been adopted. To manually adjust the brake bias, a mechanical brake bias adjuster has been developed, which can be adjusted from the cockpit. Furthermore, the car is equipped with an aerodynamic package consisting of a front wing, rear wing, undertray, and sidepods. The complete aerodynamic package can generate approximately 430 N of downforce at 50 km/h.

Figure 19 CAD assembly image of the MMR prototype.

The engine is a longitudinally arranged inline four-cylinder with a displacement of 708 cm^3 and a final drive with bevel gear, delivering approximately 73.6 kW of maximum power at 10,500 rpm. The vehicle has a total weight of about 200 kg, achieving a power-to-weight ratio of 0.36 kW/kg. Over the years, the prototype has achieved various positive results and victories in competitions, demonstrating an excellent level of performance. Hence, the idea of developing a hybrid vehicle where only the power unit is replaced to maintain these performance levels. Naturally, an electric hybrid power unit consists of a greater number of components, which will need to be installed in the same space as the current one.

To achieve this result, we have studied the spaces available for the current internal combustion engine and how it occupies them. The idea was to group the various parts of the vehicle into four categories, which are:

1. Aerodynamics,
2. Chassis,
3. Suspension,
4. Engine.

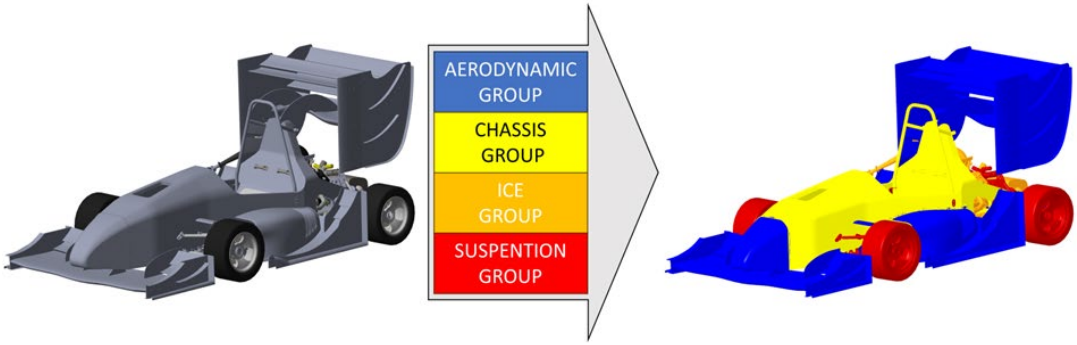

Figure 20 Image of the division into functional groups.

Once this division was made, we looked at the level of interactions within the space of these groups. In particular, focused on the engine group, and it can be easily inferred that the chassis group has the most interaction with it, while the

suspension group interacts partially with it, or rather the components of the front axle have no influence. The same can be said for the aerodynamic group. So for the next few considerations we will focus on the engine, chassis and rear suspension groups.

Once this selection was made, the next step was to consider the volume occupied in the space by the various components of the engine group, treating them as solid objects with the outer shapes of their actual geometries. With this CAD modelling, the volume of the various functional subgroups was evaluated in litres, as shown in the following *Figure 21*.

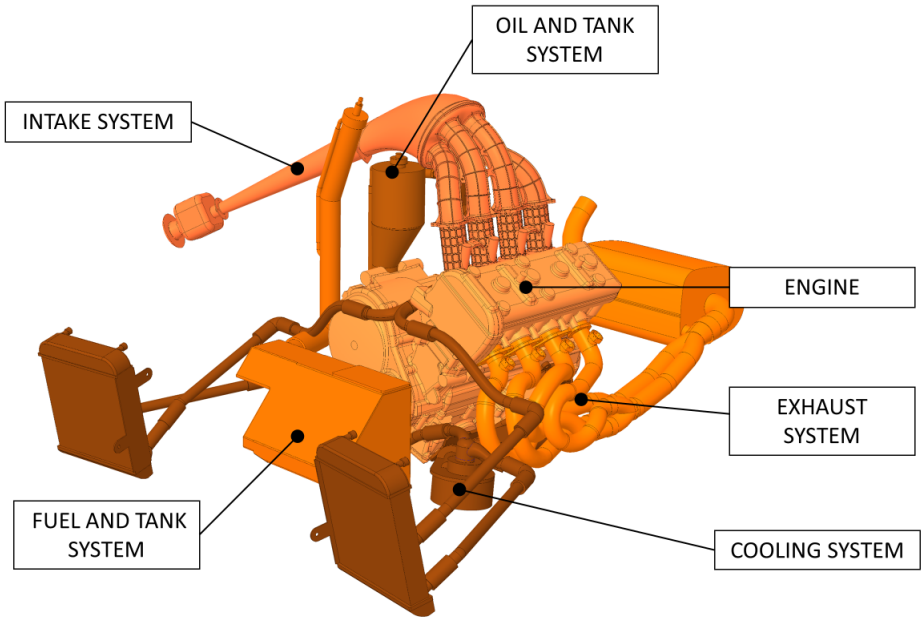

MMR COMBUSTION	Volume		
	[mm^3]	[l]	[%]
INTERNAL COMBUSTION ENGINE GROUP	**67590366,54**	**67,59**	**100,00%**
• ENGINE SYSTEM	29594502,55	29,59	**43,79%**
• COOLING SYSTEM	7405482,19	7,41	**10,96%**
• OIL AND TANK SYSTEM	3902775,05	3,90	**5,77%**
• FUEL AND TANK SYSTEM	7949543,07	7,95	**11,76%**
• INTAKE SYSTEM	4995900,15	5,00	**7,39%**
• EXHAUST SYSTEM	11268238,63	11,27	**16,67%**
• DRIVE TRANSMISSION SYSTEM	2473924,90	2,47	**3,66%**

Figure 21 Analysis of engine volumes.

From the CAD models of the chassis and suspension groups, as shown in *Figure 20*, the volume available to the engine group was extrapolated based on the

shapes of the chassis, suspension, and also considering the constraints of the regulations. This defined volume amounts to 180,87 l.

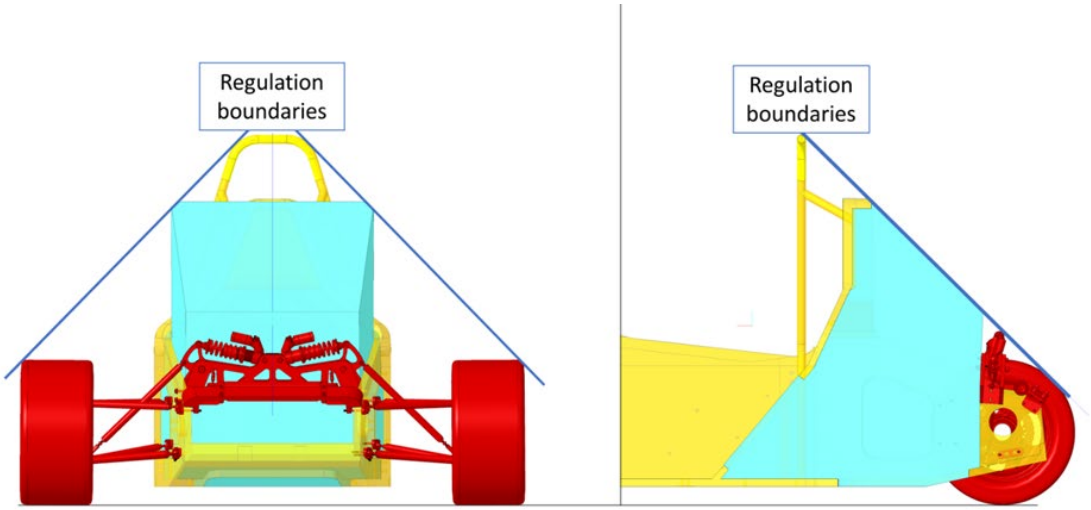

Figure 22 Image of how the available volume was defined.

Another consideration arising from this analysis is that the regulations allow for the possibility that some engine parts fall within the highlighted limits shown in *Figure 23* but at the same time do not occupy the defined volume.

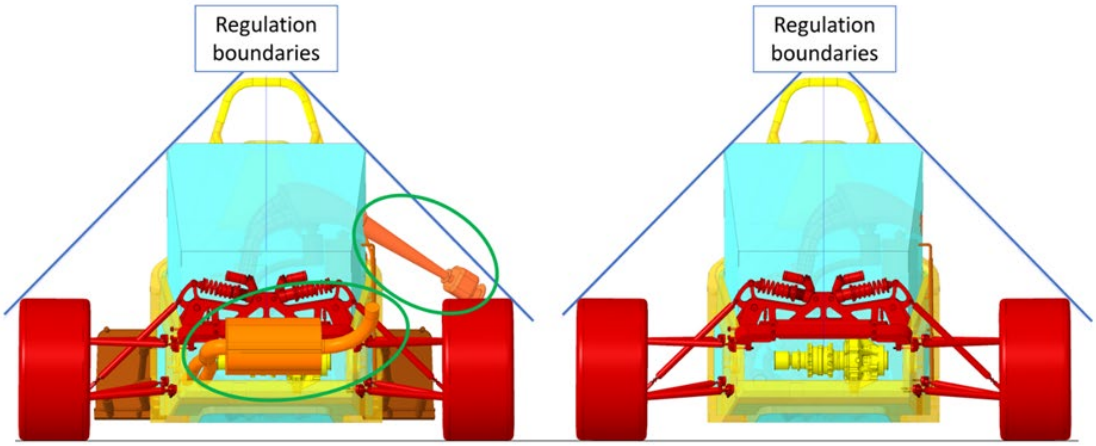

Figure 23 Imagine the areas where engine components are allowed.

With this last clarification, we evaluated how much this space is effectively utilized by the components of the engine group, disregarding the final transmission subgroup as it is overshadowed by the suspension group, reporting the analysis in *Figure 24*.

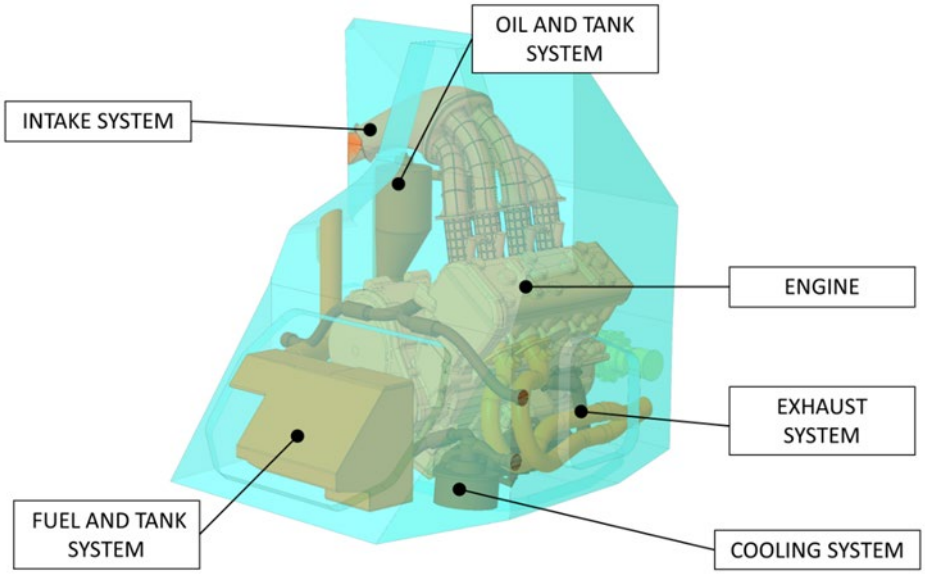

MMR COMBUSTION	Volume			Volume actually occupying the available volume		***USED VOLUME***
	[mm^3]	[l]	[%]	[mm^3]	[l]	[%]
INTERNAL COMBUSTION ENGINE GROUP	**67590366,54**	**67,59**	**100,00%**	**51351527,69**	**51,35**	**28,39%**
• ENGINE SYSTEM	29594502,55	29,59	**43,79%**	29594502,55	29,59	16,36%
• COOLING SYSTEM	7405482,19	7,41	**10,96%**	2539863,42	2,54	1,40%
• OIL AND TANK SYSTEM	3902775,05	3,90	**5,77%**	3902775,05	3,90	2,16%
• FUEL AND TANK SYSTEM	7949543,07	7,95	**11,76%**	7631918,66	7,63	4,22%
• INTAKE SYSTEM	4995900,15	5,00	**7,39%**	4099540,10	4,10	2,27%
• EXHAUST SYSTEM	11268238,63	11,27	**16,67%**	1109003,00	1,11	0,61%
• DRIVE TRANSMISSION SYSTEM	2473924,90	2,47	**3,66%**	2473924,90		0,00%
AVAILABLE VOLUME IN THE VEHICLE	**180867307,00**	**180,87**				

Figure 24 Analysis of the actual volume occupied by the engine system.

Based on this analysis, it can be deduced that only around 30% of the available volume is being utilized. While this may initially suggest that there is ample space available, it is important to note that several clarifications need to be made.

The volume required for engine installation is composed of two parts. The first part is necessary for the engine installation, while the second part is comprised of numerous small components such as wiring, control units, batteries, and gearbox actuators. These components also require installation space and must be positioned in areas permitted by the regulations. It is important to note that this analysis did not consider these small components. A crucial factor, particularly in relation to the vehicle's sporting use, is to maintain the masses as close as possible to both the vehicle's centre of gravity and the ground.

To define the layout of the hybrid power unit and develop the design of the necessary components, we will use the *AVAILABLE LIMIT VOLUME* (ALV) as a constraint. This approach ensures compliance with regulations and respects the potential of the vehicle's geometries, which have been refined over years of optimization.

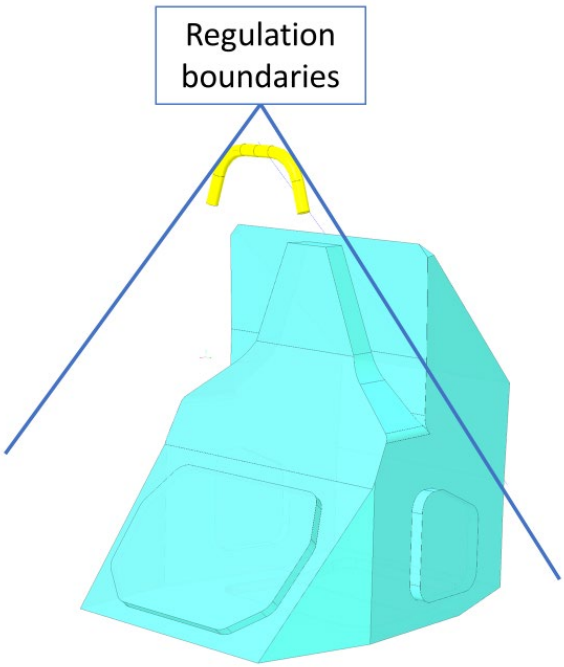

Figure 25 AVAILABLE LIMIT VOLUME *(ALV).*

5.2 Hybrid vehicle definition.

For this specific project, a parallel hybrid configuration has been chosen due to the particular simplicity of this architecture. Indeed, one of the main objectives is to carry out the hybridization process in a non-invasive manner, achieving a plug-and-go solution.

A competitive Formula SAE vehicle must be compact and lightweight; therefore, all components must be as light as possible. The engine of the Ducati 959 Panigale proves to be a good compromise between weight and power. *Figure 26* summarizes the main characteristics of the chosen internal combustion engine.

Displaced volume	955 cc
Lay-out	2-cylinders, V90°
Bore x Stroke	100 x 60,8 mm
Compression ratio	12,6:1
Number of Valves per cylinder	4
Type of valve actuation	Desmodromic
Fuel metering	Gasoline Port Injection
Maximum Power	110 kW @ 10500 rpm
Maximum Torque	102 Nm @ 9000 rpm
Dry weight	59 kg

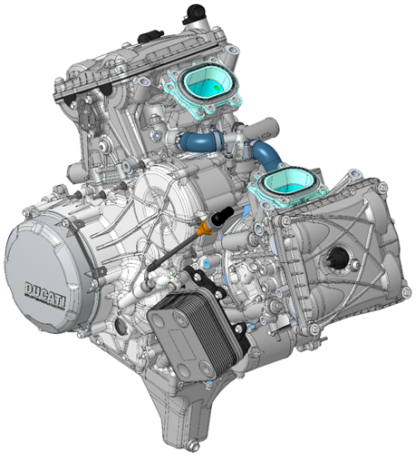

Figure 26 Characteristics of the Ducati Superquadro 959 engine.

The total displacement of this engine exceeds the maximum value agreed upon with the FSUK judges. Therefore, an important point of the project is to modify the layout of the stock engine in order to comply with the allowed displacement. In particular, the displacement almost doubles the limit, but this is what we are aiming for. Indeed, one of the cylinders has been switched to a passive mechanism, and consequently, one cylinder head has been removed (Cylinder head 1 in *Figure 27*). The head was later replaced by the electric motor (Electric motor in *Figure 27*) directly connected to the crankshaft using the original valve train chain. The goal is to achieve a solution suitable for generic V-type engines. The choice of the head to be replaced was dictated, as we will see later, by both regulatory aspects and the best use of available space. In particular, Cylinder head 2 fits better with a convenient arrangement of the intake and exhaust system.

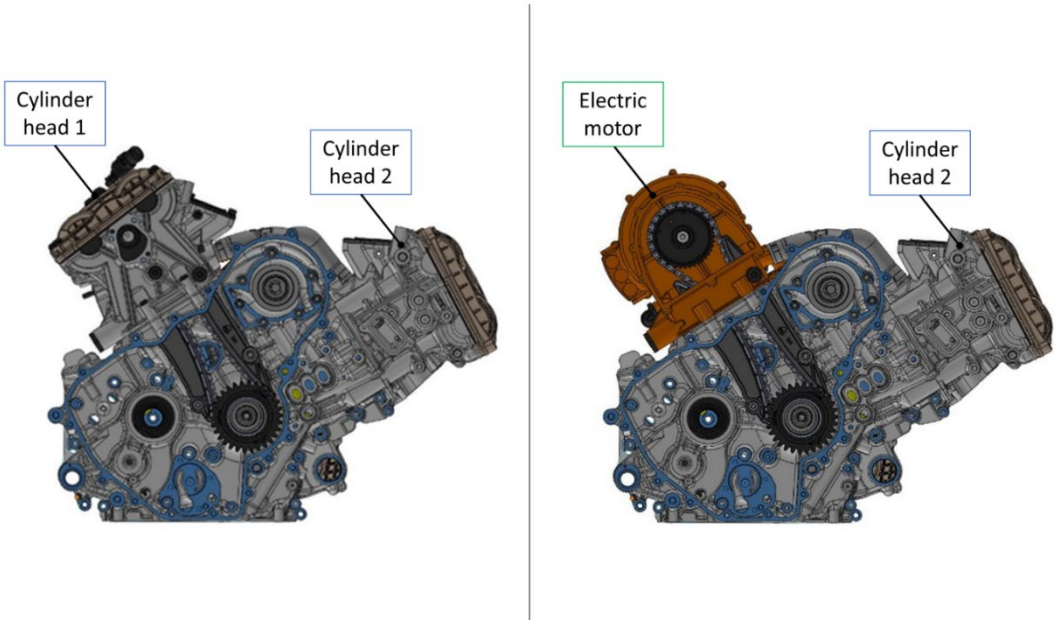

Figure 27 Electric motor installation.

The resulting hybrid architecture is referred to as a parallel hybrid [30], where the output of the engine and that of the electric motor are merged upstream of the transmission. In particular, this architecture refers to configuration P0 (described in section 2.2) as the EM is directly connected to the ICE crankshaft with a transmission chain. The electric motor provides additional thrust and enables battery charging during braking. In detail, the adopted configuration is schematically represented in *Figure 28*.

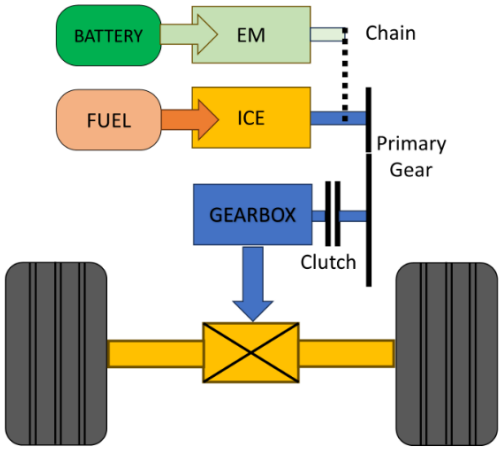

Figure 28 Parallel hybrid layout P0.

In order to confirm the correctness of the considerations made, 3D models were created using the same procedure as for the engine components of the reference vehicle, evaluating the volume occupied by the previously assumed power unit. In detail, the subgroups ENGINE SYSTEM and OIL AND TANK SYSTEM, along with part of the COOLING SYSTEM of the combustion vehicle, are compared with the ENGINE SYSTEM and ELECTRIC MOTOR SYSTEM of the hybrid vehicle. This comparison is made because the Ducati engine incorporates in the castings the water pump, an oil-water heat exchanger, and, having a semi-dry sump, the tank and a gas separation system from the lubricant.

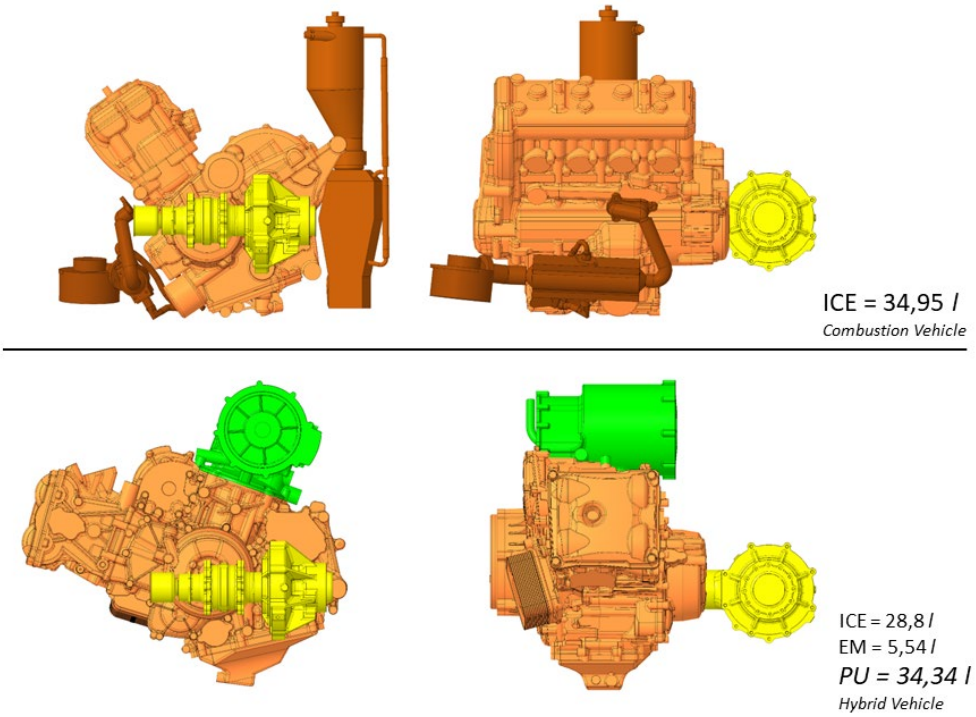

Figure 29 Comparison of the volumes occupied by the combustion engine of the reference vehicle and the hybrid power unit.

If we compare the two values of the occupied volume of the two systems, we can see that they are practically the same, with a slight delta in favour of the engine of 0,6 litres. *Figure 29* shows that the average size of the engine is smaller in the longitudinal direction than in the transverse direction, further confirming the advantage of choosing a V-engine. This characteristic will be useful later when defining the spaces for the installation of the battery pack and other components required for the electric motor. When the power unit model is inserted into the ALV, it is noticeable that the head exceeds the limit. To reduce this aspect, the bevel gear has been moved 30,5 mm to the right along the differential axis. This value was not exceeded so as not to alter the operation of the half shafts. However, even after this manoeuvre, a significant part of the head would interfere with the monocoque of the combustion engine car. This is certainly one of the points to consider when modifying the chassis.

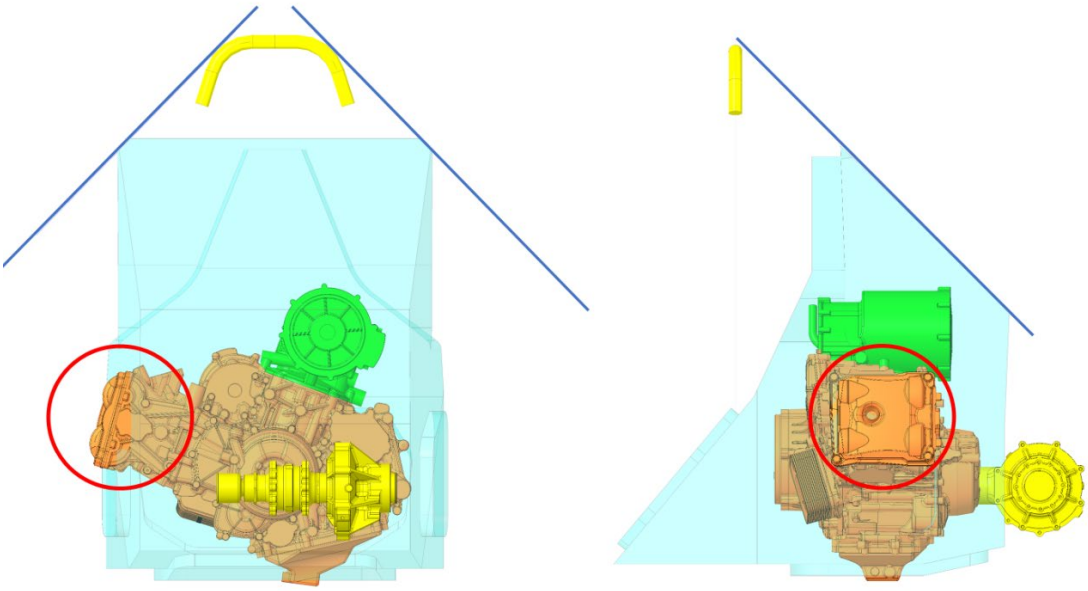

Figure 30 Areas where the cylinder head protrudes from the available volume.

As shown in *Figure 30*, the regulations allow a larger opening in that area is allowed, and the reduction in stiffness could be recovered by using the mounts present in the cylinder head, which in the original function of the engine on the motorcycle serve as structural element.

5.2.1 Internal Combustion Engine.

Based on the assumptions made, the new internal combustion engine specifications are as follows in *Figure 31*.

Displaced volume	478 cc
Lay-out	1-cylinder, V90°
Bore x Stroke	100 x 60,8 mm
Compression ratio	12,6:1
Number of Valves per cylinder	4
Type of valve actuation	Desmodromic
Fuel metering	Gasoline Port Injection
Maximum Power	46 kW @ 10500 rpm
Maximum Torque	44 Nm @ 8500 rpm
Dry weight	59 kg

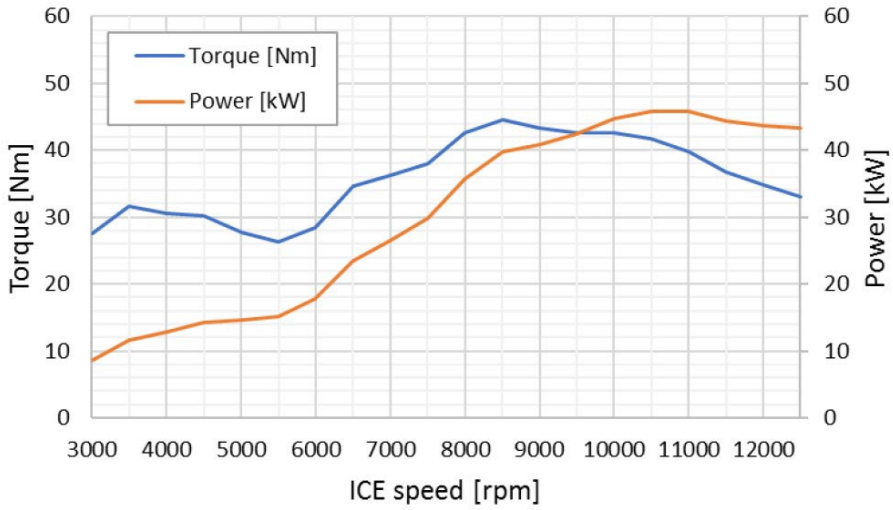

Figure 31 Single-cylinder engine characteristics.

The performance values reported are the result of a CFD-1D simulation conducted and discussed in the specific study [35].

These analyses were developed by imposing additional limits mandated by the regulations for internal combustion engines, which include a 20 mm air restriction in intake downstream of the throttle body and a maximum sound emission level of 110 $dB\ (C)$ at the equivalent engine speed corresponding to an average piston velocity of 15.25 m/s, and 103 $dB\ (C)$ at the minimum speed. In order to achieve the performance shown in the table, and to comply with the various legal limits just described, a rather complex intake system was defined by CFD 1D analysis, with a volume practically equal to that of the internal combustion engine, despite the smaller displacement. The situation is slightly worse for the exhaust system.

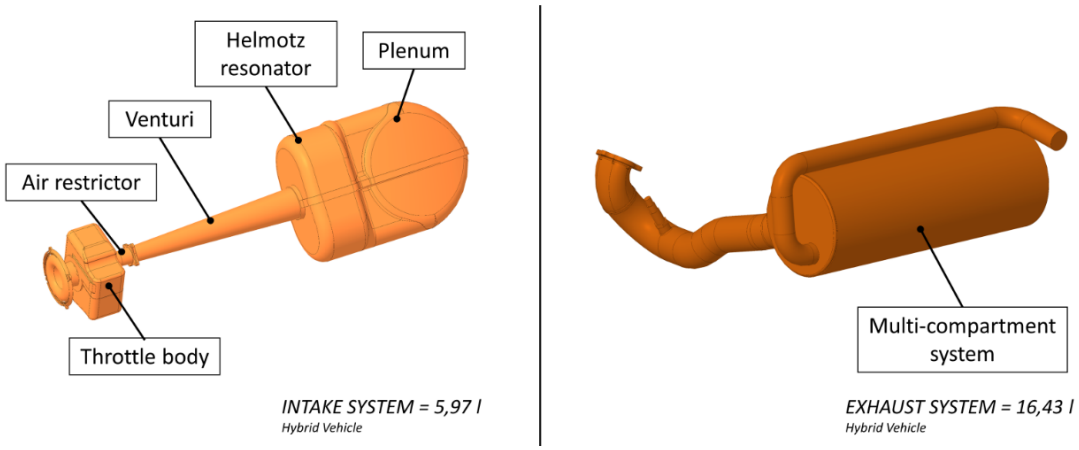

Figure 32 Intake and exhaust system defined through analysis. The occupied volumes are shown.

After a series of modelling iterations and making the best use of the regulatory limits for these systems, which must be within the main envelope, a principle also used for the internal combustion engine, the result is shown below in *Figure 33*. It has the characteristic of not significantly affecting the ALV.

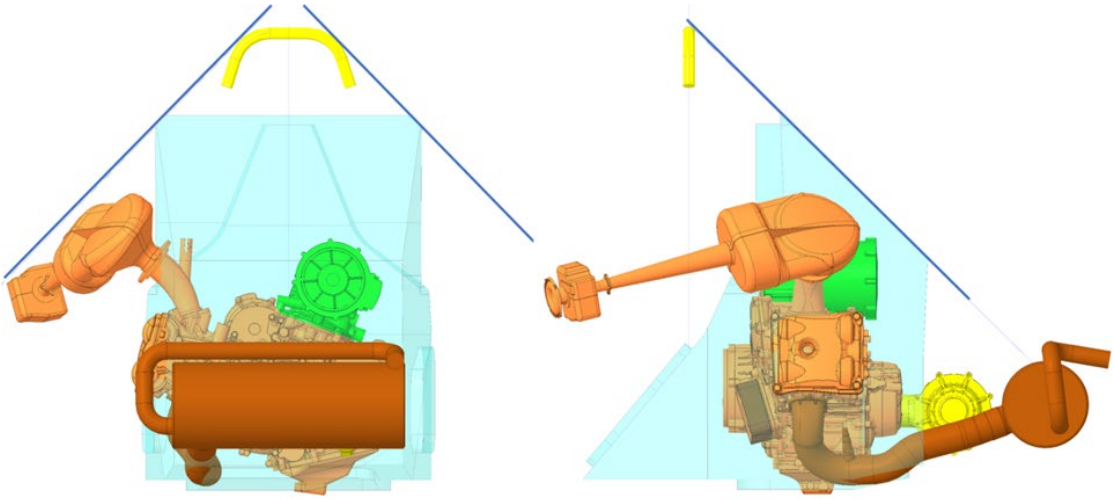

Figure 33 Installation layout of intake and exhaust systems.

An extensive experimental campaign was carried out on the single-cylinder engine using the university's dynamometer test bench. The engine was mounted on the bench without the EM, so only the thermal engine was considered to validate the ICE 1D model. During this phase, an engine calibration process focused on fuel consumption, performance, smoothness and reliability of the ICE was required. Furthermore, torque curves of the ICE were collected at various loads, obtaining a complete torque map of the ICE. Similarly, brake-specific fuel consumption (BSFC) was measured at each engine load and speed. The following data will be utilized in the analyses to define the power unit control strategy.

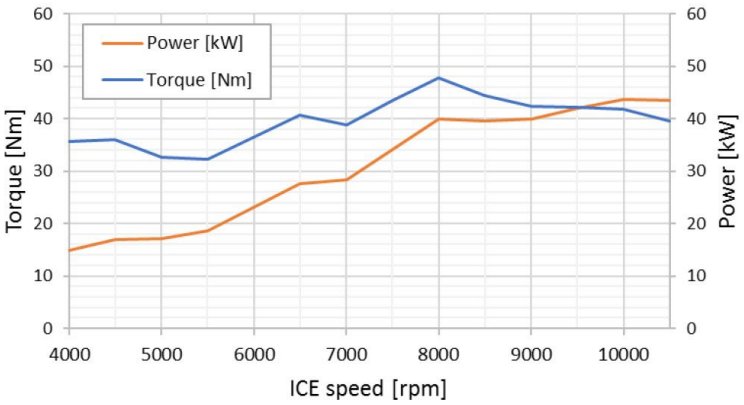

Figure 34 Experimental power and torque curves.

In converting the engine from a twin-cylinder to a single-cylinder configuration, the issue arose of how to manage the deactivated combustion chamber. Permanent deactivation of the vertical cylinder was achieved not by eliminating the entire crankshaft system, but by removing the cylinder head and sealing off the dummy combustion chamber with the electric motor case. This choice brings the benefit of not altering the characteristic of the V90° engine's ability to balance first-order inertial forces, but the drawback of generating a stagnant chamber where piston motion would trap air, subjecting it to numerous compression and expansion cycles that could lead to localized overheating and purely dissipative pumping work.

Analyses were also conducted on other balancing systems, which showed comparable weight but higher costs and potential reliability issues. The compromise solution, therefore, was to increase the volume of the dummy combustion chamber to reduce the high compression ratio of the original system, and to make perforations in the piston crown that would not significantly alter its mass, theoretically making the chamber no longer stagnant and thus nullifying the pumping effect. By reducing the compression force, the thrust force exchanged between the piston and the cylinder liner is also reduced, consequently reducing frictional losses.

Figure 35 Pictures of the piston with holes.

5.2.2 Electric Motor.

One of the most complex aspects of the design and development of both hybrid and pure electric vehicles, and one that even the automotive industry is still considering, is the choice of electric motor. Below is a brief description of the various families of such motors, in order to justify the choice of a permanent magnet synchronous motor for the application of the hybrid power unit under consideration.

The motor drives can be classified into two main groups, namely the commutator motors and commutatorless motors. Commutator motors mainly are the traditional DC motors, which include series excited, shunt excited, compound excited, separately excited, and permanent magnet (PM) excited motors. DC motors need commutators and brushes to feed current into the armature, thus making them less reliable and unsuitable for maintenance-free operation and high speed. In addition, winding excited DC motors have low specific power density. On the contrary, commutatorless electric motors present several advantages including higher efficiency, higher power density and lower operating costs. They are also more reliable and maintenance-free compared to commutator DC motors because of the lack of brushes. Thus, commutatorless electric motors are widely used for HEVs and EVs applications [37].

Focusing on the commutatorless electric motors, the major types of electric motors adopted or under serious consideration for HEVs, as well as for EVs, include the Induction Motors (IM), the Permanent-Magnet Synchronous Motors (PMSM) and the Switched Reluctance Motors (SRM) [36].

Induction Motors (IM)

Induction Motors (IM) are widely accepted as a commutatorless motor type for EV and HEV propulsion. This is because of their low cost, high reliability, and maintenance-free operation. However, conventional control of induction motors such as variable-voltage variable-frequency (VVVF) cannot provide the desired performance, suffering low efficiency at low light loads and limited constant-power operating range [38].

Permanent-Magnet Synchronous Motors (PMSM)

Permanent-Magnet Synchronous Motors can eliminate conventional brushes, slip rings, and field copper losses, by replacing the field winding of conventional synchronous motors with PMs [39]. Actually, these PM synchronous motors are also called PM brushless AC motors. When PMs are mounted on the rotor surface, they behave as nonsalient synchronous motors because the permeability of PMs is similar to that of air. By burying those PMs inside the magnetic circuit of the

rotor, the saliency causes an additional reluctance torque, which leads to facilitating a wider speed range at constant power operation [40].

Switched reluctance motors (SRM)

Switched reluctance motors (SRM) have been recognized to have considerable potential for EV and HEV applications. SRMs have the definite advantages of simple construction, low manufacturing cost, and outstanding torque-speed characteristics for EV and HEV applications. Although they possess simplicity in construction, this does not imply any simplicity of their design and control. Because of the heavy saturation of pole tips and the fringe effect of pole and slots, their design and control are difficult and subtle [46]. Traditionally, SR motors operate with shaft sensors to detect the relative position of the rotor to the stator. These sensors are usually vulnerable to mechanical shock and sensitive to temperature and dust, reducing the reliability of SRMs. Moreover, SRMs generate acoustic noise causing several NVH issues and constraining some applications [41].

Regarding the energy efficiency issue, the selection of an appropriate type of traction motor is very complicated. Motor efficiency is significantly influenced by material quality, design parameters and control technology. It is possible to consider two dominating motor losses, such as copper loss and iron loss. Copper loss is squarely proportional to the motor current. In IM and SRM, a portion of this current is also the motor magnetizing current, which produces magnetization or excitation loss. PMSM is naturally excited through magnets and, therefore, has no excitation loss. However, this is only true below the base speed of the motor. Above the base speed, PMSM requires external excitation to weaken its naturally existing magnetic field. Therefore, torque per copper loss is inherently better below the base speed in PMSM. Moreover, at very high speed, iron loss becomes significant. Iron losses are a function of flux density and frequency of flux alternation. The PMSM has rotor magnets, so it has theoretically zero rotor iron loss. The only iron loss in PMSM is in the stator side [42,43].

Therefore, as previously anticipated, a PMSM has been chosen for the described advantages of reliability, efficiency, and also greater adaptability to the specific layout of the applied case.

The necessary requirements for defining the EM are listed below:

1. The outer dimensions of the stator and rotor, such as diameter and length, must not exceed the space occupied by the replaced cylinder head. Indeed, the EM must fit into the free space created by the removal of the ICE head. Since the position of the EM axis is constrained by the original transmission layout, the maximum outer diameter of the stator is limited.

2. Considering that the EM must be directly connected to the ICE, the maximum speed of the EM depends closely on the transmission ratio between the engine shaft and the EM shaft. Knowing the maximum speed of the ICE allows evaluating the corresponding maximum speed of the EM. In particular, the specific considerations on the transmission ratio are discussed in the following section.
3. The power that the EM must handle is imposed by the FSAE rules. The goal is therefore to obtain a continuous power below this limit and a slightly higher peak power to be able to use the EM under safe conditions.

Based on these requirements, the dimensions of the stator and rotor are summarized below.

EM dimensional request	***Stator***	***Rotor***
Out diameter	135 mm	80 mm
Inner diameter	82 mm	30 mm
Length	94 mm	96 mm

Figure 36 Characteristics dimensions of the EM.

The outer diameter of the stator influences the external profile of the EM housing. Furthermore, considering both the outer diameter and axial length of the stator, it is possible to determine the necessary interference, based on the maximum torque to be transmitted. The difference between the inner radius of the stator and the outer radius of the rotor represents the air gap thickness, in this case chosen to be 1 mm. Finally, the inner diameter and length of the rotor are parameters that influence the design of the EM shaft.

Given all the constraints described below, the performance characteristics of the chosen electric motor are as follows.

Supply Voltage	96 VAC
Continuous torque	19,5 Nm
Speed @ continuous torque	0/9600 rpm
Continuous power	19,5 kW
Speed @ continuous power	9600 rpm
Peak torque	36,5
Speed @ peak torque	0-8600 rpm
Peak power	32,5 kW
Speed @ peak power	8600 rpm

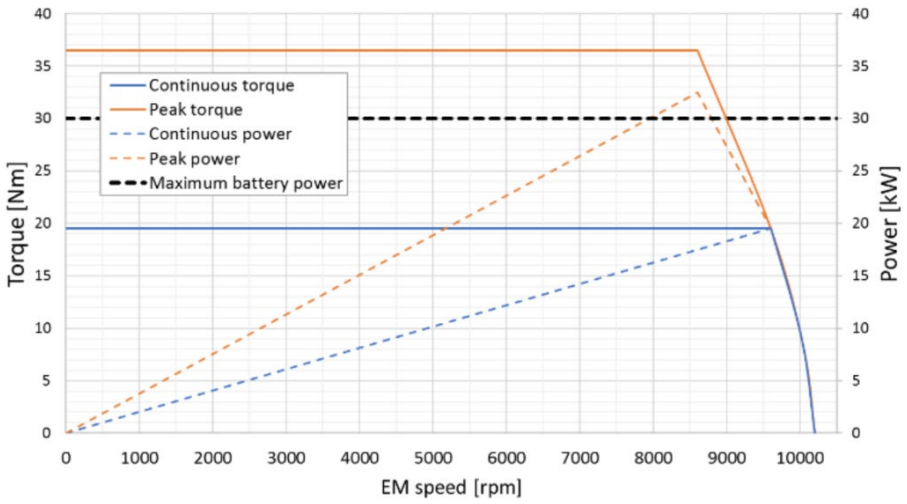

Figure 37 Electric motor power and torque curve.

Figure 37 shows the theoretical power and torque curves of the electric motor. The blue lines represent the continuous power and torque delivered by the EM, while the orange curves refer to overload conditions. In reality, it is not possible to overload the motor beyond 30 kW due to the value imposed by the regulations that limit the maximum power that can be delivered by the battery.

Once the performance characteristics and constraints for sizing the electric motor have been defined, the following are additional aspects considered for its realization.

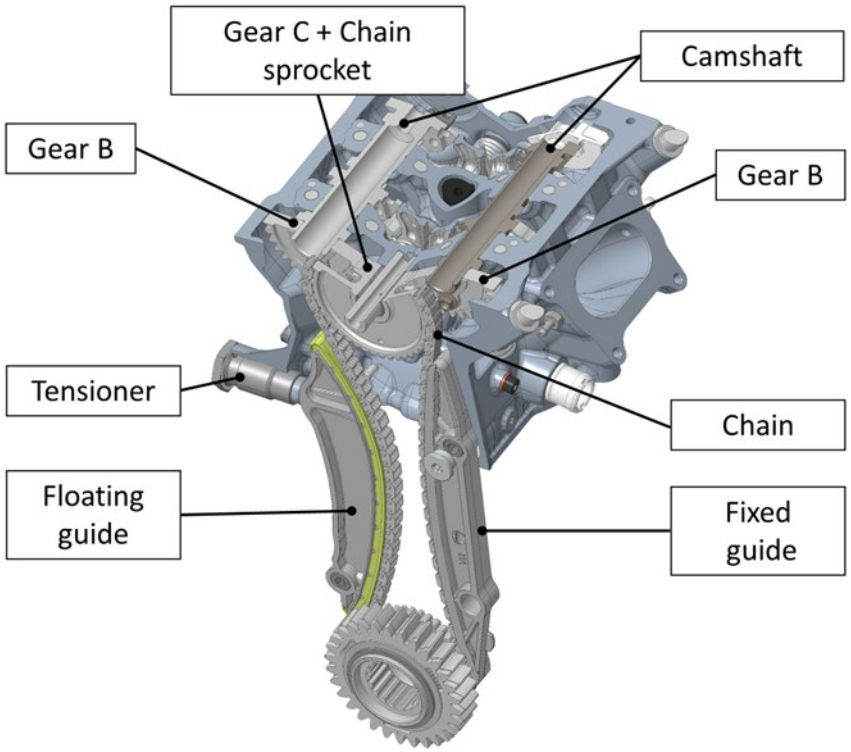

Figure 38 The system transmits motion from the crankshaft to the desmodromic camshafts.

The valvetrain transmission system of the original engine consists of both a timing chain and transmission gears *Figure 38*. Consequently, two different transmission ratios must be considered, referring respectively to the chain and the gears. The chain is kept in position by two guides: one is fixed (fixed guide in *Figure 38*) and the other can rotate to adjust the chain tension (floating guide in *Figure 38*). This task is entrusted to the hydraulic tensioner that ensures correct tension during operational conditions.

Of course, the original total transmission ratio is such as to rotate the camshafts at half the speed of the crankshaft. Specifically:

$$\tau_{tot} = \tau_{chain}\tau_{gear} = 1{,}2 * 1{,}667 = 2$$

Where τ_{chain} is the transmission ratio of the chain alone, and τ_{gear} is the transmission ratio between gears B and C (*Figure 38)*. However, by removing the camshafts, gears B are also eliminated (*Figure 38*). Consequently, the EM shaft is directly connected to the upper sprocket of the chain (Chain sprocket in *Figure 38*), with the transmission ratio in this configuration being 1.2 (τ_{chain}). Originally, the wheel hub did not include any torque transmission device as it was a freewheel gear. Therefore, a splined profile was added to the original wheel design to allow torque transmission from the EM shaft to the ICE motor shaft.

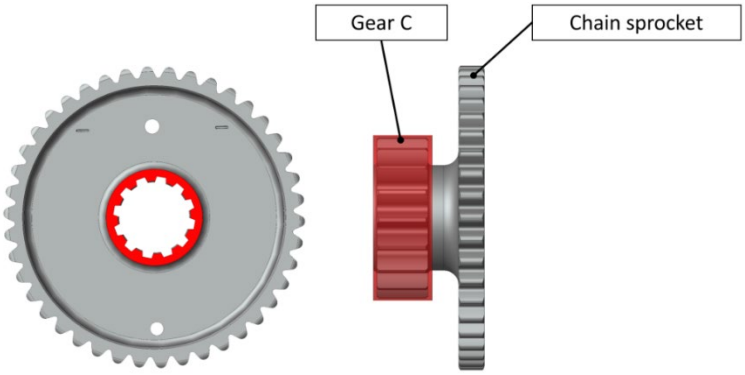

Figure 39 New sprocket design.

In *Figure 39*, the specific modifications applied to the sprocket are highlighted in red. Additionally, the original wheel also contains the teeth of gear C (*Figure 38*), which no longer mesh with gears B. Consequently, this part can be removed to reduce the weight of the component and the rotational inertia of the EM rotating parts. Indeed, the rotating inertia of these components is significant for the performance analysis of the power unit [44]. Additionally, the rotating inertia also affects the loads acting on the transmission chain [45].

The ICE has a maximum rotation speed (limiter) of 12000 rpm (see *Figure 31*), therefore the maximum allowed speed for the electric motor has been appropriately defined.

Specifically:

$$\omega_{EM} = \omega_{ICE}\tau_{chain} = 12000 * 1{,}2 = 10000\ rpm$$

where ω_{ICE} is the maximum speed of the internal combustion engine and ω_{EM} is the speed that the electric motor must not exceed. In fact, the characteristic of the EM presents a speed range that varies up to 10000 rpm (*Figure 37*). Finally, the drive is entrusted to a silent-type chain. A silent chain is a set of racks composed of two teeth each. This type of chain can operate at high speeds transmitting high loads while ensuring noise reduction [46,47].

The analysis of loads derived from the original desmodromic drive and the maximum load declared by the chain manufacturer are considered in order to assess the feasibility of using the original chain for the connection between the electric motor and the engine shaft. In particular, a specific structural analysis was performed considering the dynamic behavior of the entire transmission system to evaluate the use of the OEM chain [45].

Another important component involved in the torque transmission mechanism is the shaft of the electric motor. It must match the rotor of the EM and be supported by the housing of the EM. Suitable bearings have been selected during the design process, taking into account the maximum speed and operating loads. *Figure 40* shows a sectional view of the EM assembly showing the shaft, stator, rotor and all other functional components.

The position of the shaft seal has been chosen to keep the EM chamber clean by isolating of the engine crankcase. On the opposite side is an encoder sensor capable of accurately sensing the rotary motion. This is done by attaching a magnet to the end of the shaft using a special adapter. The rotor is connected to the shaft by two diametrically opposed keys to prevent unbalanced forces. Finally, the shaft is provided with a through hole to reduce the mass of the shaft and the rotational inertia.

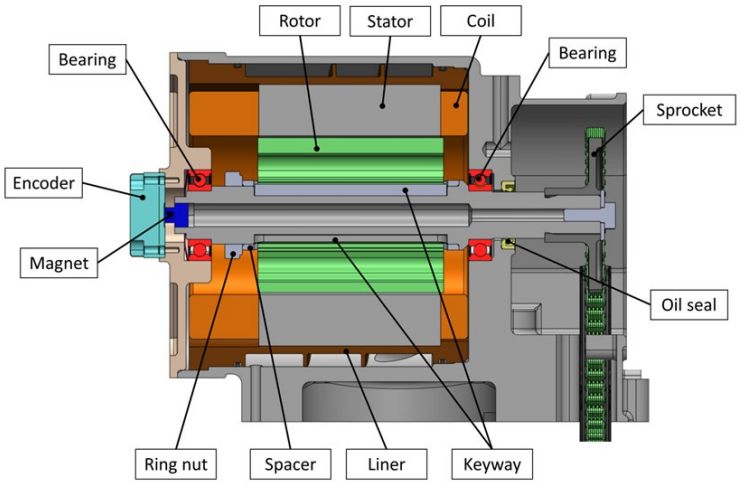

Figure 40 Electrical motor assembly.

5.2.3 Cooling system analysis.

Another aspect considered in the development of the EM is the introduction of a cooling system. The cooling of an electric motor is crucial as it has a direct impact on efficiency. Indeed, there should be a strong interaction between electromagnetic and thermal design, as it is impossible to accurately analyse one without the other (for example, losses are critically dependent on temperature and vice versa) [48]. In general, an electric motor provides about 60% of the total energy conversion from electric to mechanical [49].

It is therefore necessary to implement a dedicated cooling circuit to keep the EM temperature as low as possible. However, this means considering separate cooling lines, radiators and pumps from the ICE system [50], resulting in increased weight and cost. In addition, the project aims for a *plug&play* solution with as few components as possible. In particular, the water pump body is integrated into the engine block, through which it is connected directly to the cylinders.

From there, the coolant rises into the cylinder head and the EM cooling circuit, as shown in *Figure 41*.

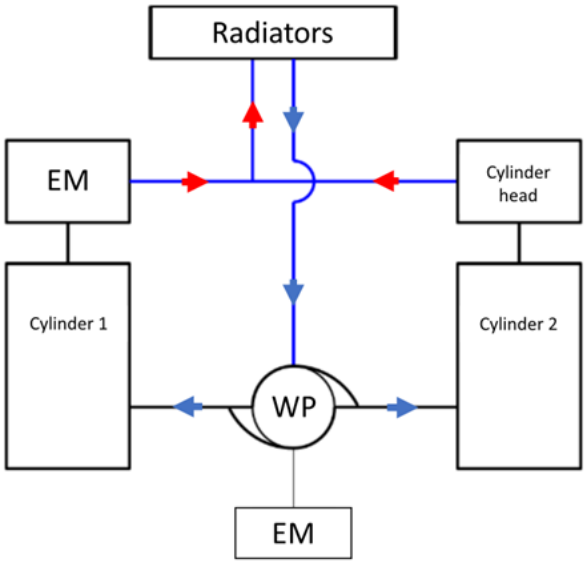

Figure 41 Cooling circuit diagram of the power unit.

The black lines represent the channels inside the engine block and cylinder head, while the blue lines represent the pipes of the external circuit to the radiator. The outlets from the cylinder head and the EM are combined towards the radiator, which is located in the side of the vehicle. The two circuits are therefore connected in parallel. The fluid used in the cooling system is distilled water, as the Formula SAE regulations expressly prohibit the use of additives.

The cooling circuit designed in this way therefore imposed the following constraints on the definition of the final geometry:

- Firstly, the characteristics of the EM cooling circuit had to be defined in such a way as to maintain the balance of the original circuit and ensure the same flow to the ICE head.
- Secondly, the particular geometry analysed must maximise the heat transfer between the EM case wall and the fluid.

To achieve these results, the cooling circuit of the standard production head was first characterised (*Figure 42*). This was done in order to determine the target pressure drop to be achieved by the new EM circuit (*Figure 43*). *Figure 44* shows only the version that allows the same flow characteristics as the OEM cylinder head and maximises the heat exchange surfaces with the stator of the electric machine.

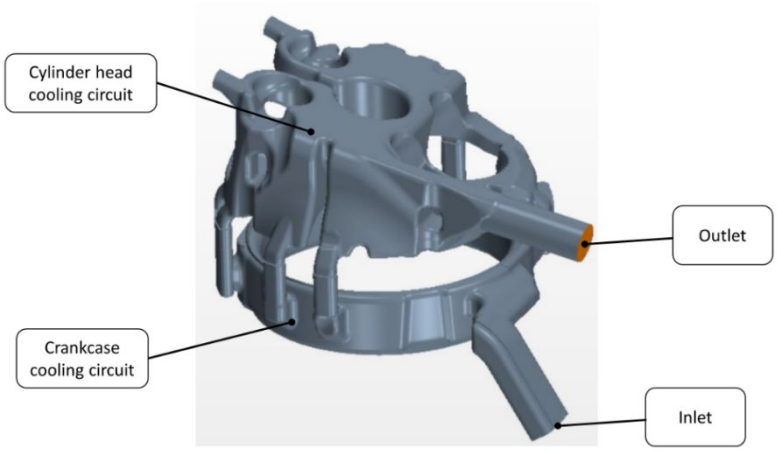

Figure 42 OEM cooling circuit of the internal combustion engine.

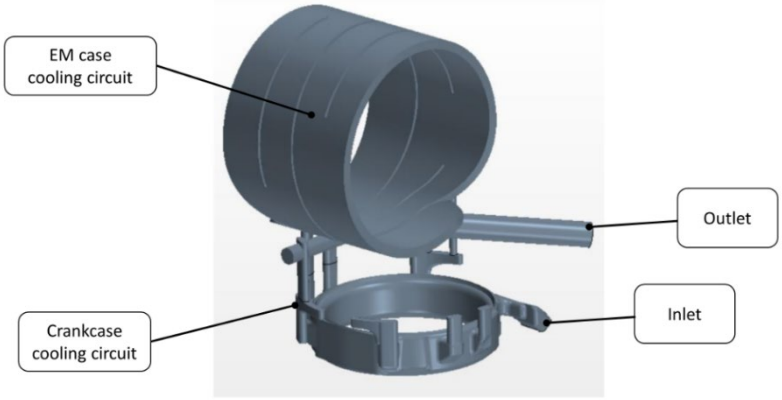

Figure 43 Electric machine cooling circuit.

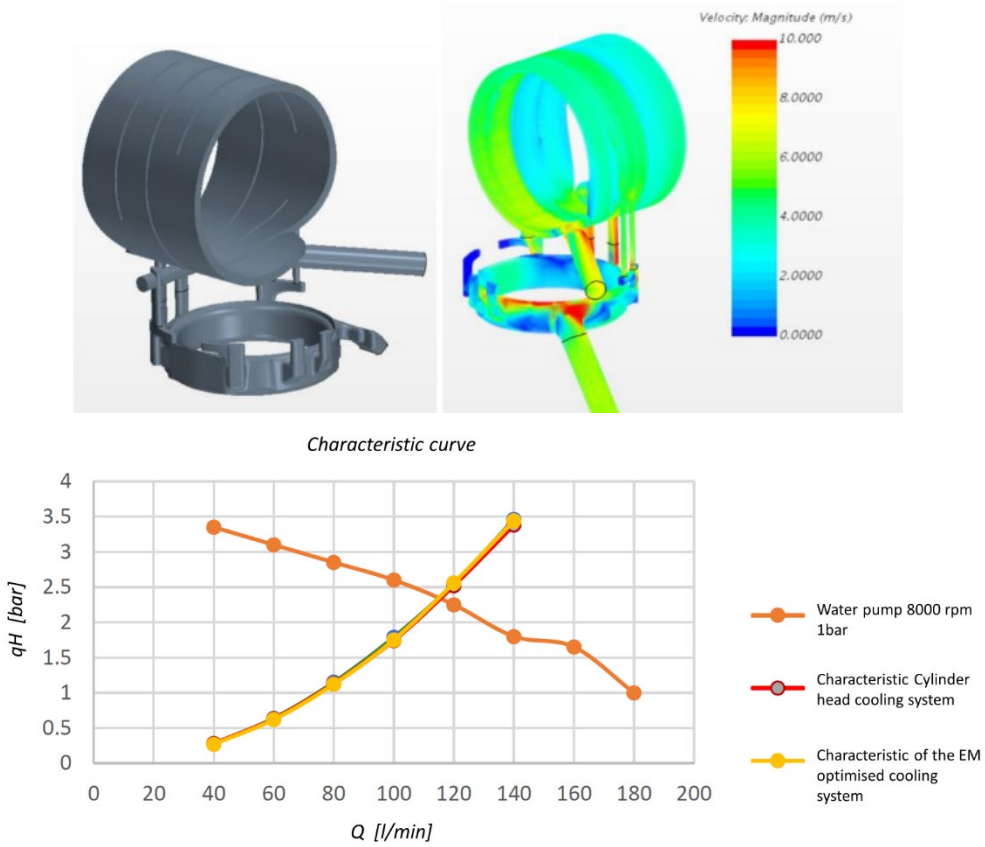

Figure 44 Optimized range of speeds for the cooling circuit of the electric machine.

Following these 3D CFD analyses, a thermostructural analysis was carried out to identify any fatigue-related issues in the EM housing, which is not particularly stressed as it is not subject to significant thermal stresses such as those resulting from combustion. This analysis did, however, provide information on how to modify the interface flange with the crankcase. Between this flange and the one on the crankcase is the OEM cylinder head gasket. Which is a metal gasket that must be compressed to the same extent as the cylinder head to ensure the sealing of the high and low pressure water and oil circuits.

5.2.4 Battery pack.

As described earlier, energy storage systems in a hybrid vehicle are fundamentally two-fold. The first is high-energy density, characteristic of chemical fuels in liquid or gaseous form that are non-renewable. The second is low-energy density but has the ability to be regenerated or self-regenerated by the vehicle itself by recovering kinetic or chemical energy used by the combustion engine. These latter systems, known as RESS (Rechargeable Energy Storage Systems), are used to store energy for later use in vehicle operation and can be of various types. In general,

the most common energy storage systems developed in the automotive field are batteries, supercapacitors, flywheels, and fuel cells.

Supercapacitors are devices capable of handling high power rates compared to batteries but are unable to store the same amount of charge as batteries. Supercapacitors can be used for high-power requirements such as energy recovery during regenerative braking [51]. The flywheel system consists of a large rotating disk where kinetic energy is stored and a motor/generator that is coupled to the flywheel to convert kinetic energy into electrical energy. Therefore, this system stores energy in the kinetic form, which can then be transformed into electricity. Sometimes, this type of architecture is called a mechanical hybrid because the energy accumulator consists of a kinematic device [52]. Fuel cells are devices that take in fuel as input and produce electricity as output. Fuel cells are powered by hydrogen, which could be produced remotely as part of the hydrogen economy. Consequently, this system requires onboard tanks for hydrogen storage [53].

Electrochemical batteries are devices that convert chemical energy into electrical energy. In recent years, much research has been conducted on those based on reversible reactions, namely those that can convert chemical energy into electrical energy and vice versa. These batteries allow for a high energy density and therefore find significant application in the automotive industry. *Figure 45* illustrates how power and energy demands can be grouped based on the type of vehicle under consideration [54].

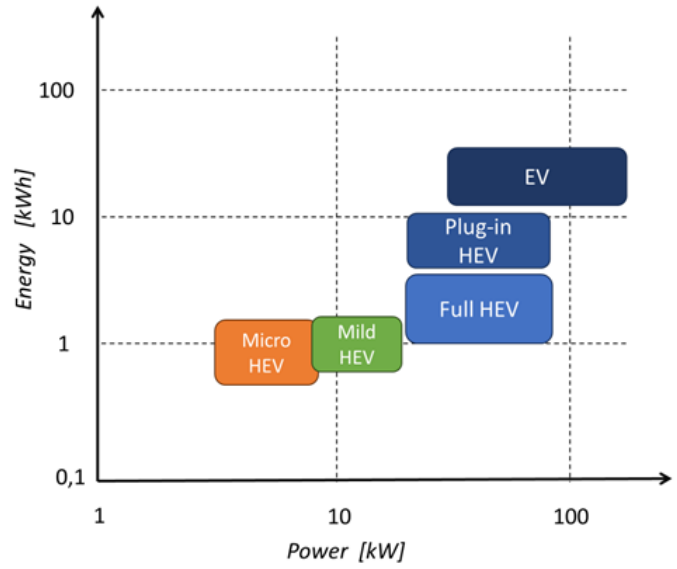

Figure 45 Energy and power demands on batteries for different types of vehicles [54].

In general, batteries can be classified based on their energy density, charge and discharge characteristics, system integration, and costs. Other relevant performance parameters include cycle life, performance at low and high temperatures, and safety.

Specifically:

- Gravimetric power density (also known as specific power density) and volumetric power density are among the most important parameters for hybrid vehicles. High values generally imply low electrical resistance, resulting in low energy losses and high-power capacity.
- The ratio of discharged energy to charged energy is energy efficiency. Energy losses are converted into heat and must be removed to prevent battery overheating.
- Cycle life, on the other hand, describes how many cycles the battery can perform before failing. Cycle life depends on the depth of discharge, current rate, and average state of charge (SOC). Capacity turnover is measured in full equivalent cycles.
- In addition to technical aspects, costs are relevant for the choice of a battery system. However, costs strongly depend on specific requirements and battery quality.

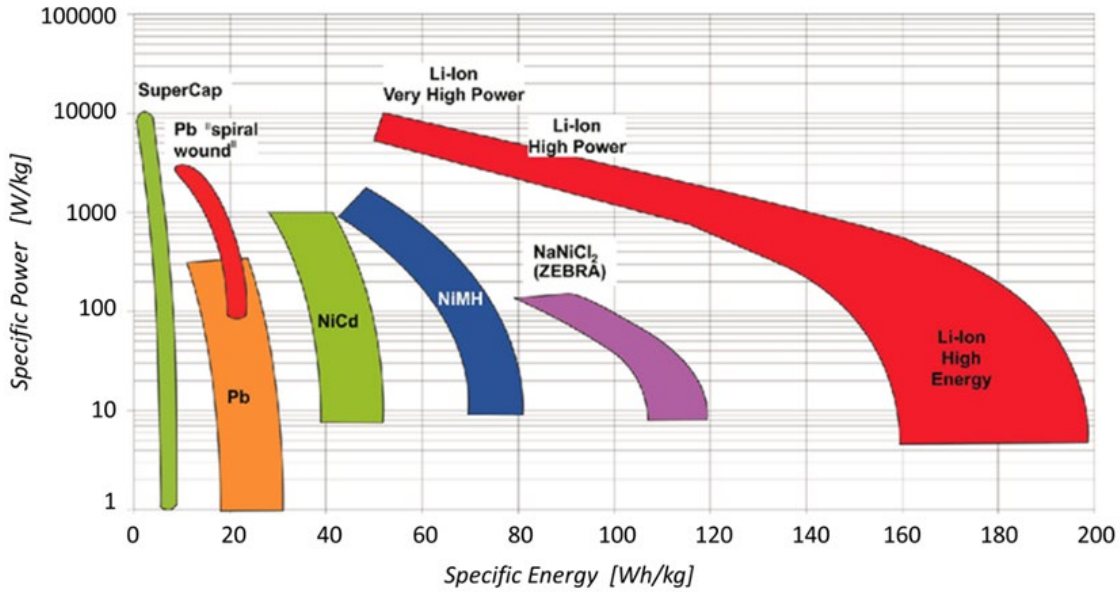

Figure 46 Ragone plot of various battery technologies with specification at cell level for automotive applications [54].

Some of the widely used batteries in the automotive sector are lead-acid batteries, nickel-metal hydride (NiMH) batteries, and lithium-ion batteries. Lead-acid batteries are the cheapest batteries used in vehicles where there is not a strong demand for power and energy density, typically employed in traditional vehicles for starting, lighting, and ignition (SLI) (e.g., for auxiliary devices and vehicle starting). Nickel-metal hydride batteries are used in mild hybrid and full hybrid vehicles. They provide higher energy and power density compared to lead-acid batteries, but at a significantly higher cost. Lastly, lithium-ion batteries, introduced in the early 1990s, are the most expensive but can provide high energy and power density values, approximately 3-4 times higher than lead-acid

batteries. They are currently widely used in new electric and hybrid vehicles [55]. Shows the main characteristics of the listed battery types in *Figure 47*.

MATERIALS	***Lead Acid***	***Metal Hydrocarbon***	***Lithium Ions***
SPECIFIC ENERGY [Wh/kg]	30-50	60-120	100-265
SPECIFIC POWER [W/kg]	75-300	250-1000	250-340
ENERGY EFFICIENCY [%]	70-80	60-70	85-98
AUTO-DISCHARGE [%/DAY]	0,033	2,5-3,0	0,1-0,3
LIFE CYCLES	100-2000	500-1000	500-3000
COST for POWER UNIT [$/kW]	175-600	150-1500	175-4000
COST for ENERGY UNIT [$/kWh]	150-400	150-1500	500-2500

Figure 47 Key features of the three battery categories: Lead Acid, Metal Hydrocarbons, and Lithium Ions.

The lithium-ion battery technology has been considered for this specific application. In particular, the cell utilizes the chemical intercalation mechanism, which involves the insertion of lithium ions between the graphite layers during the charging phase, while during the discharging phase, the lithium ions move out of the material towards the carbon. The lithium ions shuttle through the electrolyte and separator, from one electrode to the other. During the discharge process, the ions move from the negative electrode to the positive one, and vice versa during the charging process, leaving the graphite structure intact [56].

The main lithium-ion battery types are: Lithium Cobalt (LCO), which despite being used by some automakers is not considered safe for the automotive sector, Lithium Manganese Oxide (LMO), Lithium Nickel Manganese Cobalt (NMC), Lithium Nickel Cobalt Aluminum (NCA), and Lithium Iron Phosphate (LFP). Another category is Lithium Titanium (LTO), whose acronym comes from the lithium titanium oxide anode and the cathode is graphite [56]. Below are brief descriptions of the main characteristics of each battery family:

1. Lithium Cobalt (LCO): It has a cell nominal voltage of 3,6V and a specific energy density of 200 Wh/kg. It has low self-discharge allowing for 500 to 1000 discharge cycles. Disadvantages include high cost due to cobalt, safety concerns, low thermal stability, and capacity loss with deep charge-discharge cycles.
2. Lithium Manganese Oxide (LMO): It has a cell nominal voltage of 3,8 V, a specific energy density of 100-150 Wh/kg, and can achieve 300-700 life cycles. It is not a toxic material, costs less, and has higher thermal stability compared to Lithium Cobalt.
3. Lithium Nickel Manganese Cobalt (NMC): The combination of these elements results in higher energy density and longer battery life. It has a nominal voltage of 3,6-3,7 V, specific energy density of 150-220 Wh/kg,

and 1000-2000 life cycles. Additionally, the use of a lower cobalt concentration reduces costs and safety issues.

4. Lithium Nickel Cobalt Aluminum (NCA): It has similar characteristics to the above-described battery: nominal voltage of 3,6 V, specific energy density of 150-220 Wh/kg, and long battery life. Moreover, the presence of aluminum improves thermal stability and electrochemical performance. Disadvantages include high cost and low safety.
5. Lithium Iron Phosphate (LFP): It has a nominal voltage of 3.2 V, a specific energy density of 90-120 Wh/kg, and 1000-2000 life cycles. The main advantages are thermal stability at high temperatures, high safety, and low cost. On the other hand, it has higher self-discharge.
6. Lithium Titanium (LTO): It has a nominal voltage of 204 V, a specific energy density of 70-110 Wh/kg, and a lifespan of 1000 cycles. The main advantages are safety due to the absence of carbon and high thermal stability, while the cost is high.

The battery type chosen for this specific application is the Sony VTC6 cylindrical cells in the 18650 format. The cell dimensions are a diameter of 18 mm and a length of approximately 65 mm. The chemistry of the Sony VTC6 batteries is lithium manganese oxide. Each cell has a capacity of 3000 mAh and a maximum continuous discharge current of 15 A, according to Sony; however, if the cell temperature remains below 80 °C, the continuous discharge current increases significantly to 30 A.

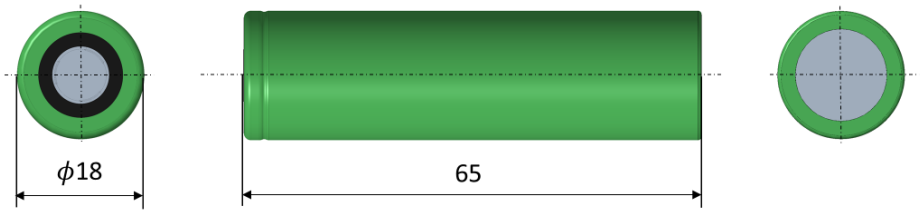

Figure 48 Sony VTC6 cylindrical cells 18650.

In both hybrid and electric vehicles, the battery is created by combining these cylindrical cells, which can also have different geometries, defining combinations in series and parallel to determine the performance characteristics, and consequently, the geometric features of the storage system. For this specific application, the battery pack was sized starting from a power of 30 kW, corresponding to the limit imposed by FSUK rules. Additionally, each pack must consist of modules with a maximum of 90 cells. To achieve the power target, 270 cells are therefore required, grouped into three modules, generating a layout of 27 series by 10 parallel. Consequently, the total nominal voltage is approximately 100V and the maximum current is 300A. Lithium-ion batteries also require a monitoring system to check each cell for temperature and voltage. The Battery Management System (BMS) is an electronic system that also manages voltage

balancing of individual cells during charge and discharge phases to ensure maintenance of the storage system's performance.

To maintain appropriate cell temperatures during frequent charge and discharge cycles, a cooling system was added to the electrical energy storage system. In the *Figure 49*, the characteristics of the battery pack are depicted.

Total allowed power	30 kW
Cell typology	Cylindrical LMO
Cells number	270
Connection scheme	27 series of 10 parallel
Total Voltage	100 V
Maximum current	300 A
Capacity	3 kWh
Cooling system	Liquid

Figure 49 Characteristics of the battery pack.

One final regulatory consideration is that all the systems described above must be contained within a case that meets both mechanical stress and electrical isolation requirements. Therefore, with all the performance and regulatory characteristics defined, it is necessary to evaluate the remaining space available in the vehicle, taking into account the previous considerations. The available space for installing the battery pack is essentially the same as the space occupied by the gasoline tank in a combustion vehicle. This space is located between the driver's seat and the engine and has an estimated volume of approximately 38 l (see *Figure 50*). It must be shared with both the gasoline tank and the inverter, which is required for managing the current sent to the electric motor.

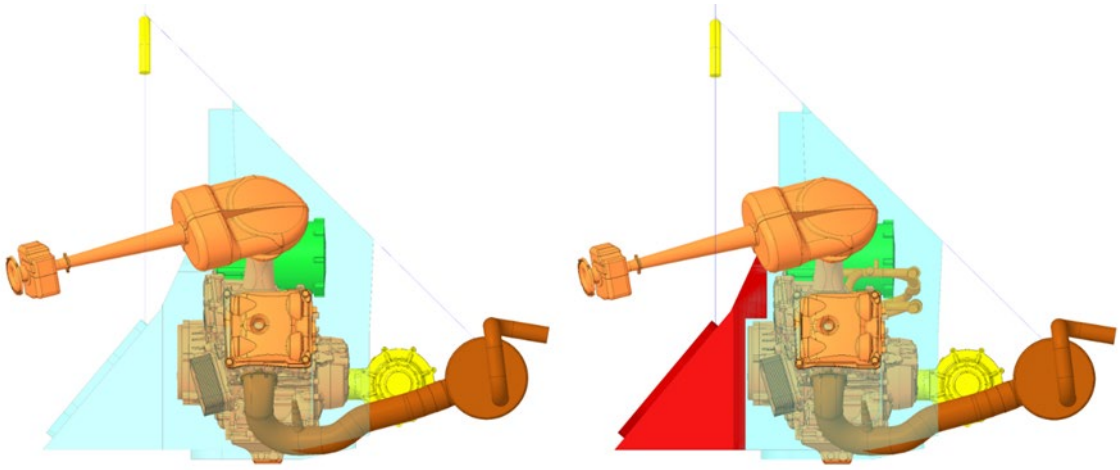

Figure 50 Red-highlighted area of the ALV is for installation of the battery pack, petrol tank and inverter.

To create a battery pack that optimally utilizes the available space, an analysis was conducted to determine the best arrangement of cells, starting from the

consideration that each cell occupies a volume of 0,02 l, and therefore the volume occupied by 270 cells is equal to 4,64 l. To see how the arrangement of cells could best manage the space, several considerations were made on how to arrange the 10 cells in parallel. The best solution is described in *Figure 51*, where the cells are arranged in two columns of 5 cells each, with their axes spaced 19 mm apart in all directions. By alternating the arrangement of cells and connecting them with shaped copper plates, it is possible to connect the sub-modules of ten cells in parallel.

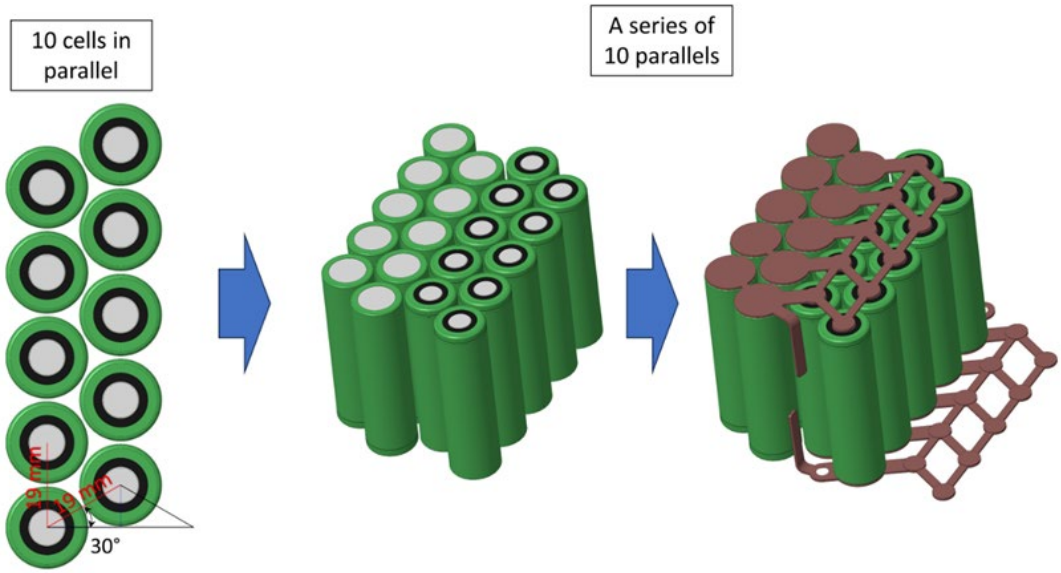

Figure 51 Primary module of 10 cells in parallel, with optimised arrangement.

With this layout, the volume occupied by the module of 90 cells is 2 l, a good compromise considering it is only about 1,4 l larger than just the cells alone. However, this configuration allows for the width of the available volume to be utilized, limiting the space taken up in the side view, which is greatly restricted by the firewall that protects the driver from the engine compartment.

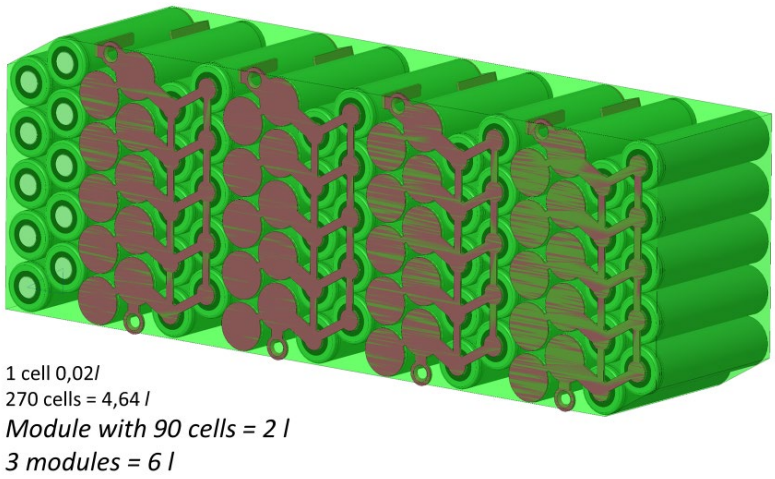

Figure 52 90-cell module evaluation of occupied volume.

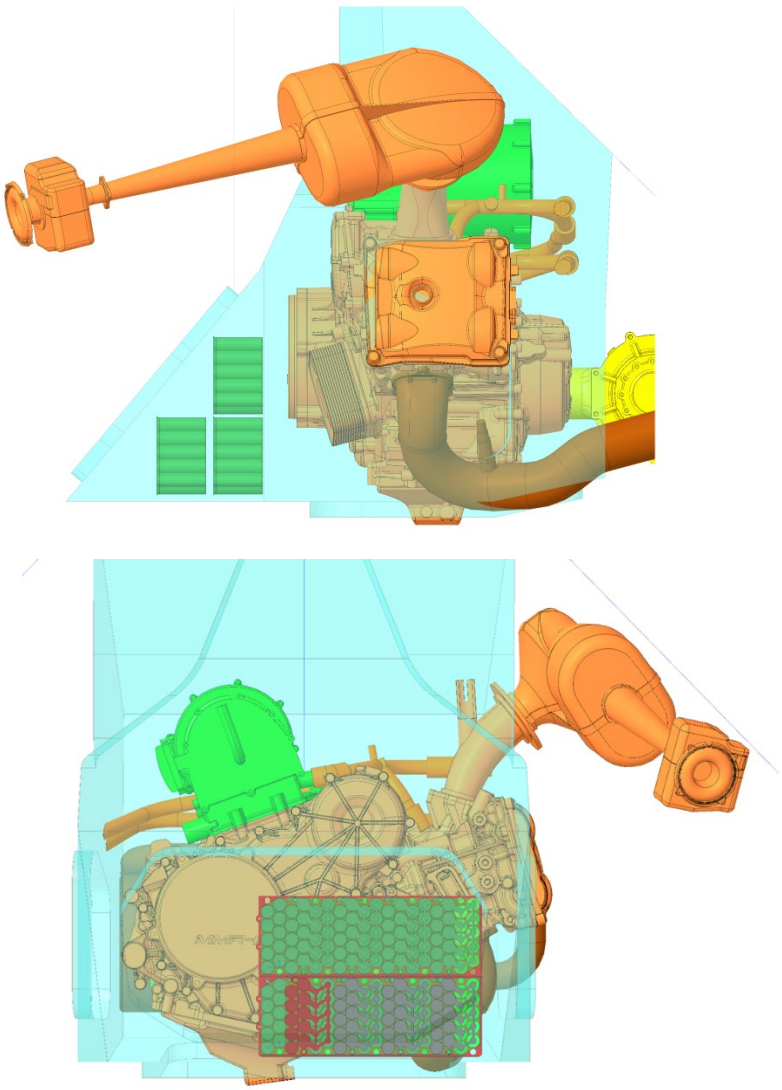

Figure 53 Battery Pack Installation Assessment.

In this initial analysis, we arrived at defining a configuration that broadly outlines the general dimensions of the pack and where it is best positioned in the compartment. However, as mentioned earlier, the storage system, in addition to the cells, must integrate numerous other components for management and safety. To try to keep the dimensions under control, a new concept has been developed for the installation of the cells in the pack, avoiding soldering and enabling efficient water cooling (*Figure 54*). In particular, the cells are connected to each other by a copper plate acting as a conductor. An important role is played by the contact area between the conductor and the cell. Although the soldering process is easier to develop, it rarely guarantees a repeatable and predictable contact area. Consequently, another solution involves applying axial force on the cells, generating a certain contact pressure, ensuring a minimum contact area that closely influences electrical contact resistance [58]. However, the cells considered have a certain dimensional tolerance on the cell length. Therefore, specific cup springs have been considered under each cell to ensure a constant force (and thus

contact area) on each individual cell. The spring is designed considering the stiffness of the individual spring, the minimum force required, and achieving a displacement control assembly using specific spacers. Additionally, this solution favours maintenance.

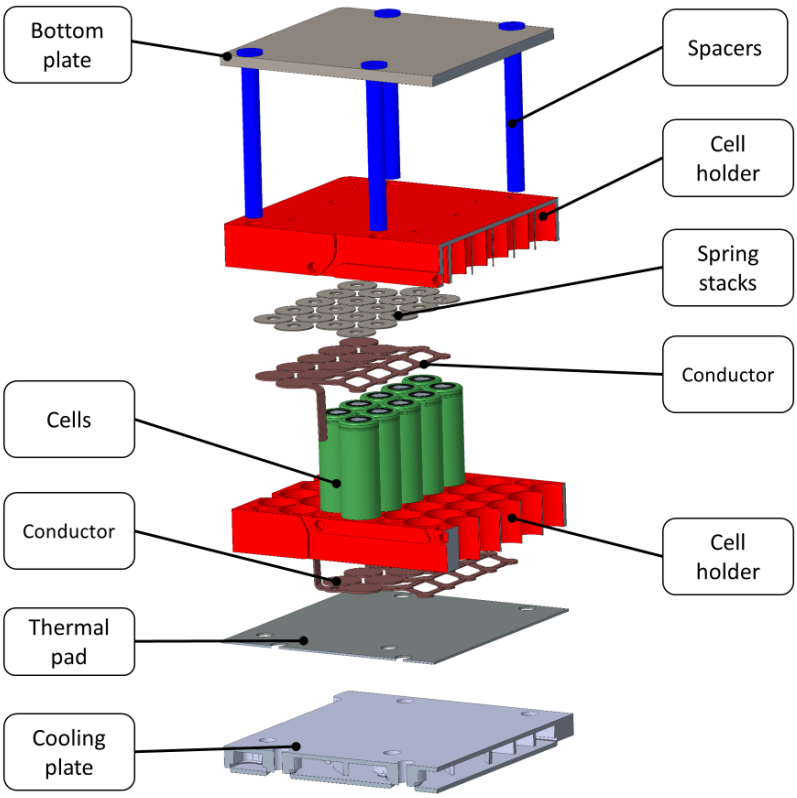

Figure 54 Describing the battery pack proposed concept.

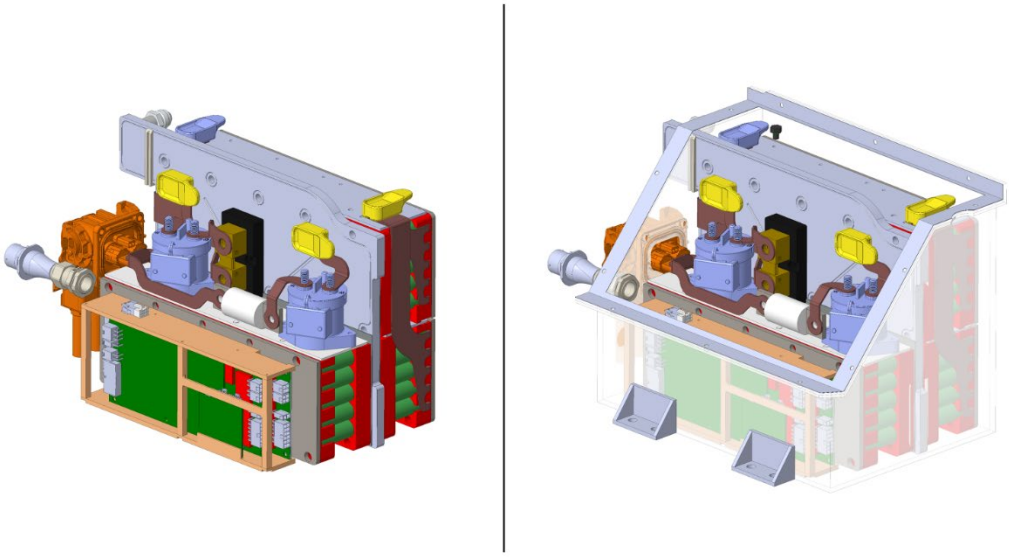

Figure 55 Final battery pack.

Lithium-ion batteries also require a monitoring system in order to control each cell, in terms of temperature and voltage. The battery monitoring system (BMS) is an electronic system that manages the battery pack protecting it from operating outside its safe operating area, monitoring its state, reporting that data, controlling its environment and providing the balance of the cells [59].

To complete the battery pack, space had to be found for the control system boards (BMS) and the various safety systems required by regulations. These were mainly inserted into the remaining space between the three modules and the firewall. The entire setup was enclosed in a case made of composite materials consisting of kevlar and carbon fibre laminated with resin, which has fire-resistant and electrically insulating properties. See *Figure 55*.

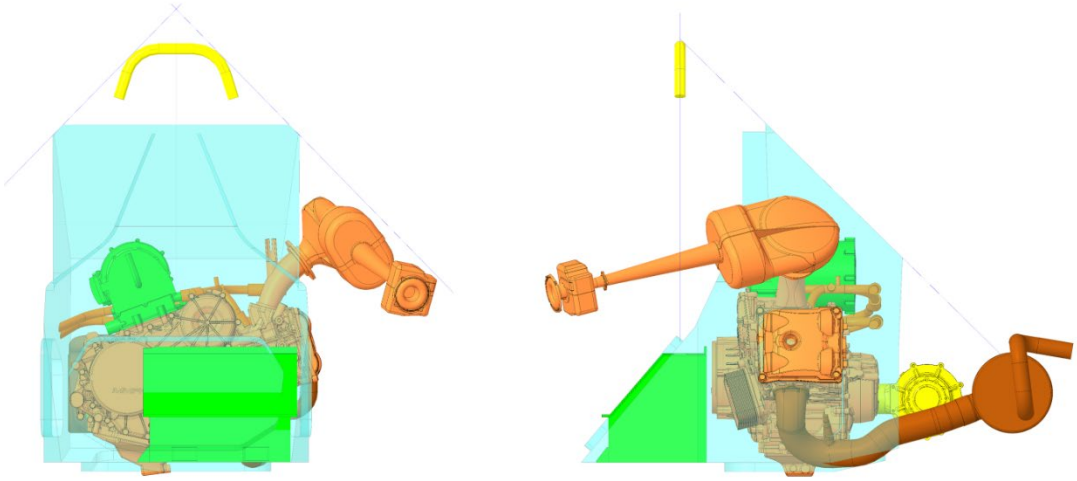

Figure 56 Volume occupied by the final battery pack.

Finally, it is reported that the battery pack thus constructed has a volume of 15,8 liters, slightly less than half of the 38 liters described in *Figure 50*. This means that there are approximately 22 liters available for the installation of the gasoline tank and inverter. However, this space is slightly smaller because a minimum volume must be considered, evaluated through installation tests on the vehicle, for the handling of battery pack installation.

5.3 Analysis of volumes of HEV Formula Student.

After all the considerations and a series of iterations to define the layout of the final components required for the power unit, such as the fuel tank, the inverter and the cooling circuits, *Figure 57* shows the final assembly. As before, all the occupied volumes were evaluated using the same procedure.

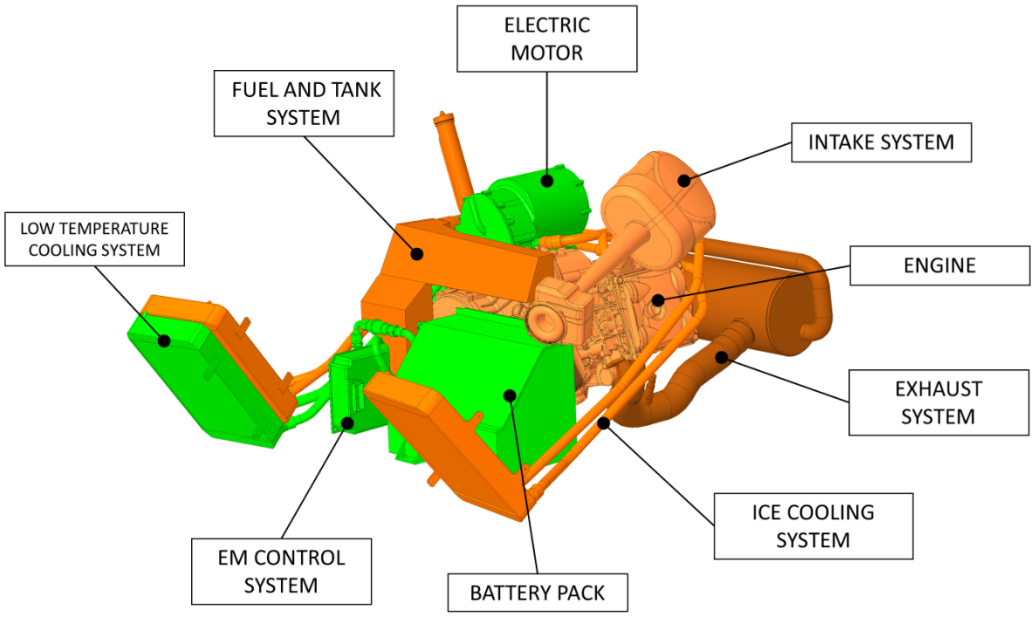

MMR HYBRID	Volume		
	[mm^3]	[l]	[%]
INTERNAL COMBUSTION ENGINE GROUP *Conventional Vehicle*	67590366,54	**67,59**	***RIF***
POWER UNIT GROUP (PUG)	**96929112,96**	**96,93**	***30,27%***
ELECTRIC MOTOR GROUP (PU)	**29309204,53**	**29,31**	100,00%
• ELECTRIC MOTOR CONTROL SYSTEM	3209351,755	3,21	10,95%
• ELECTRIC MOTOR SYSTEM	5538456	5,54	18,90%
• COOLING SYSTEM (LOW TEMPERATURE)	4757923,408	4,76	16,23%
• BATTERY PACK SYSTEM	15803473,37	15,80	53,92%
INTERNAL COMBUSTION ENGINE GROUP (PU)	**67619908,43**	**67,62**	100,00%
• ENGINE SYSTEM	28801194,93	28,80	42,57%
• COOLING SYSTEM	8689896,62	8,69	12,81%
• FUEL AND TANK SYSTEM	5251603,09	5,25	7,73%
• INTAKE SYSTEM	5971703,97	5,97	8,79%
• EXHAUST SYSTEM	16431584,92	16,43	24,27%
• DRIVE TRANSMISSION SYSTEM	2473924,90	2,47	3,62%

Figure 57 Analysis of PU volumes.

From this analysis, it can be stated that the power unit as designed and implemented occupies a volume of approximately 29 liters more than the internal

combustion propulsion system taken as a reference, which is a 30% increase in percentage terms.

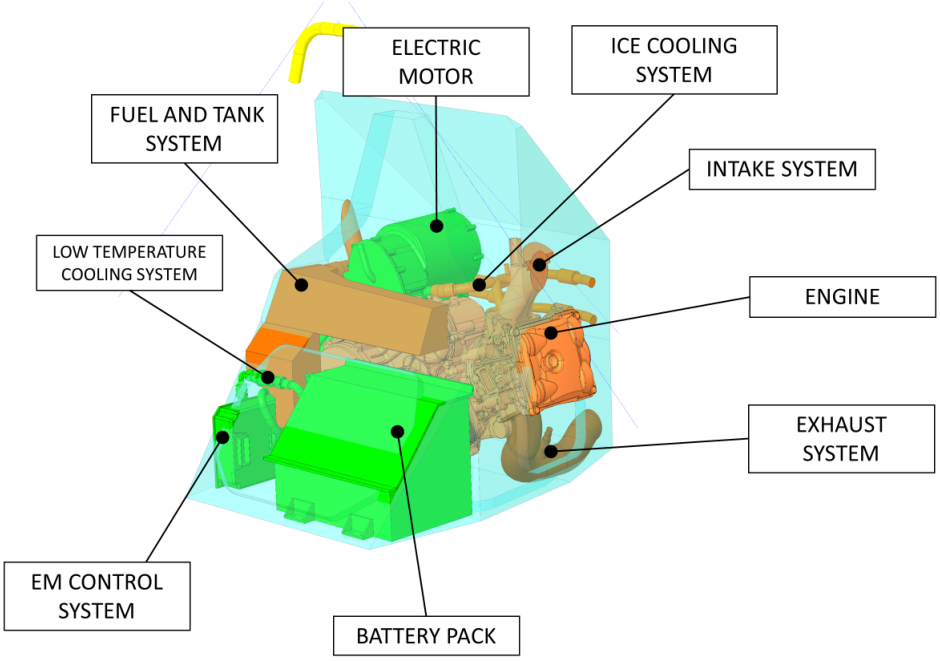

MMR HYBRID	Volume			Volume actually occupying the available volume		***USED VOLUME***
	[mm^3]	[l]	[%]	[mm^3]	[l]	[%]
INTERNAL COMBUSTION ENGINE GROUP *Conventional Vehicle*	67590366,54	**67,59**	***RIF***	**51351527,69**	**51,35**	**28,39%**
POWER UNIT GROUP (PUG)	**96929112,96**	**96,93**	***30,27%***	**64117534,40**	**64,12**	**35,45%**
ELECTRIC MOTOR GROUP (PU)	**29309204,53**	**29,31**	100,00%	**25456738,13**	**25,46**	**14,07%**
• ELECTRIC MOTOR CONTROL SYSTEM	3209351,755	3,21	10,95%	8747807,755	8,75	4,84%
• ELECTRIC MOTOR SYSTEM	5538456	5,54	18,90%			
• COOLING SYSTEM (LOW TEMPERATURE)	4757923,408	4,76	16,23%	905457	0,91	0,50%
• BATTERY PACK SYSTEM	15803473,37	15,80	53,92%	15803473,37	15,80	8,74%
INTERNAL COMBUSTION ENGINE GROUP (PU)	**67619908,43**	**67,62**	100,00%	**38660796,27**	**38,66**	**21,38%**
• ENGINE SYSTEM	28801194,93	28,80	42,57%	28801194,93	28,80	15,92%
• COOLING SYSTEM	8689896,62	8,69	12,81%	650468,44	0,65	0,36%
• FUEL AND TANK SYSTEM	5251603,09	5,25	7,73%	5039087,00	5,04	2,79%
• INTAKE SYSTEM	5971703,97	5,97	8,79%	438162,00	0,44	0,24%
• EXHAUST SYSTEM	16431584,92	16,43	24,27%	1257959,00	1,26	0,70%
• DRIVE TRANSMISSION SYSTEM	2473924,90	2,47	3,62%	2473924,90		0,00%
AVAILABLE VOLUME IN THE VEHICLE	**180867307,00**	**180,87**				

Figure 58 Analysis of the actual volume occupied by the PU system.

As mentioned earlier, not all additional components need to be contained within the chassis bay, but certainly many are subject to regulatory constraints. Nevertheless, the result obtained was excellent as it managed to occupy 35.45% of the available volume, which means using about 10% more than what was done in the internal combustion vehicle.

6 Definition the control system.

This chapter describes the development of the control system for the Formula Student single-seater power unit. These are based on the theories described earlier in chapters for the design of control logic and for fuel consumption optimization using Dynamic Programming.

6.1 Description of the power unit control logic.

The MoTeC M150 ECU, which has been selected to manage the power unit, uses a rule-based method to determine the percentage of torque requested from the two motors through a series of tables. *Figure 57* illustrates this control logic.

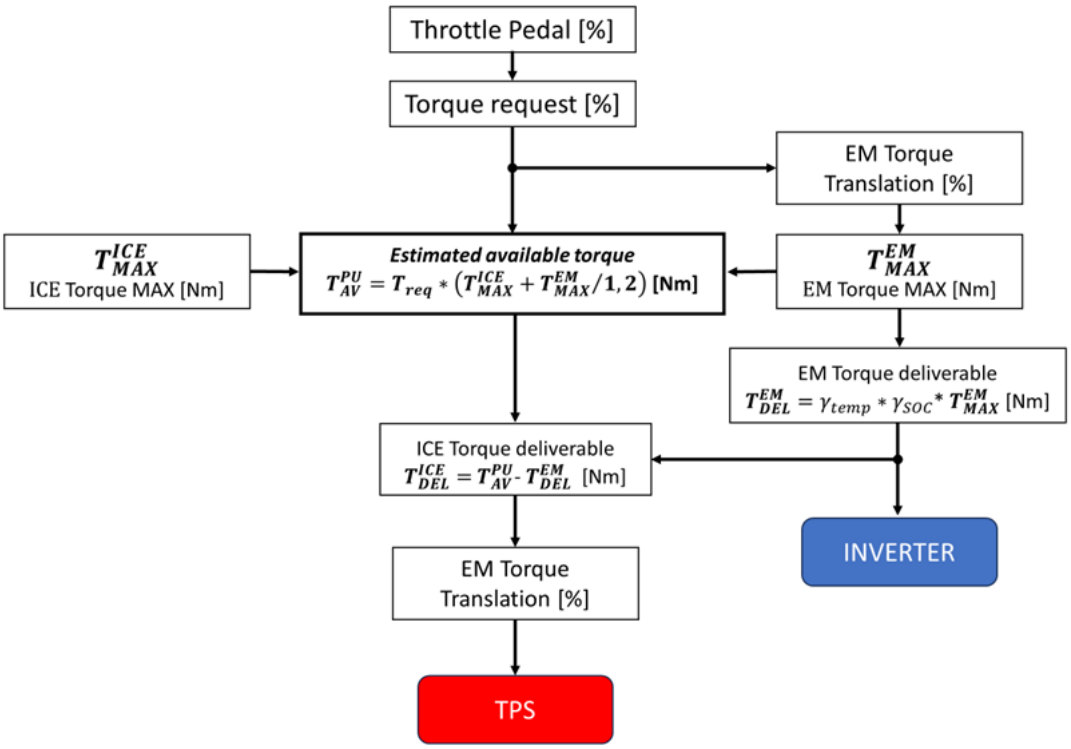

Figure 59 Flow chart EMS.

This system utilizes a total of seven tables, including:

- *ICE Max Torque*: contains the maximum torque value of the internal combustion engine obtained at full load on the dynamometer (WOT).
- *EM Max Torque*: comprises three mappings of the maximum torque of the electric motor based on the type of test the vehicle must perform.

- *MAP-A*: contains the maximum torque achievable by the electric motor and is designed for Acceleration, Skidpad, and Autocross events. This allows the power unit's power to be fully utilized by delivering the maximum allowed current according to regulations.
- *MAP-B*: contains an intermediate torque curve designed for Endurance event and is particularly used during test sessions.
- *MAP-C*: the electric motor's torque is zero at all operating points, allowing the power unit to operate purely in thermal configuration. This map is mainly used during vehicle warm-up in the initial phases of track testing.
- *Total PU Torque*: translates the driver's request (% pedal) into the percentage of total torque requested from the power unit at various engine speeds.
- *ICE Torque Translation*: contains the throttle opening values in % necessary to meet the remaining torque request after accounting for the torque provided by the electric motor. This table reports the requested torque on the ordinate axis and the rpm on the abscissa axis.
- *EM Torque Translation*: of the two torque split tables, it is the first to intervene, effectively influencing the other; it defines the percentage of torque to be requested from the electric part from the initial moments, which will then be influenced by corrective factors.
- *Temperature Torque Cut*: is the first of the two corrective factors and defines a torque cut to the electric motor based on the temperature reached by the battery pack, specifically the cell with the highest temperature. This control is crucial for safety and compliance with regulations; in this case, the maximum allowable temperature is 60°C, exceeding which the vehicle must shut down completely.
- *SOC Torque Cut*: unlike the first one, it simply takes into account the typical operating range of the batteries used, which rarely reach SOC values below 15/20%. By cutting the torque near these values, it directs the torque request towards the thermal source, reducing the rate of SOC reduction.

The strategy currently in use can be summarised as follows: when the driver presses the pedal, a signal is sent to request a certain percentage of total torque from the system. The maximum torque that the power unit can produce is calculated by adding the two maximum torque curves based on the engine speed, while also taking into account the *1,2* gear ratio between the rotor and the crankshaft.

At this stage, the torque request is split into two branches. The first branch calculates the corresponding torque for the requested percentage on the thermal side, while the second branch enters the electric side as an input into the table that returns the electric portion (also expressed as a percentage) to be requested.

After calculating the percentage of electric torque, it is multiplied by the maximum torque value available at that point and proceeds to the "*correction phase*". Here, the two corrective factors described previously come into play, and the corrected torque output is sent to both the inverter and the final torque calculation part for the thermal engine. During this phase, the electric torque is subtracted from the total torque, and the remaining portion is translated into throttle opening percentage, completing the torque request for the two sources.

An example of the logic at an operating point is presented in *Figure 58*.

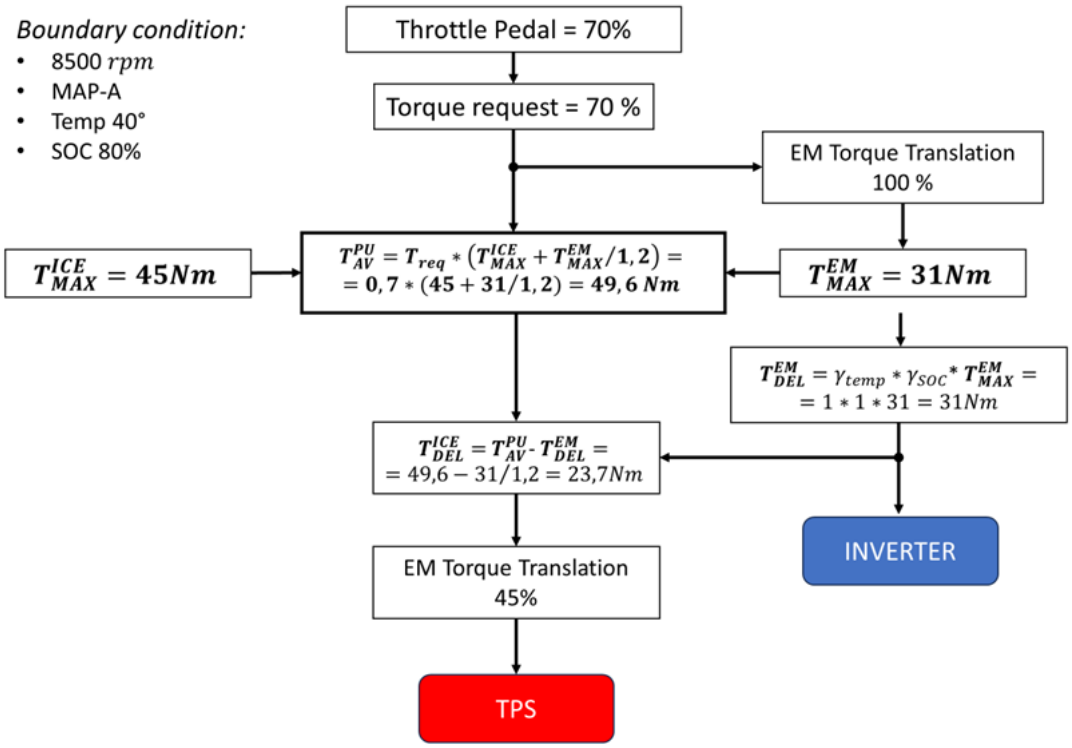

Figure 60 Example of an EMS operating point.

Once the control logic was defined, below is the development of the control strategy that allows the vehicle to complete the Endurance event, considering the main constraints as the consumption of the two energy sources: fuel and electrical energy. To achieve this, as described in Chapter 4, working by applying the Dynamic Programming technique, which allows deriving the history of electricity consumption stored in the battery during a reference lap, considering the minimum fuel consumption for a given starting state of charge as the cost variable.

6.2 Dynamic Programming implementation.

The analysis is based on the use of a model for solving the equations of longitudinal motion of the vehicle in a *backward* manner. This model has been implemented using a Matlab code, with the aim of simulating a single lap of the track (due to the high computational load) of approximately 1 km, while setting limits on the state of charge (SOC) of the batteries and using the fuel consumption of the internal combustion engine as the cost-to-go.

To achieve this, it was necessary to provide as input the speed profile derived from telemetry, various characteristics of the two engines, including peak torque and power, and the drag resistance of the vehicle.

At the end of the simulation, graphs were generated showing the state of charge (SOC) space over time (a set of points where the minimum cost point is identified) and the line connecting all the points identified as optimal, moment by moment.

6.2.1 Variables.

The first step in creating such an optimisation algorithm was to define all the variables that characterise the vehicle and to define the driving cycle. For the definition of the driving cycle, the reference was taken from the best endurance lap performed during the Formula ATA event at the Varano de' Melegari circuit. From the telemetry, the speed traces and the gear value were extracted with a sampling frequency of 10Hz, corresponding to a time step of one tenth of a second. It was necessary to filter the data due to excessive acceleration peaks caused by local peaks in the speed trace. These spikes are the result of uncertainty in the encoder measurement due to the use of phonic wheels positioned directly on the wheel set. As for the definition of all the constants that characterise the vehicle, their values are given below.

Vehicle mass	263 kg
Driver mass	60 kg
Wheels inertia moment	0,30062 $kg\ m^2$
Gearbox primary shaft inertia moment	0,000575 $kg\ m^2$
Gearbox secondary shaft inertia moment	0,00035 $kg\ m^2$

Bevel gear efficiency	0,95
Gearbox efficiency	0,98
Primary efficiency	0,98
Timing drive chain efficiency	0,95
Electrical Motor efficiency	0,85

EM/ICE Transmission ratio	0,833
Primary Transmission ratio	1,767
1st gear transmission ratio	2,467
2nd gear transmission ratio	1,875
3rd gear transmission ratio	1,5
4th gear transmission ratio	1,25
Bevel gear transmission ratio	3,3
Wheel radius	0,205 m

Figure 61 Vehicle characteristic data.

As for the efficiencies, they have been assumed on the basis of average values given in the main engineering manuals. However, the electro-mechanical efficiency deserves a closer look. This efficiency is the ratio between the power actually developed by the electric motor and the power supplied by the battery, i.e:

$$\eta_{el} = \frac{P_{mech}}{P_{el}} = \frac{T_{EM}\omega_{EM}}{V_{batt}I_{batt}}$$

The way it's defined includes all the losses that can be dissipated between the battery pack and the motor, including the inverter, cables, connections, etc. For this reason, the value is quite low. The estimate of its average value was based on the analysis of data from various telemetry datasets containing several endurance laps, calculating the reduction in SOC generated by the consumption of mechanical power compared to the actual electrical power.

Once the time, speed and acceleration vectors had been established, calculations were carried out for various angular speeds and accelerations, starting from the wheels and working backwards to the engine shaft, using the previously defined transmission ratios.

With all the quantities known, we can now define the forces required to solve the equations of motion. As described in Chapter 3.1, the force required to move the vehicle is defined as follows:

$$F_{trac} = F_{inertia} + F_{roll} + F_{aero} + F_{grade}$$

So, starting from the definition of the inertia force, we obtain:

$$F_{inertia} = m\,a \qquad \begin{cases} m = m_{veh} + m_d \\ a = \dfrac{v(i) - v(i-1)}{t} \end{cases}$$

Where m_{veh}, m_d are the masses of the vehicle and the driver respectively, expressed in kilograms, while a is the acceleration of the vehicle calculated as the change in velocity over the sampling time.

For the vehicle mass, the value measured during the pre-race setup phase was used, while for the driver's weight, an average value among the weights of the currently present team drivers was chosen.

To calculate the total resistant forces acting on the vehicle, some track tests were conducted, with a total of five trials to ensure consistent and reliable data. The test in question was carried out by reaching the vehicle's maximum speed limit, followed by deceleration without using the brakes and with the clutch disengaged to avoid any drag from the power unit. This test was conducted on a runway for tourist airplanes, providing sufficient space for its proper execution.

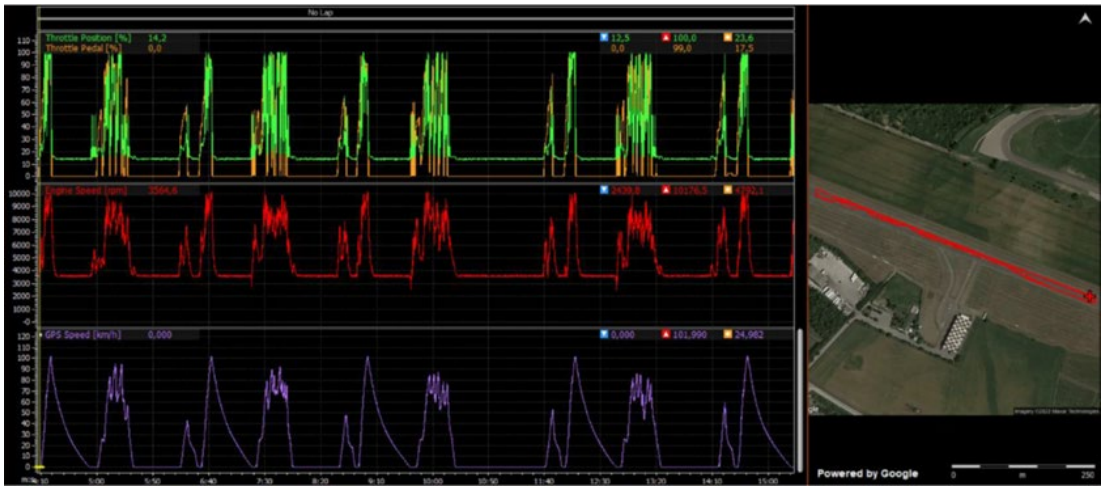

Figure 62 Telemetry of the five experimental track tests.

The tests carried out simultaneously considered mechanical friction, aerodynamic and rolling resistance forces, thus characterising a trend in the total drag force acting on the vehicle as a function of the measured deceleration. The braking force was then calculated from the deceleration and the braking torque from the wheel radius. Using the derived trend, it was possible to associate each speed of the considered cycle with a corresponding braking force obtained by interpolation.

The final trend line, shown in red, is a second-degree polynomial iteratively calibrated to reflect the average trend of the individual trend lines from the five tests. This is the equation used:

$$F_{res} = F_{roll} + F_{aero} = F_0 + 4{,}8 \cdot v + 0{,}58 \cdot v^2$$

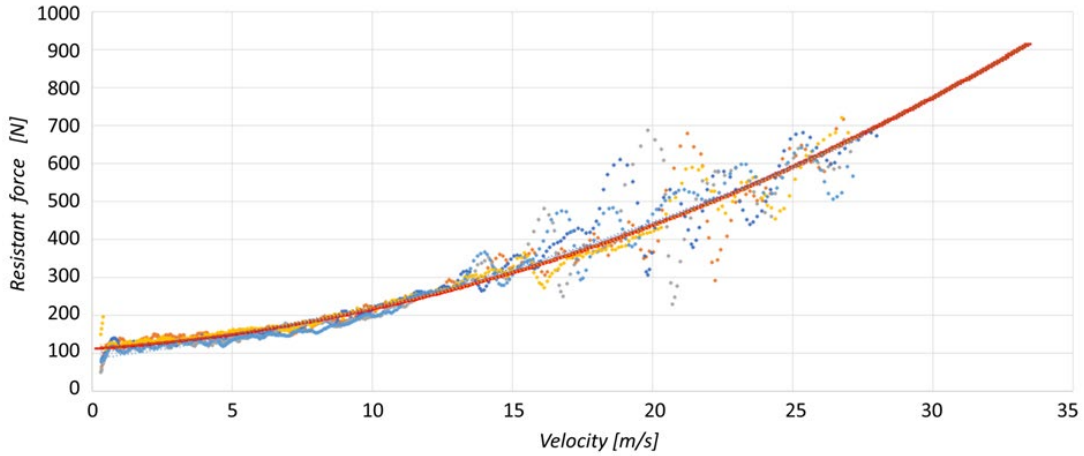

Figure 63 Experimental resistant force.

After summing up the two force contributions (inertial and resistive), the calculation of the corresponding torque applied to the wheel was carried out, then retracing the vehicle's transmission kinematic chain backward. During this phase, the various transmission ratios of the bevel gear, gearbox, clutch basket with the crankshaft, and their efficiencies were considered. The torques from the wheels were added to the moments of inertia calculated using the moment of inertia J in $kg \cdot m^2$ and the angular acceleration $\dot{\omega}$ in $\frac{rad}{s^2}$. Below is a schematic representation of the path followed.

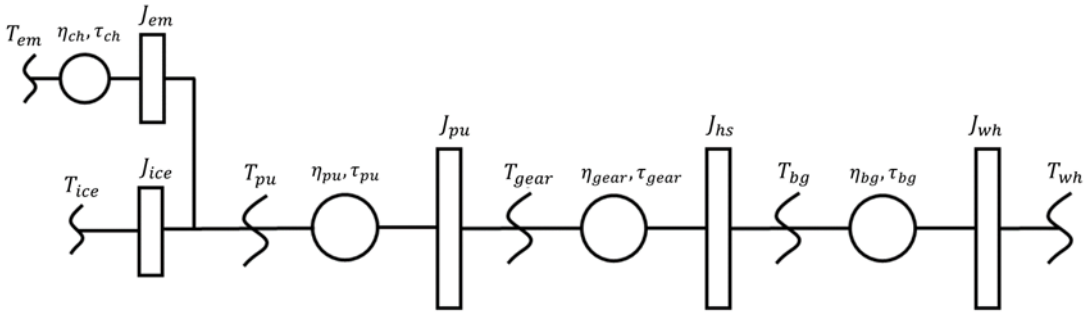

$$T_{pu} = \left(\left(\left(\left((T_{wh} + J_{wh} \cdot \dot{\omega}_{wh}) \cdot \frac{\tau_{bg}}{\eta_{bg}}\right) + J_{hs} \cdot \dot{\omega}_{hs}\right) \cdot \frac{\tau_{gear}}{\eta_{gear}}\right) + J_{pu} \cdot \dot{\omega}_{pu}\right) \cdot \frac{\tau_{pu}}{\eta_{pu}} \qquad \begin{cases} T_{em} = (T_{pu} + J_{em} \cdot \dot{\omega}_{em}) \cdot \frac{\tau_{ch}}{\eta_{ch}} \\ T_{ice} = T_{pu} + J_{ice} \cdot \dot{\omega}_{ice} \end{cases}$$

Figure 64 Kinematic chain block diagram.

Once the file containing all the system variables had been imported, the next step was to define the number of iterations to be carried out, corresponding to the tenths of a second required to complete one lap of the track.

As explained in the introduction to Dynamic Programming, it is necessary to define state and control variables. In this case, the maximum power of the electric motor was used as the control variable and the state of charge (SOC) of the battery as the state variable. In particular, the SOC variable defined the initial and final conditions to which the simulation had to adhere. The simulation was based on the prediction of a total distance travelled of approximately 20 km. For this reason, an initial SOC delta of 4% was set as a first attempt, assuming a total battery consumption of 80%. Corrective factors related to battery state of charge and temperature are not currently considered, although these factors have a significant impact on battery performance in reality.

After defining the battery pack capacity, which is 10800 kJ, the constraints mentioned above were translated into terms of energy, also introducing the resolution of the SOC itself, which is the step between the various available energy levels at each moment in time. To ensure the stability of the SOC history and prevent it from deviating from the optimal one, a penalty function was introduced:

$$pSOC = 1 - \left(\frac{SOC - SOC_f}{\frac{SOC_{max} - SOC_{min}}{2}} \right)^3$$

To complete the preparation phase, a minimum torque that the internal combustion engine must produce to balance internal losses was identified.

6.2.2 Torque calculations.

For the calculation of the various torques acting during the cycle (i.e., torques from the electric motor, internal combustion engine, and brakes), three main cases have been defined based on the value of the total torque requested at the crankshaft:

- $T_{pu} = 0$: all torques equal to zero.

$$T_{em} = 0$$
$$T_{ice} = 0$$
$$T_{brk} = 0$$

- $T_{pu} < 0$: can be divided into two sub-cases.
  - $|T_{pu}| < \tau_{chain} \cdot \eta_{chain} \cdot T_{em}^{max}$: braking torque required less than the maximum recoverable torque from the electric motor; braking only with the electric motor.

$$T_{em} = {T_{pu}}/{\tau_{chain} \cdot \eta_{chain}}$$
$$T_{ice} = 0$$

$$T_{brk} = 0$$

- $|T_{pu}| > \tau_{chain} \cdot \eta_{chain} \cdot T_{pu}^{max}$: braking torque greater than that recoverable; maximum recovery from the electric motor and the remaining difference is requested from the brakes.

$$T_{em} = -T_{pu}^{max}$$
$$T_{ice} = 0$$
$$T_{brk} = T_{pu} + {}^{T_{pu}^{max}}\!/_{\tau_{chain} \cdot \eta_{chain}}$$

- $T_{pu} > 0$: this is where the algorithm comes in and selects the best strategy.

$$T_{em} = T_{pu}^{vector} entire\ operating\ range\ of\ the\ electric\ motor$$
$$T_{ice} = T_{pu} - \tau_{chain} \cdot \eta_{chain} \cdot T_{em}$$
$$T_{brk} = 0$$

The amount of burned fuel mass m_{fuel} was also calculated through a dedicated script, which takes as input the engine speed and the torque required by the internal combustion engine.

This function uses the torque map obtained on the dynamometer, and after isolating the torque vector referred to the current engine speed, it allows to derive the relative throttle percentage through another interpolation. At this point, it becomes possible to use the fuel consumption map (also obtained on the dynamometer) expressed as a function of engine speed and throttle percentage; a double interpolation is then performed to provide the value of m_{fuel} in kg/h.

So far, the choice between the various torque splits has not yet taken into account the maximum torque deliverable by the internal combustion engine, which, as seen earlier, depends on the rotational speed of the engine shaft; to address this issue, all possible combinations of T_{ice}, T_{em}, T_{bkr}, and m_{fuel} where the condition $T_{ice} > T_{ice}^{max}$ holds have been eliminated.

Once the vector of available torques to be requested from the electric motor has been obtained, the mechanical power was calculated, and through the efficiency, it was then translated into electrical power, thus allowing to start reasoning in terms of energy to be requested from the battery.

$$P_{em} = \frac{T_{em} \cdot \omega_{em}}{\eta_{em} \cdot 1000}$$

6.2.3 Calculation of SOC limits and application of Dynamic Programming.

Once all the possible vectors of electric powers for each time step have been calculated, they are multiplied by the corresponding time, which is the timestep

of 0,1 s, to obtain the value of energy lost (in the case of discharge) or recovered (in the case of regeneration) from the battery.

In particular, two factors have been defined:

- SOC_d (descendant): corresponding to the maximum expendable energy at the previous step*

$$SOC_d = max(P^*_{em} \cdot t)$$

- SOC_a (ascendant): corresponding to the maximum recoverable energy at the previous step*

$$SOC_a = min|P^*_{em} \cdot t|$$

Subsequently, starting from these, the minimum and maximum local SOC values were created:

$$SOC_{\min_{local}} = min(SOC) - SOC_d$$

$$SOC_{\max_{local}} = max(SOC) - SOC_a$$

An *"if"* condition was applied to these two values; if they exceeded the minimum and maximum values initially defined (100% and 20%) respectively, they would be set equal to the energy corresponding to these two limits, namely 2160 kJ in the case of the minimum and 10800 kJ in the case of the maximum. This condition is essential to prevent the optimisation process from carrying out regeneration when the battery is fully charged or when the lower limit is exceeded, with the risk of damaging the cells. Obviously, this condition only makes sense in the case of simulations lasting several laps, until the end of the race, or in simulations with very high or very low SOC values.

This is where the most important part of the definition of the SOC state space comes into play, namely a control that allows the projection of the SOC history from the current iteration. It is based on corrections to the current maximum and minimum SOC values (local) and the energy available up to the end of the simulation, ensuring the link with the previously defined final SOC value (SOC_f).

Therefore, we define:

$$SOC_{to\_loose} = \sum_{j=i}^{t\_end} max\left(P_{em_j} \cdot t\right)$$

$$SOC_{to\_gain} = \sum_{j=i}^{t\_end} min\left|P_{em_j} \cdot t\right|$$

These two values define the available energy that can be discharged or gained from the i^{th} iteration until the end of the computation. If the local maximum value is greater than the sum of the "energy to be lost" and the final SOC, it is adjusted

to equal the value from this sum. The same logic is applied when the local minimum value is less than the same sum, considering the "energy to be gained".

Once the correction is completed, the SOC vector is created for each iteration from the local minimum $SOC_{\min\ \_local}$ to the local maximum $SOC_{\max\ \_local}$, with the initially defined step determining the SOC resolution.

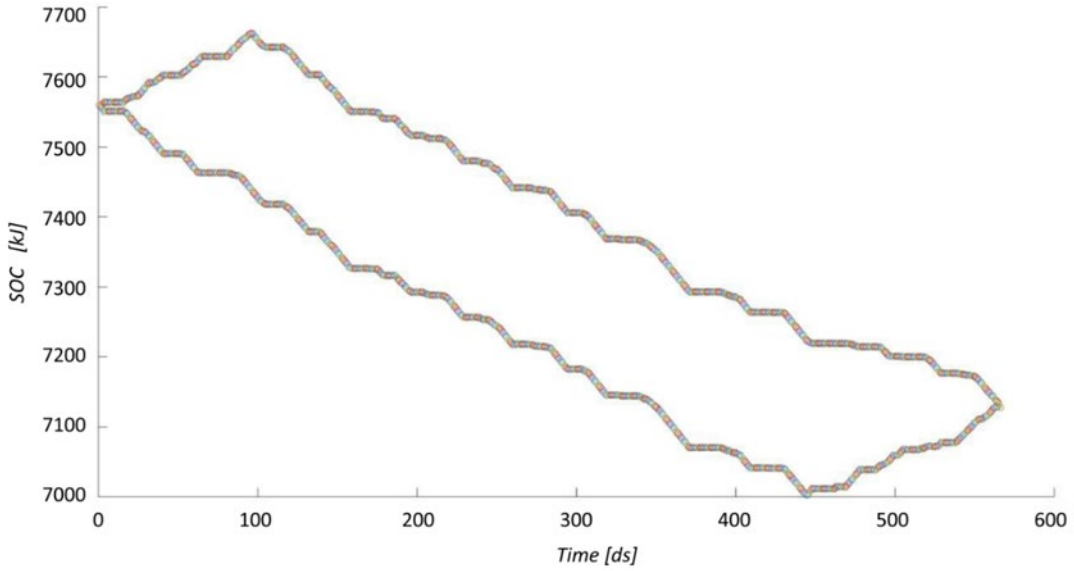

Figure 65 Limits of SOC utilization over time.

In conclusion, a graph representing the state of charge (SOC) space is plotted, with the energy value expressed in kJ on the ordinate and time in ds on the abscissa. From the graph, it can be observed that in the initial phase, the upper and lower limits tend to diverge, but after approximately ten seconds from the start of the cycle, they assume a parallel descending behaviour. This reversal of the upper limit is caused by the *"if"* controls described earlier; similarly, the same occurs inversely for the lower limit towards the end of the cycle, thus allowing the two limits to reconverge.

In this phase, Dynamic Programming is implemented as defined in *Chapter 4*, but with a backward approach by reversing the time matrix. After initializing the variables, the cycle is traversed in reverse, calculating the instantaneous cost function $L_k(arc\ cost)$ and the cost-to-go Y. These are computed for every possible SOC and applied electrical power. Once the results are obtained, for each SOC at a given time, the power that minimizes the cost-to-go is selected.

The computational load is almost entirely concentrated in this part of the algorithm, as it requires nesting three *"for"* loops: the first loop (i) iterates over each time step, the second loop (j) iterates over each SOC value, and the third (z) iterates over each available electrical power value.

Initially, the SOC for the next time step (i.e., $i-1$ because of the backward approach) is calculated, considering for each SOC the expendable or regenerable energy that decreases or increases it.

At this point, I choose fuel consumption as the variable to associate with the instantaneous cost function.

$$L_k(j,k) = m_f(k).$$

Next, the 'hypothetical' next SOC value is checked to see if it falls within the available state space previously calculated. There are two possible cases:

- Feasible SOC: I calculate the cost-to-go values, which will be the progressive sum of each instantaneous consumption, giving as a final result the total fuel consumed during the lap.
$$Y_k(j,k) = L_k(j,k) + \sum_{k=1}^{N-1} \min\big(L_k(k)\big)$$
- Infeasible SOC: I assign an extremely high value to the cost-to-go in order to exclude this point from the candidates (in this case, 1000 was chosen).

By doing this, vectors of cost-to-go are obtained for each individual SOC value referring to a specific instant. Now, within this vector, the minimum cost-to-go value is sought to be used in the next iteration; in addition to the fuel value, I store the corresponding electrical power P_k. At the end of the calculation for each simulation instant, n vectors of cost-to-go are obtained, equal to the number of possible SOCs related to that instant, and the same applies to those containing the powers.

In the next phase of Dynamic Programming, the time matrix is inverted again to return to a forward approach; at this point, matrices $Y(j,i)$ and $\mu(j,i)$ are created containing the vectors summarizing the various cost-to-go and powers.

6.2.4 Data Analysis from DP and Definition of the Optimized Map.

From the results obtained from Dynamic Programming optimization, the following were analysed:

- The history of SOC trend;
- Total fuel consumption;
- History of the requested torque to the electric motor.

Initially, attention was focused on the requested torque trace to the electric motor, particularly analysing the maximum values reached and the regions where regeneration was applied, seeking a possible characteristic behaviour of such choices (*Figure 66*).

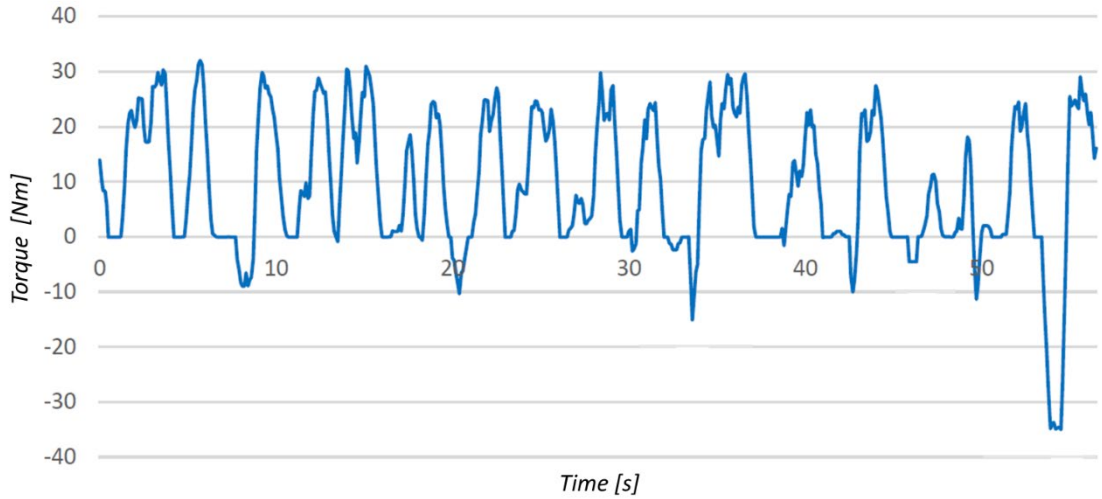

Figure 66 Torque request to the electric motor resulting from Dynamic Programming.

The maximum peak values all hover around 30 Nm, despite the available torque being higher. As for the regeneration zones, they are found in very similar situations, namely during partial load conditions near the entry into curves. These points are of great interest, as even a slight improvement in regeneration allows us to have much more energy available during the race and significantly increases the safety margin regarding the final SOC prediction.

It is easy to notice how a significant recharge was performed in the final part of the cycle; however, this negative torque peak has limited relevance, as it is heavily influenced by the Dynamic Programming's decision-making process and the characteristic of the examined cycle. In fact, starting from the end of the cycle, the algorithm is tasked with meeting a relatively high total torque request for which the thermal contribution alone is not sufficient, thus forcing the SOC to adhere to the maximum discharge profile. As soon as there is an opportunity to halt the electric motor's output and use combustion energy for regeneration, the control maximizes this condition, returning to the optimal SOC profile. It is also worth noting that in this phase, there were no limits considered in terms of regeneration, using the same characteristics of the electric motor both in motor and generator operation. This is why the final negative regeneration peak has such a high absolute value (approximately 35 Nm).

Taking into account considerations related to the reliability of the power unit and the battery pack, these results have been elaborated to generate a control map that seeks to follow the optimization analysis indications as closely as possible. However, this has led to a more conservative use of the electric motor during

regeneration phases. With this approach, SOC trends like those shown in *Figure 67* have been generated.

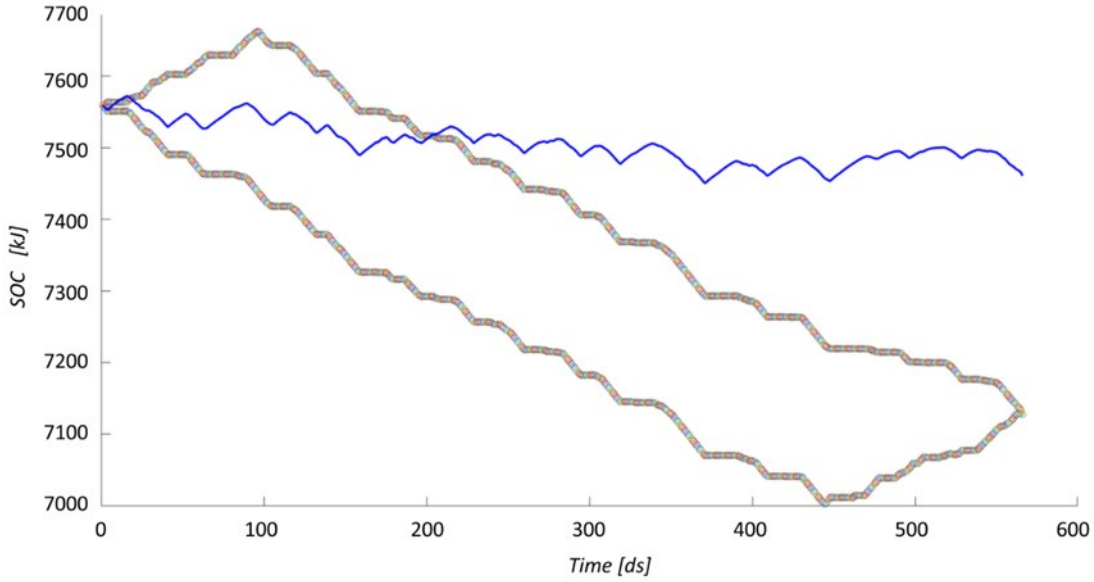

Figure 67 SOC trend over time with the first attempt map.

Seeking to maximize the optimization indications while preserving the battery pack cell temperatures, which are regulated, after several iterations, a power unit management map was defined, yielding the following results over a distance of 20 *km*.

	Fuel consuption *[l/km]*	Energy consuption *[SOC%/km]*
Ideal solution to DP	0,08	4
Safety control	0,108	2,5
Track result	0,13	3,44

7 Conclusion.

The aim of this thesis was to gather considerations for the design of a high performance vehicle with compact dimensions, using an electric hybrid power unit. In addition, the study focused on the theory of Dynamic Programming in order to develop a control logic for the optimisation of energy consumption so that the vehicle could effectively tackle the dynamic endurance event of the Formula Student. Starting from a volume analysis of the Engineering Department team's Formula Student single-seater, which currently uses a conventional internal combustion engine, the available volume was defined and further reduced by regulatory aspects. This was done in order to assess the design setup before proceeding with the detailed design of all the parts required for the electric hybrid power unit.

The process led to the selection of a parallel hybrid power unit layout, known as P0, which met all the regulatory limits imposed by the Formula Student UK event. The electric motor was integrated as a plug-and-go conversion kit. This was facilitated by the choice of a 90° V-engine layout, which provided the benefits of balancing first-order inertia forces, a dedicated distribution chain for introducing the electric motor, and a form factor that facilitated its installation in the vehicle. Another advantage of this type of engine is the highly integrated cooling and lubrication circuits, which can be easily modified to define a new circuit that effectively integrates the cooling requirements of the electric motor and the entire power unit.

The study of volumes was crucial to the definition of the energy storage systems, particularly in the development of the shapes and all the choices made to define the battery pack. This component posed a challenge as it required a significant amount of space, which was not readily available in a Formula Student single-seater chassis. However, this led to the research of solutions that proved to be efficient in terms of volume utilisation, maintenance and electrical energy storage.

The other aspect that was addressed and could be further explored was the definition of optimised energy management strategies. Through the development of codes in the Matlab environment, it was possible to make use of the theory of Dynamic Programming, which led to the definition of control maps for the power units that allowed them to make the best use of their capabilities.

It is reported that over the three-year period of activity, a vehicle was produced each year for participation in the British Formula Student event. In particular, in 2023, a significant portion of the dynamic tests was completed with good results.

It can be said that this approach can be applied to the design of two-wheeled vehicles characterised by small dimensions, such as the single-seater discussed in the thesis. In fact, starting from a blank slate, iterative analyses can be carried out to define a power unit that is guided by the available space. The idea is to use the theory of Dynamic Programming in combination with volume analysis to also choose the type of hybrid [60]. Currently, the automotive industry favours power-split or parallel hybrid systems, which undoubtedly optimise energy use, but are mechanically complex and bulky. These characteristics are hardly suitable for two-wheeled vehicles.

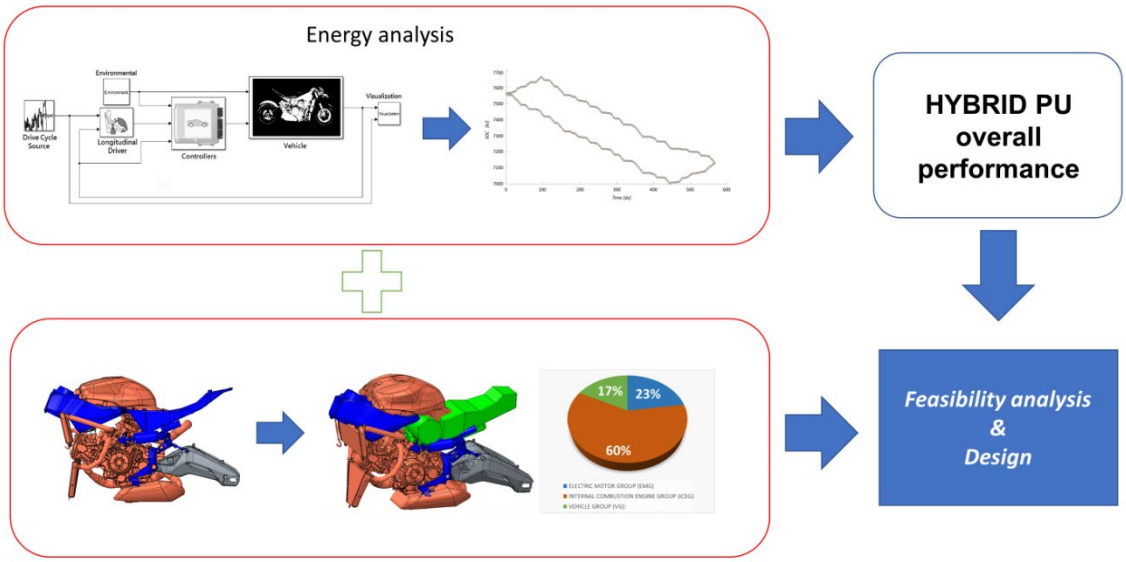

Figure 68 Logical schema of the design method for a two-wheeled electric hybrid vehicle.

Abbreviations

ALV available limit volume

BEV battery electric vehicle

BMS battery management system

CAD computer aided design

CFD computational fluid dynamic

EM electric motor

ESS energy storage system

FE finite element

HEV hybrid electric vehicle

HTC heat transfer coefficient

ICE internal combustion engine

ICEV internal combustion engine vehicle

IM induction motor

LCO lithium cobalt oxide

LDV light-duty vehicle

LFP lithium ferro phosphate

LMO lithium manganese oxide

LTO lithium titanium oxide

NCA (lithium) nickel cobalt aluminium

NMC (lithium) nickel manganese cobalt

OEM original equipment manufacturer

PMSM permanent magnet synchronous motor

SRM switched reluctance motor

TKE turbulent kinetic energy

VSI voltage source inverter

VVVF variable-voltage variable-frequency

ZEV zero emission vehicle

References.

1. Chapman, L., “Transport and climate change: a review,” *J. Transp. Geogr.* 15(5):354–367, 2007, doi:10.1016/j.jtrangeo.2006.11.008.

2. Saboori, B., Sapri, M., and Baba, M. bin, “Economic growth, energy consumption and CO2 emissions in OECD (Organization for Economic Co-operation and Development)’s transport sector: A fully modified bi-directional relationship approach,” Energy 66:150–161, 2014, doi:10.1016/j.energy.2013.12.048.

3. Fontaras, G., Zacharof, N.G., and Ciuffo, B., “Fuel consumption and CO2 emissions from passenger cars in Europe – Laboratory versus real-world emissions,” Prog. Energy Combust. Sci. 60:97–131, 2017, doi:10.1016/j.pecs.2016.12.004.

4. Hawkins, T.R., Gausen, O.M., and Strømman, A.H., “Environmental impacts of hybrid and electric vehicles-a review,” Int. J. Life Cycle Assess. 17(8):997–1014, 2012, doi:10.1007/s11367-012-0440-9.

5. Zdeněk, Č. and Pavel, M., “Electric, hybrid electric and combustion engine driven cars and their impact on environment,” Proc. 2011 14th Eur. Conf. Power Electron. Appl. EPE 2011 739–743, 2011.

6. González Palencia, J.C., Furubayashi, T., and Nakata, T., “Energy use and CO 2 emissions reduction potential in passenger car fleet using zero emission vehicles and lightweight materials,” Energy 48(1):548–565, 2012, doi:10.1016/j.energy.2012.09.041.

7. Szymlet, N.; Rymaniak, Ł.; Lijewski, P. Two-Wheeled Urban Vehicles—A Review of Emissions Test Regulations and Literature. Energies 2024, 17, 586. doi:10.3390/en17030586.

8. Singh, S.; Kulshrestha, M.J.; Rani, N.; Kumar, K.; Sharma, C.; Aswal, D.K. An Overview of Vehicular Emission Standards. Mapan J. Metrol. Soc. India 2023, 38, 241–263. doi:10.1007/s12647-022-00555-4.

9. Pacura, W.; Szramowiat-Sala, K.; Gołaś, J. Emissions from Light-Duty Vehicles—From Statistics to Emission Regulations and Vehicle Testing in the European Union. Energies 2024, 17, 209. doi:10.3390/en17010209.

10. Wang, P.; Duan, X.; Chen, C.; Liu, S. Experimental Investigation on the Exhaust Emissions and Performance of a Hybrid Electric Motor Coupled with an Energy Recovery System. Case Stud. Therm. Eng. 2023, 45, 102994. doi:10.1016/j.csite.2023.102994.

11. Elango, P.; Mathivanan, A.; Kakani, R.; Das, H.B.; Asvathanarayanan, R. Numerical Evaluation of Fuel Consumption and Transient Emissions of Different Hybrid Topologies for Two-Wheeler Application. SAE Int. J. Electrified Veh. 2023, 12, 389–402.

12. IMechE website, http://www.imeche.org/events/formula-student/team-information/rules, Feb. 2019.

13. Sciarretta, A., Back, M., and Guzzella, L., “Control of Parallel Hybrid Electric Vehicles,” IEEE Trans. Control Syst. Technol. 12(3):352–363, 2004, doi:10.1109/TCST.2004.824312.

14. Chan, C.C., “The State of the Art of Electric, Hybrid, and Fuel Cell Vehicles With their superior fuel economy and performance, hybrid vehicles will likely increase in popularity in coming years; further development of control theory for hybrids is essential for their,” Fellow IEEE 95(4):704–718, 2007, doi:10.1109/JPROC.2007.892489.

15. Çağatay Bayindir, K., Gözüküçük, M.A., and Teke, A., “A comprehensive overview of hybrid electric vehicle: Powertrain configurations, powertrain control techniques and electronic control units.” EnergyConvers. Manag. 52(2):1305–1313,2011, doi:10.1016/j.enconman.2010.09.028.

16. Fellini, R., Michelena, N., Papalambros, P., and Sasena, M., “Optimal design of automotive hybrid powertrain systems,” Proc. - 1st Int. Symp. Environ. Conscious Des. Inverse Manuf. EcoDesign 1999 400–405, 1999, doi:10.1109/ECODIM.1999.747645.

17. Chan, C.C., Bouscayrol, A., and Chen, K., “Electric, hybrid, and fuel-cell vehicles: Architectures and modelling.” IEEE Trans. Veh. Technol. 59(2):589–598, 2010, doi:10.1109/TVT.2009.2033605.

18. M. Sabri, M.F., Danapalasingam, K.A., and Rahmat, M.F., “A review on hybrid electric vehicles architecture and energy management strategies,” Renew. Sustain. Energy Rev. 53:1433–1442, 2016, doi:10.1016/j.rser.2015.09.036.

19. Onori, S.; Serrao, L.; Rizzoni, G. “*Hybrid Electric Vehicles: Energy Management Strategies.”*; Springer: London, UK, 2016.

20. Emadi, A., Rajashekara, K., Williamson, S.S., and Lukic, S.M., “Topological overview of hybrid electric and fuel cell vehicular power system architectures and configurations.” IEEE Trans. Veh. Technol. 54(3):763–770, 2005, doi:10.1109/TVT.2005.847445.

21. Ross, M. and Wu, W., “Fuel economy analysis for a hybrid concept car based on a buffered fuel-engine operating at an optimal point,” SAE Tech. Pap. (41 2), 1995, doi:10.4271/950958.

22. Gökce, K. and Ozdemir, A., “An instantaneous optimization strategy based on efficiency maps for internal combustion engine/battery hybrid vehicles,” Energy Convers. Manag. 81:255–269, 2014, doi:10.1016/j.enconman.2014.02.034.

23. Yang, Y., Ali, K.A., Roeleveld, J., and Emadi, A., “State-of-the-art electrified powertrains - hybrid, plug-in, and electric vehicles,” *Int. J. Powertrains* 5(1):1, 2016, doi:10.1504/ijpt.2016.075181.

24. Sai, L.W., Schultz, G., and Higuchi, N., “A novel parallel hybrid transmission,” J. Mech. Des. Trans. ASME 123(2):161–168, 2001, doi:10.1115/1.1365118.

25. Chau, K.T. and Wong, Y.S., “Overview of power management in hybrid electric vehicles,” Energy Convers. Manag. 43(15):1953–1968, 2002, doi:10.1016/S0196-8904(01)00148-0.

26. Picarelli, A. and Dempsey, M., “Simulating the complete 2014 hybrid electric Formula 1 cars,” 9.2-9.2, 2015, doi:10.1049/cp.2014.0960.

27. Genta G., “Meccanica dell’autoveicolo.”; Levrotto&Bella: Torino, Italy, 2000.

28. Limebeer, D.J.N., Perantoni, G., and Rao, A. V., “Optimal control of Formula One car energy recovery systems,” Int. J. Control 87(10):2065–2080, 2014, doi:10.1080/00207179.2014.900705.

29. Ehsani, M.; Singh, K.V.; Bansal, H.O.; Mehrjardi, R.T. State of the Art and Trends in Electric and Hybrid Electric Vehicles. Proc. IEEE 2021, 109, 967–984. doi:10.1109/JPROC.2021.3072788.

30. Nüesch, T., Cerofolini, A., Mancini, G., Cavina, N., Onder, C., and Guzzella, L., “Equivalent Consumption Minimization Strategy for the Control of Real Driving NOx Emissions of a Diesel Hybrid Electric Vehicle,” Energies 7(5):3148–3178, 2014, doi:10.3390/en7053148.

31. Musardo, C., Rizzoni, G., Guezennec, Y., and Staccia, B., “A-ECMS: An adaptive algorithm for hybrid electric vehicle energy management,” Eur. J. Control 11(4–5):509–524, 2005, doi:10.3166/ejc.11.509-524.

32. Onori, S., Serrao, L., and Rizzoni, G., “Adaptive equivalent consumption minimization strategy for hybrid electric vehicles,” ASME 2010 Dynamic Systems and Control Conference, DSCC2010, ISBN 9780791844175: 499–505, 2010, doi:10.1115/DSCC2010-4211.

33. Park, J. and Park, J.H., “Development of equivalent fuel consumption minimization strategy for hybrid electric vehicles,” Int. J. Automot. Technol. 13(5):835–843, 2012, doi:10.1007/s12239-012-0084-6.

34. Rezaei, A., Burl, J.B., and Zhou, B., “Estimation of the ECMS Equivalent Factor Bounds for Hybrid Electric Vehicles,” IEEE Trans. Control Syst. Technol. 26(6):2198–2205, 2018, doi:10.1109/TCST.2017.2740836.

35. Mattarelli, E., Rinaldini, C.A., Scrignoli, F., and Mangeruga, V., “Development of a Hybrid Power Unit for Formula SAE Application: ICE CFD-1D Optimization and Vehicle Lap Simulation,” SAE Tech. Pap. Ser. 1, 2019, doi:10.4271/2019-24-0200.

36. Zeraoulia, M., Benbouzid, M.E.H., and Diallo, D., Electric motor drive selection issues for HEV propulsion systems: A comparative study, IEEE Trans. Veh. Technol. 55(6):1756–1764, 2006, doi:10.1109/TVT.2006.878719.

37. Ehsani, M., Gao, Y., Longo, S., and Ebrahimi, K., “Modern electric, hybrid electric, and fuel cell vehicles,” CRC press, ISBN 0429998244, 2018.

38. Ehsani, M., Gao, Y., and Gay, S., “Characterization of Electric Motor Drives for Traction Applications,” *IECON Proc. (Industrial Electron. Conf.* 1:891–896, 2003, doi:10.1109/IECON.2003.1280101.

39. Hanselman, D., “Brushless permanent magnet motor design,” 2003.

40. Awadallah, M., Tawadros, P., Walker, P., and Zhang, N., “Selection and Characterisation of PMSM motor for mild HEV Applications,” *EVS 2016-29th International Electric Vehicle Symposium*, ISBN 151083270X, 2016.

41. Yang, Z., Shang, F., Brown, I.P., and Krishnamurthy, M., “Comparative study of interior permanent magnet, induction, and switched reluctance motor drives for EV and HEV applications,” *IEEE Trans. Transp. Electrif.* 1(3):245–254, 2015, doi:10.1109/TTE.2015.2470092.

42. Rahman, Z., Ehsani, M., and Butler, K.L., “An investigation of electric motor drive characteristics for EV and HEV propulsion systems,” *SAE Tech. Pap.* (724), 2000, doi:10.4271/2000-01-3062.

43. Rahman, K.M. and Ehsani, M., “PERFORMANCE ANALYSIS OF ELECTRIC MOTOR DRIVES FOR ELECTRIC AND HYBRID ELECTRIC VEHICLE APPLICATIONS,” 49–56, 1998.

44. Jeongwoo, L. and Nelson, D.J., “Rotating inertia impact on propulsion and regenerative braking for electric motor driven vehicles,” *2005 IEEE Vehicle Power and Propulsion Conference, VPPC*, ISBN 0780392809: 308–314, 2005, doi:10.1109/VPPC.2005.1554575.

45. Valerio Mangeruga, Fabio Renso, Francesco Raimondi, Saverio Giulio Barbieri, Matteo Giacopini, “Influence of the Crankshaft Dynamic Phenomena on the Fatigue Behaviour of a Transmission Chain in a Hybrid Power Unit”, Journal of Multiscale Modelling Vol. 14, No. 2 (2023) 2350002 (29 pages) doi: 10.1142/S1756973723500026 2023

46. Feng, Z.M., Li, J.L., and Liu, G.W., “Dynamic Analysis of Silent Chain Drive System for Hybrid Car,” Adv. Mater. Res. 694–697:84–89, 2013, doi:10.4028/www.scientific.net/amr.694-697.84.

47. Meng, F., Feng, Z., and Chu, Y., “MESHING THEORY AND DESIGN_ METHOD OF NEW SILENT CHAIN AND SPROCKET,” *Chinese J. Mech. Eng. Ed.* 19(3):425–427, 2006.

48. Boglietti, A., Cavagnino, A., Staton, D., Shanel, M., Mueller, M., and Mejuto, C., “Evolution and modern approaches for thermal analysis of electrical machines,” *IEEE Trans. Ind. Electron.* 56(3):871–882, 2009, doi:10.1109/TIE.2008.2011622.

49. Schofield, N., Bilgin, B., Kasprzak, M., Emadi, A., Preindl, M., Nalakath, S., Sadek, H., Cotton, J., and Yang, Y., “Thermal management of electric machines,” *IET Electr. Syst. Transp.* 7(2):104–116, 2016, doi:10.1049/iet-est.2015.0050.

50. Cao, M., Kovent, I., and Ku, J., “Efficient thermal modeling and integrated control strategy of powertrain for a parallel hybrid EcoCAR2 competition vehicle,” *SAE Tech. Pap.* 1, 2014, doi:10.4271/2014-01-1927.

51. González, A., Goikolea, E., Barrena, J.A., and Mysyk, R., Review on supercapacitors: Technologies and materials, *Renew. Sustain. Energy Rev.* 58:1189–1206, 2016, doi:10.1016/j.rser.2015.12.249.

52. Barr, A. and Veshagh, A., “Fuel economy and performance comparison of alternative mechanical hybrid powertrain configurations,” *SAE Tech. Pap.* (724):776–790, 2008, doi:10.4271/2008-01-0083.

53. O’hayre, R., Cha, S.-W., Colella, W., and Prinz, F.B., “Fuel cell fundamentals,” John Wiley & Sons, ISBN 1119113806, 2016.

54. Budde-Meiwes, H., Drillkens, J., Lunz, B., Muennix, J., Rothgang, S., Kowal, J., and Sauer, D.U., “A review of current automotive battery technology and future prospects,” *Proc. Inst. Mech. Eng. Part D J. Automob. Eng.* 227(5):761–776, 2013, doi:10.1177/0954407013485567.

55. Kwade, A., Haselrieder, W., Leithoff, R., Modlinger, A., Dietrich, F., and Droeder, K., “Current status and challenges for automotive battery production technologies,” *Nat. Energy* 3(4):290–300, 2018, doi:10.1038/s41560-018-0130-3.

56. Higashimoto, K., Homma, H., Uemura, Y., Kawai, H., Saibara, S., and Hironaka, K., “Automotive Lithium-ion Batteries,” 2011.

57. John T. Warner, “The Handbook of Lithium-Ion Battery Pack Design,” 2015, doi:10.1016/c2013-0-23144-5.

58. Babu, S.S., Santella, M.L., Feng, Z., Riemer, B.W., and Cohron, J.W., “Empirical model of effects of pressure and temperature on electrical contact resistance of metals,” Sci. Technol. Weld. Join. 6(3):126–132, 2001, doi:10.1179/136217101101538631.

59. Pattipati, B., Pattipati, K., Christopherson, J.P., Namburu, S.M., Prokhorov, D. V., and Qiao, L., “Automotive battery management systems,” AUTOTESTCON (Proceedings) (September):581–586, 2008, doi:10.1109/AUTEST.2008.4662684.

60. Mangeruga, V., Cusati, D., Raimondi, F., Giacopini, M., ”Feasibility Study on MHEV Application for Motorbikes: Components Sizing, Strategy Optimization through Dynamic Programming and Analysis of Possible Benefits.” Vehicles 2024, 6, 1442–1467. doi:10.3390/vehicles6030068.